NEARSHORE AND SURFZONE MORPHODYNAMICS

OF A STORM WAVE ENVIRONMENT:

EASTERN BASS STRAIT, AUSTRALIA

L.D.WRIGHT, P.NIELSEN, A.D.SHORT, F.C.COFFEY and M.O.GREEN

CONTENTS

ABSTRACT

A field investigation of inner shelf, surf-zone, and beach
processes and associated morphodynamic changes was carried out on and
seaward of Eastern Beach, on the Gippsland Coast, in Eastern Bass
Strait, Australia. The beach is part of a long straight beach system
fronted by a wide continental shelf. Frequent passage of gales through
Bass Strait results in relatively high energy but variable and rapidly
changing deepwater wave conditions. Time series of benthic currents
(u and v) were recorded at depths of 20m and 10m over the nearshore
profile and from different regions of the surf zone.

Over the nearshore profile, wave-induced oscillatory flows
dominate to depths of 20m and are responsible for agitating and
suspending sediments. Despite the microtidal range, reversing shore-
parallel currents and superimposed wind driven currents are second in
importance and determine the fate of sediments suspended by waves.
Frictional dissipation of the obliquely incident waves over the rough,
rippled and low-gradient nearshore profile is particularly pronounced
and, as a result, bottom orbital velocities measured at 10m depth were
slightly weaker than those measured at 20m. Of fundamental importance
to surf zone processes, nearshore energy dissipation by bed friction
causes not only a reduction in average breaker height but also signifi-
cantly reduces the temporal range of breaker conditions.

The morphodynamic state of the surf zone and beach remains inter-
mediate between the reflective and dissipative extremes and is
characterized for most of the time by pronounced longshore bar-trough
or rhythmic bar and beach topography. A relatively deep (h= 2m) trough

separates a dissipative bar from a steep reflective beach face. In
addition to the oscillations at incident wave frequency which are
dominant throughout the surf zone, important roles are played by
surf zone standing waves at subharmonic and infragravity frequencies
and by longshore currents and rips. Vertical profiles of longshore
current velocity within the trough revealed velocities as high as
$0.25m \ sec^{-1}$ to within 0.075m above the bed and were not at all loga-
rithmic. The profiles are explained in terms of the large near-bottom
eddy viscosity caused by wave induced vortices over a rippled bed.
Direct measurement of vertical profiles of suspended sediment concen-
trations showed that, despite the presence of longshore currents,
sediment suspension can be well modelled in terms of entrainment by
waves alone.

Although temporal variability of deepwater wave conditions is
very large, the substantial reductions in breaker variability caused
by increased nearshore dissipation of larger waves also reduces the
range of morphodynamic variability of the beach and surf zone. The
longshore-bar-trough and rhythmic-bar-and-beach states represent the
modal states and other states rarely develop. However, profile mobility
is considerable. Most of this mobility is expressed by onshore-offshore
migrations of the bar and, to a lesser extent, by longshore migrations
of rhythmic features. The mobility of the subaerial beach face is
comparatively low and this is attributable to the relative constancy
of the shore-break amplitude. The Eastern Beach model is compared to
an analog at Duck, North Carolina, U.S.A.

INTRODUCTION

It is apparent that, on the southeastern coast of Australia at least, the onshore-offshore and alongshore exchange of sediments is not confined to the surf zone but extends out onto the inner continental shelf to depths of over 20 metres. In addition, processes operating over the inner continental shelf partially predetermine the nature, intensity, and variability of the processes which operate within the surf zone. In turn, the complex processes of the surf zone are fundamental in effecting the transfer of sediments between the shelf and the subaerial beach. The problem of beach and nearshore morphodynamics is thus one which involves the entire Coastal Boundary Layer (Fig.1). The Coastal Boundary Layer is defined in this context as the region in which oceanic processes are measurably modified by the presence of the coast. The seaward limit is approximately the 50 metre depth contour and the landward limit is the beach. In this report we are concerned with morphodynamic aspects of the Coastal Boundary Layer including the region seaward of the surf zone, the surf zone, and the beach.

All deterministic models aimed at predicting changes, either erosional or accretional, of beaches, nearshore sea beds, or any other morphologic feature are underlain by this axiom: morphodynamic changes result from gradients in sediment transport. Sediment transport depends in part on the instantaneous or time averaged shear stresses, τ, which disturb sediment or place it in suspension and in part on the net drift pattern, $\vec{V}$, which advects the entrained sediment. Fundamental to understanding sediment transporting processes and their gradients which produce either accretion or

erosion is an appreciation of the roles played by different modes
of fluid motion in contributing to τ and $\vec{V}$ within the benthic
regime over different regions of the Coastal Boundary Layer.
Seaward of the surf zone, we must understand the relative roles
played by interacting waves, tidal currents, and other currents
in determining the fate of nearshore sediments. In the presence
of complex bar-trough surf zone topography the process signature
is even more complex and includes the effects of breaking incident
waves, standing waves and edge waves, and wave-generated longshore
currents and rips.

Our field studies of Australian beaches and surf zones over the
past few years have shown that nearshore and surf zone process
signatures, associated sediment transport, and beach response are
all mutually related and are strongly dependent on coastal environ-
mental conditions as well as on the predominant modal state of the
beach and surf zone (Wright et al 1979 a and b; Short 1979 a and b;
Wright 1981, 1982; Wright et al 1981, 1982; Wright et al 1982;
Wright and Short in press). Depending on local environmental
conditions, sediments, inner shelf processes and antecedent wave
conditions, beaches and surf zones may be dissipative, reflective,
or in one of four intermediate states. The intermediate states,
particularly states characterized by pronounced longshore bar and
trough and crescentic bar topographies with rip circulation cells
are typically the most dynamic in terms of morphologic mobility
and exhibit the most complex sets of processes (Short, 1981;
Wright 1981; Wright and Short in press).

The Gippsland coast of Victoria bordering Bass Strait in the
extreme southeastern corner of Australia, exhibits an uninterrupted

sandy beach (Ninety Mile Beach), 145 kilometres in length fronted by a comparatively wide, petroleum rich, continenta shelf. Ninety Mile Beach and its associated nearshore system face oughly toward the south and into Bass Strait (Fig.2) through which the frequent passage of mid-latitude storms and gales produce rapidly changing deep water wave conditions. This highly variable and relatively high energy wave climate combines with tidal and wind driven currents to produce a complex set of sediment-transporting processes but is also filtered appreciably by the wide nearshore profile to reduce the temporal variability in beach morphology. As a consequence of the regional environmental conditions and sediment properties, the modal morphodynamic state of the beach and surf zone tends to remain intermediate between the dissipative and reflective extremes and is characterized by pronounced bar-trough and crescentic bar topography. The region thus offers an excellent laboratory for studying the processes which operate in the presence of this globally-important morphodynamic state as well as the processes which operate seaward of the surf zone and predetermine the probability that this surf zone state will exist.

The Gippsland coast provides us with a case study for illustrating some of the processes which operate within and seaward of intermediate bar-trough and rhythmic bar and beach type surf zones. The functions of the report are twofold: (1) to present the results of a set of experiments carried out on and seaward of Eastern Beach near the eastern end of Ninety Mile Beach in eastern Bass Strait, and (2) to use this "case study" as a medium for illustrating the application of recently developed ideas and discussing some processes of general importance. To
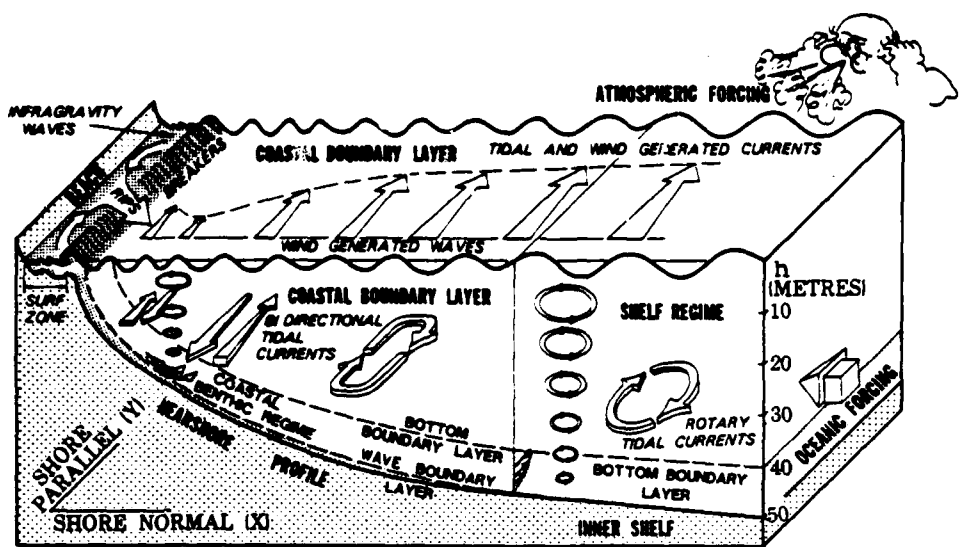
Figure 1.   Components and Processes of the Coastal Boundary Layer.
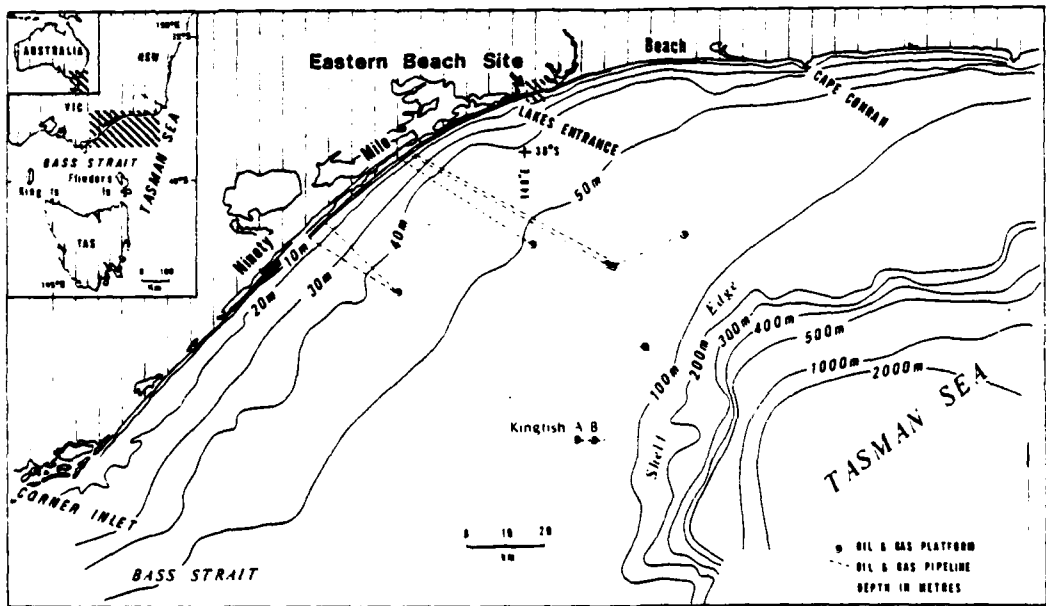
Figure 2.   Bathymetry and Coastline Configuration of Eastern
            Bass Strait.

a large degree, the emphasis is on principles rather than place. We will discuss the relative magnitudes of several important processes at different positions over the nearshore zone and in the surf zone; draw some inferences about nearshore sediment transport; and discuss the beach variability and mobility that result from these processes.

THE GIPPSLAND COASTAL ENVIRONMENT

Coastal Configuration and Geology

The Gippsland coast extends 440 km along an arc from Wilsons
Promontory to Cape Howe at the New South Wales border (Fig.3).
North from Snake Island the coast consists of an almost continuous
364 km sand beach-barrier system facing Bass Strait. The low
energy, tidal dominated Shallow Inlet region occupies the south-
western corner. North of the first 34 km, exposure to wave energy
has produced a continuous beach, Ninety Mile Beach, extending
from Shallow Inlet to Red Bluff a distance of 144 km or 90 miles.
Beyond Red Bluff the beach-barrier continues almost unbroken for
another 132 km to Ram Head. Only the mouth of the Snowy River and
Cape Conran, Pearl Point, Clinton Rocks and Point Hicks interrupt
the curve of the coast. Beyond Ram Head the coast abruptly trends
northeast resulting in initially low wave energy and a sediment
deficient coast. Rocky coastline dominates 17 of the next 32 km
with sand increasing in abundance toward Gabo Island. At the New
South Wales border a wide sand plain and transgressive coastal
dunes dominate the morphology. In total, 92% of the 336 km between
Shallow Inlet and Cape Howe is composed of sand beaches backed by
barriers and dunes. Changes in coastal orientation along the arc
(Fig.3) result in systematic variation in levels of wave energy
and onshore wind velocities, which in turn control the beach and
dune sediment supply and ultimately the form of the beach-barrier
system. In addition, the overall orientation relative to the
dominant west and southwest waves and winds produces a pronounced

northeastward increase in wave energy and associated littoral drift.

The coast lies in a Tertiary depositional basin called the Gippsland Basin (see Franklin and Clifton, 1971 for a description of the stratigraphy). It is bordered on the north and west by Palaeozoic rocks of the Eastern Highlands, and in the southwest by Cretaceous rocks of the Gippsland Highlands and the high granite of Wilsons Promontory. The eastern boundary of the basin lies at the edge of the continental shelf. Because of the present high sea level the shoreline lies approximately in the middle of the basin. East of Red Bluff the east-west trend of the Eastern Highlands dominates the coast and controls the coastal orientation. South of Red Bluff the present coastline lies along the axis of basin tilting with slight uplift landward and extensive downwarping seaward across the shelf with sediments exceeding 2000 m in thickness. The Basin is composed of Tertiary fluvial and marine deposits. Uplifted marine deposits outcrop at numerous locations across the subaerial plain. During the Quaternary at least three major barrier systems were built: the Prior, Inner and Outer Barriers (Bird 1978), the Outer representing the Holocene barrier system.

Evidence suggests that periodic high wave energy and pronounced north-eastward littoral drift has delivered Holocene beach-barrier sediments both from offshore where they have eroded down to Tertiary sands and gravels, and from alongshore, resulting in erosion of Pleistocene deposits between Seaspray and Reeves Beach. The littoral drift has resulted in continual Holocene inlet and river mouth migration northward along the coast. On Ninety Mile

Beach numerous abandoned recurved inlet spits and flood tide deltas extend from Stockyard Hill for 16 km to Bunga Arm, and Bunga Arm itself is the result of eastward spit growth leaving an abandoned Holocene barrier abutting Boole Poole Peninsula. Similar eastward spit growth and truncation was a characteristic of Cunningham Arm before the construction of training walls at Lakes Entrance (Bird, 1978).

Climate and Wind Regime

The Gippsland coast lies between latitudes 37° 34'S and 39° 08'S which places it near the southern margins of Australia's dominant pressure system, the subtropical anticyclonic belt, and in the path of the mid-latitude cyclones. Superimposed on the general westerly airflow, stronger westerly and southwesterly winds (locally called gales) accompany the passage of fronts. Although these fronts occur throughout the year, they are most frequent and their effects most intense during the winter months. Following passage of fronts, the winds usually moderate and turn south or southwest. Northeast and easterly winds, which are subdominant, prevail during intervening periods of high pressure. The winter period of most frequent frontal passage is also the period of greatest rainfall. Figure 4 shows the mean annual distribution of temperature and rainfall at the two ends of the region. Wind roses for Tidal River, Lakes Entrance, and Gabo Island are shown in Figure 5. Additonal wind data can be found in Appendix A.

Winds from the westerly sector (SW, W, NW) dominate at all stations. However, there is considerable variation along the coast, presumably reflecting local topographic effects. There is also a
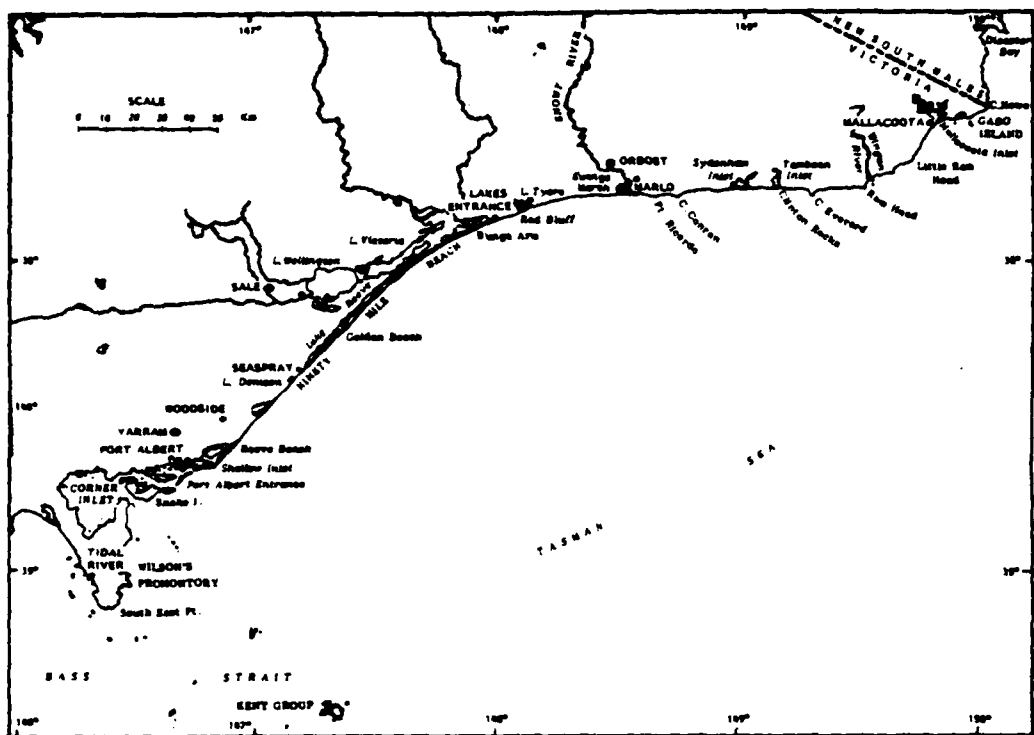
Figure 3.   Location Map
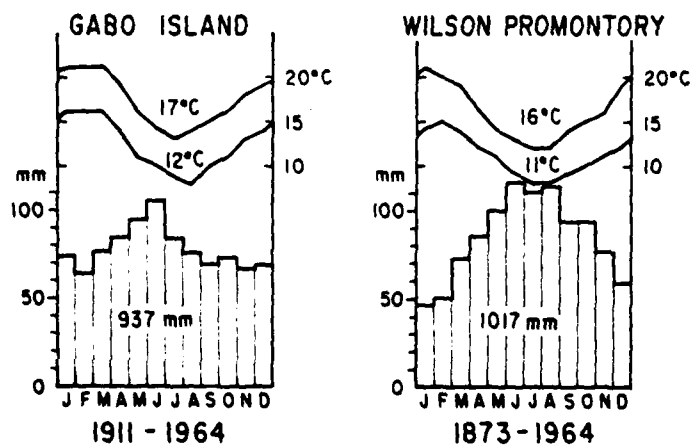
Figure 4.   Annual distribution of temperature and precipitation.
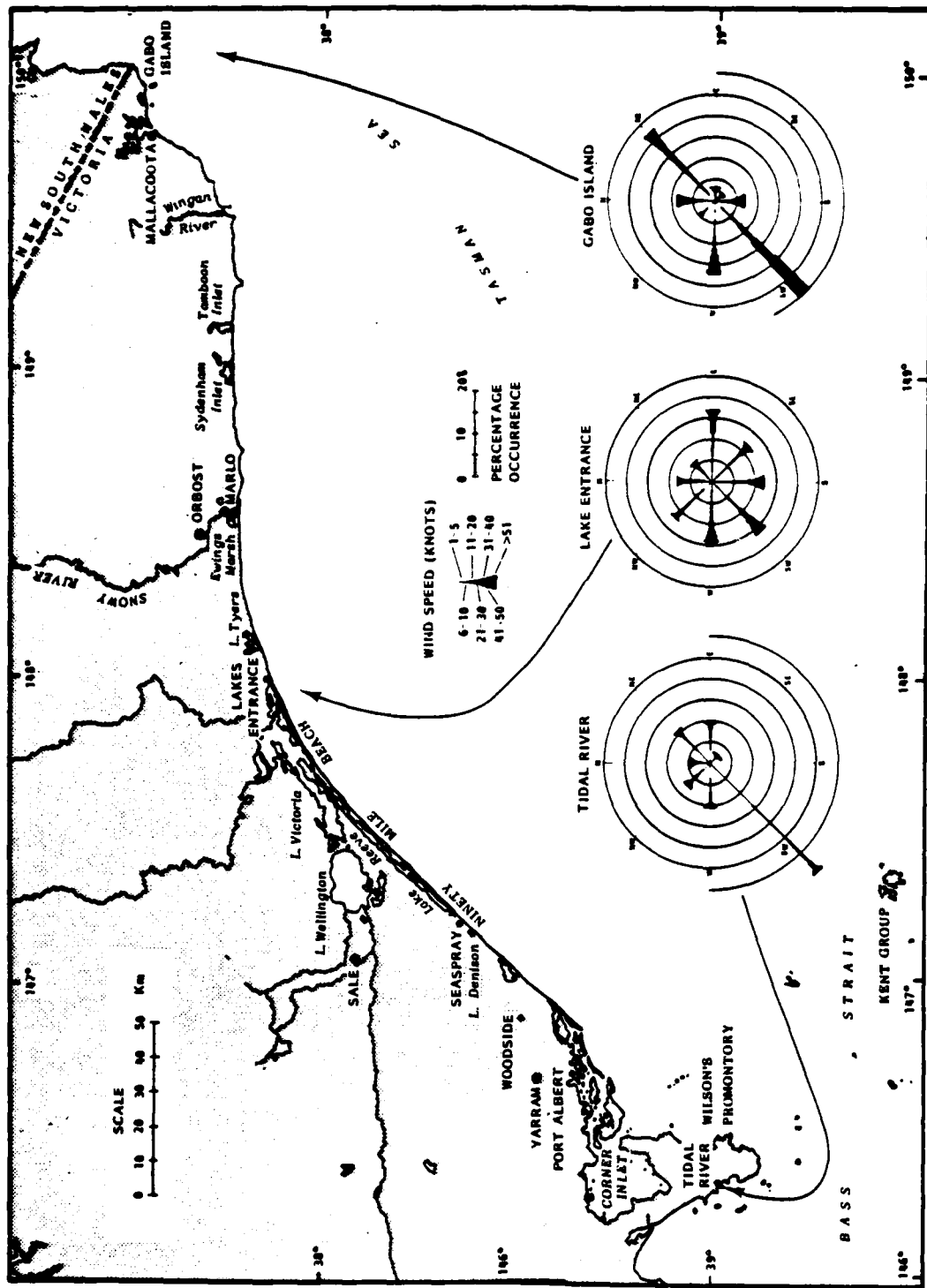
Figure 5. Wind Roses for Tidal River, Lakes Entrance and Gabo Island.

significant gradient in wind velocity between Tidal River and Gabo Island. At Tidal River, which is partially sheltered the "modal" wind speed is between 1-5 km hr^{-1} and only 12% of the winds exceed 21 km hr^{-1}, at the more exposed locality of Lakes Entrance, the "modal" wind speed is about 10 km hr^{-1} and speeds of 21 km hr^{-1} are exceeded for 20% of the time. The strongest winds prevail at Gabo Island which is fully exposed: there the modal speed is 20 km hr^{-1} which is exceeded for 50% of the time. At all three locations, the strongest winds are associated with westerly gales. The data in Appendix A suggests that diurnal seabreezes also contribute significantly to the wind regime. At all stations there is a significant increase in onshore velocities between 0900 and 1500 hours.

Wave Climate

The coastal wave regime of the region is controlled by four factors. The first is that the prevailing westerlies blow generally offshore to the south of Lakes Entrance and alongshore to the east whereas the southwesterly winds produce obliquely-incident waves. Second, fetch lengths from the west and south increase eastward. Third, Wilsons Promontory and offshore islands north of Tasmania partially, but not wholly reduce the westerly and southwesterly swell reaching eastern Bass Strait from generation centres to the west and southwest in the Southern Ocean. Finally, the wide, low-gradient continental shelf fronting the coast reduces the heights of the larger waves before they reach the surf zone. This effect is discussed further in the next section. Overall, the wave climate is thus strongly

influenced by locally generated wind waves related to the passage
of cyclones and gales. Accordingly, deep water wave conditions are
subject to appreciable and rapid temporal variations.

Although deepwater wave conditions have been recorded from
offshore petroleum platforms for several years, those data are
proprietary and not publicly available. We have used some of
these data from the period of our experiments (with permission from
Esso Australia) elsewhere in the report; however we do not have
access to records of sufficient length to describe the long-term
wave climate. Hence, we base our description here on two sources:
(1) hindcasted wave statistics for western Bass Strait for 1951-
1965 (Spillane et al 1972); and (2) visual observation data from
the Gabo Island lighthouse. Summaries of these data can be found
in Appendix A. Unfortunately, both sets of data must be considered
suspect, at least quantitatively.

Figure 6a shows the average annual distribution, by direction,
of energy flux as computed from the hindcasted wave statistics for
western Bass Strait (Spillane 1972). Figure 6b shows the percentage
of occurrence of waves arriving from different directions at Gabo
Island. The western Bass Strait data suggests that the dominant
energy flux arrives from the southwest. However, the Gabo Island
data indicate that southerly waves dominate, at least in terms of
frequency of occurrence.

Figure 7 indicates the probability of exceedance of wave heights
based on data from both sources. It is worthy of note that the
hindcasted data from western Bass Strait and the sea state data from
Gabo Island show reasonable agreement. Swell height data from
Gabo Island (which are suspect owing to the difficulty of obtaining

(a)

AVERAGE ANNUAL ENERGY FLUX (Kilowatts per metre)

7·0 6·0 5·0 4·0 3·0 2·0 1·0 0·5   0·5 1·0 2·0 3·0 4·0 5·0

1·99 Kw m⁻¹

0·24 Kw m⁻¹

0·55 Kw m⁻¹

0·70 Kw m⁻¹

6·96 Kw m⁻¹

MODAL WAVE   H = 3·0m, T = 8·5 sec, from SW
AVERAGE (rms) WAVE   H = 1·6m, T = 8·5 sec

DEEPWATER WAVES
HINDCASTING
BASED ON 1951-1965

(b)

GABO ISLAND
DIRECTION OF SWELL
1973 — 1982

N

30 25 20 15 10 5

NE (14%)

E (16%)

SW (17%)

SE (17%)

S (30%)

CALM = 5%
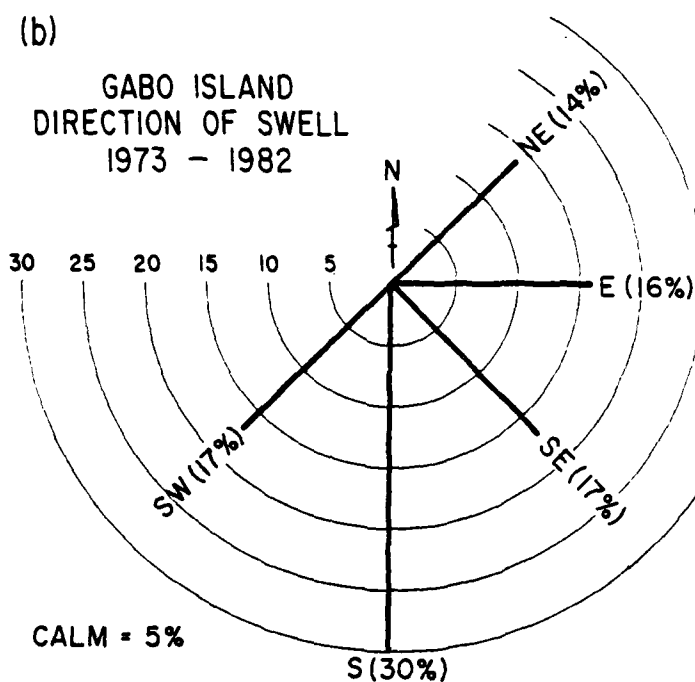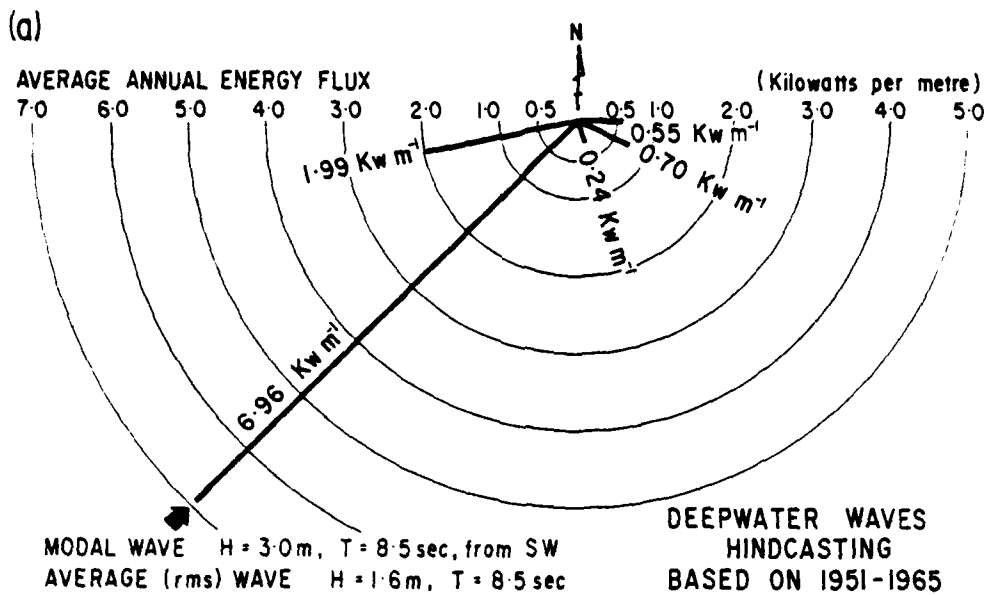
Figure 6.   Deepwater Wave Climate of Bass Strait: (a) directional
distribution of energy flux (watts per metre) based on
hindcast data for western Bass Strait; (b) frequency of
occurrence of waves from different directions based on
lighthouse observations at Gabo Island.
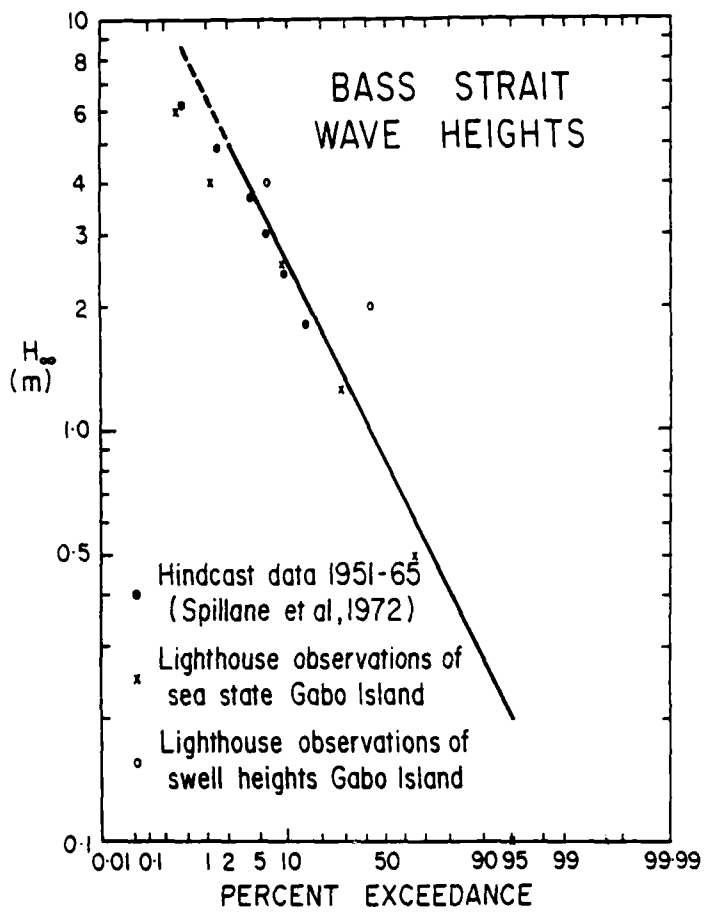
Figure 7. Bass Strait wave climate: average annual exceedance of deepwater wave heights, H_∞. Based on hindcasted data for western Bass Strait and lighthouse observation from Gabo Island.

accurate visual estimates of swell height when seas are superimposed)
reveal an unusually high frequency of occurrence of high swell. If
we take the line on Figure 7 as representative, we can make the
following generalizations about the wave climate: deepwater waves
exceed 1 metre for 40% of the time; they exceed 2 metres for 20%
of the time; they exceed 3 metres for 4% of the time; and they
exceed 5 metres for nearly 2% of the time. From the western Bass
Strait data (Spillane et al 1972), we estimate the modal wave
(defined as the set of conditions for which the product of energy
flux and frequency of occurrence is at a maximum) to be a 3 metre,
8.5 second southwesterly wave. The "average" (root-mean-square)
wave conditions are 1.6 m, 8.5 seconds from the data of Spillane
et al (1972) and roughly 1.5 m, 10 seconds from the Gabo Island
lighthouse data. The "storminess" of the Bass Strait environment
is reflected in the hindcasting statistics which indicate that the
average interval separating the occurrence of waves of 2 metres or
more in height is a little less than 3 days.

Tides

The tides in eastern Bass Strait are semidiurnal with a moderate
diurnal inequality. The M_2 tide is strongly dominant and the S_2
constituent is low in amplitude so that neap-to-spring variations
are modest. The Australian Tide Tables indicate mean spring tide
ranges of 1.0 m at Gabo Island and 2.1 m in the Kent Island Group
southeast of Wilsons Promontory. The approximate mean spring range
at Lakes Entrance is only 0.9 m; however, this estimate is based
on a gaging station located inside the entrance and is thus likely
to be an underestimate of the "open coast" tides.

METHODS

This report is based largely on a set of experiments carried out at Eastern Beach, near Lakes Entrance (Fig.2) over a relatively short period from 4 May through 16 May, 1981, supplemented by an additional set of surveys made in December 1981. Despite the limited duration, the main experiments were conducted during one of the stormiest months of the year and included measurements obtained during two gales as well as during intervening calm periods. The data should thus be reasonably representative of the modal conditions.

Surveys of the beach and surf zone were carried out using a conventional theodolite and a surveying level. A specially designed staff permitted the staff handler to operate in the surf zone to water depths of about 4 metres. Surveys were extended seaward of the surf zone using a Raytheon Model DE719 surveying echo sounder on a 7 metre workboat. Horizontal positions for bathymetric surveys were determined by theodolite angles from shore. At the main Eastern Beach experiment site a survey grid was established consisting of six profiles spaced at intervals of 50 metres alongshore. These lines were surveyed daily over the experiment period. Nearshore sediment samples were obtained by divers and by means of a dredge from the survey boat. Ripple dimensions on the nearshore bed were measured directly by divers.

Benthic currents seaward of the surf zone were recorded from depths of 10 metres and 20 metres using a pair of InterOcean Model 195 m recording electromagnetic current meters. These instruments

employ Marsh McBirney two-component electromagnetic current sensors with a range of 0-3 m sec^{-1} and a precision of ± 2 cm sec^{-1}. They may be programmed for different sampling intervals, burst durations and intervals between bursts. In this case, we used a sampling interval (Δt) of 2 seconds, a burst duration of 15 minutes, and an interval of 1 hour between the start of each burst. The instruments were mounted on tripods weighing 220 kilogrammes with sensors situated at elevations of 1 metre above the bed. Figure 8 shows one of these instruments mounted on its tripod. Data were recorded on magnetic tape cassettes and subsequently read into files for analysis on the University of Sydney's Cyber computer.

Within and near the surf zone, strain-gage-type pressure transducers with 0-5 bar range absolute were used to measure pressure which was converted to water surface elevation, η. Horizontal surf zone currents were measured by means of small, low inertia bidirectional ducted-impellor flow meters (Bradshaw et al 1978; Sonu et al 1974). Flow meters were mounted orthogonally to obtain time series of u and v. Pressure transducers and flow meters were mounted together on masts with 50 kilogramme flat bases in various arrays, an example of which is shown in Figure 9. Several such installations were deployed simultaneously. Signals from the sensors were transmitted by cables to a mobile van housing a chart recorder, multiplexing digital tape recording facilities and mini-computers. The field monitoring system has been described by Bradshaw et al (1978). Sensors were sampled simultaneously at intervals (Δt) of 1-1.5 seconds. Data were corrected for frequency response characteristics (Nielsen and Cowell, 1981).

Data tapes from nearshore and surf zone instruments were
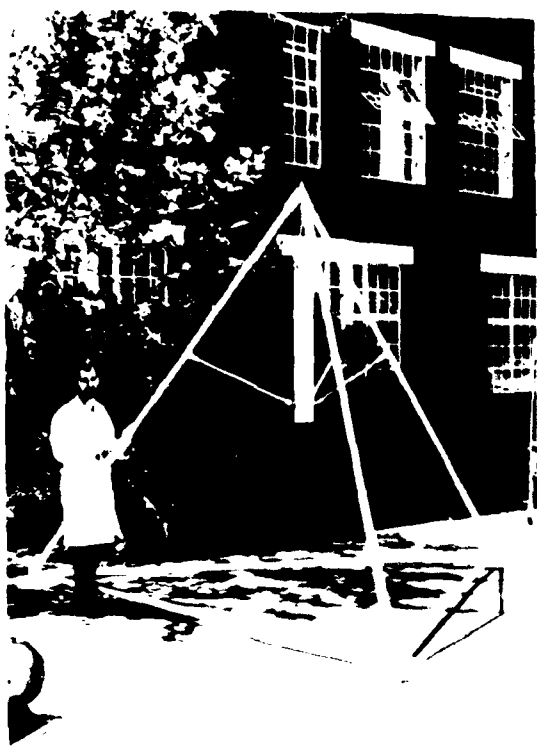
Figure 8.   Inter Ocean Model 195M recording electromagnetic current
             meter attached to weighted tripod for measuring nearshore
             benthic currents.

transferred into files for analysis on the University of Sydney's Cyber computing system. Analyses included computing instantaneous and time-average vector resultants and performing spectral and cross-spectral analyses to determine the magnitudes of currents and surface oscillations corresponding to different frequencies and forcings. A fast Fourier transform was used to compute spectral estimates. A phase relationship of 90° ($\pi/2$) between water surface elevation, η, and shore-normal current, u, at any given frequency was used as a test for the existence of surf zone standing waves at that frequency. Current and surface oscillation amplitudes related to different frequency bands were determined from the total variance within that band.

Vertical profiles of suspended sediment concentration in the surfzone were measured using the suction sediment sampler developed by Nielsen (Nielsen and Green in press). This device, shown in Figure 10 has been extensively field tested and proven to be the most effective system for obtaining concentration profiles presently in use. Water and sediment enters by way of thin metal intake tubes which minimize flow disturbance and enable concentrations to be measured to within 1 centimetre of the bed. This includes much of what has traditionally been regarded as bed load. Intakes were situated at seven different levels with a maximum distance of 0.55 m between top and bottom intakes. Filling of 2.2 litre glass jars via the intake tubes takes place over a time of about 3.5 minutes. The filling and suction through the intakes is driven simply by the pressure difference between the tops of the jars and an elevated air outlet from the jars. The distance from intakes to the jars is 1.25 m and the jars are always oriented so as to minimize flow disturbances.
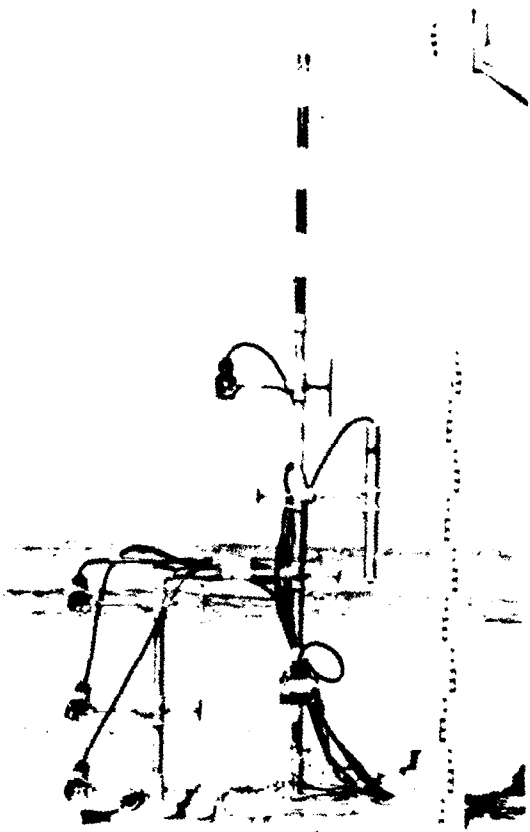
Figure 9.   Bidirectional ducted flow meters and pressure transducer.
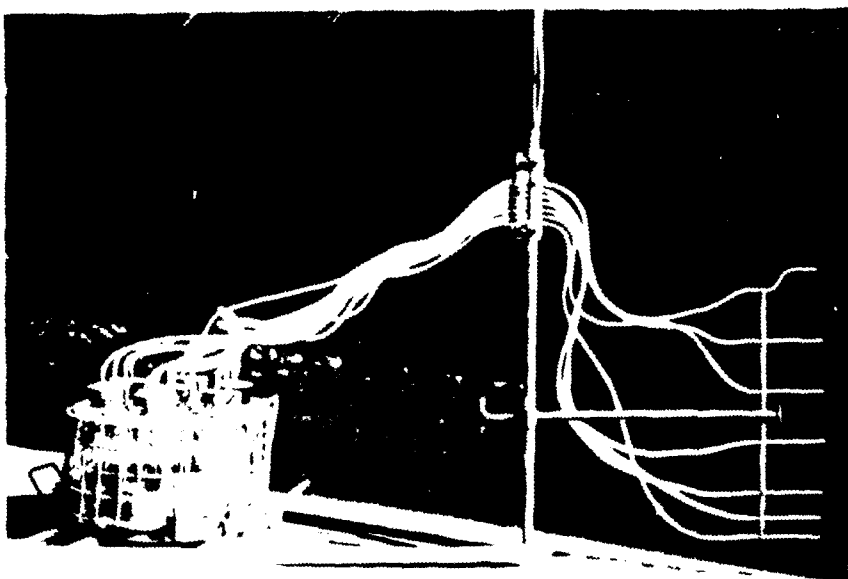
Figure 10.   Suspended sediment sampler.

NEARSHORE PROCESSES

The nearshore zone, defined here as the region of the inner continental shelf over which shoaling unbroken waves agitate sediment, is the fundamental 'valve' linking shelf and surf zone processes, (Fig.1). The nearbottom hydrodynamic processes of this region determine the rates and directions of nearshore sediment transport while the configuration of the nearshore profile itself determines the extent of shallow water wave modifications and, hence, influences the amount of energy which reaches the surf zone. We will confine our attention, in this discussion, to the region between the surf zone and the 20 metre depth contour.

Characteristics of the nearshore profile

Figure 11 shows the nearshore profile fronting Eastern Beach. Several important features are evident: (1) overall, the profile exhibits a pronounced concave-upward shape, typical of wave-built "equilibrium" profiles (e.g. Dean 1977). (2) The innermost 200 metres of the profile consists of a shallow plateau 2 to 3 metres deep which is surmounted by the surf zone and its associated bar and trough features. (3) Seaward of the inshore plateau, the bed descends steeply to a depth of about 15 metres but with gradients decreasing progressively seaward yielding an exponential profile shape. (4) Seaward of a rather sharp break in slope at 15 metres ($x \cong 600m$), the profile flattens onto a near-horizontal outer nearshore "plain"; the 20 metre depth contour lies nearly 3 kilometres seaward of the 15 metre contour.

Dean (1977), among others, has shown that the wave-dominated nearshore equilibrium profile can be expressed in the general form

$$h = a\ x^m \qquad (1)$$

where h is local depth, x is distance seaward and a and m are empirical constants. The exponent, m, has been theoretically evaluated by Dean (1977) in terms of two alternative equilibrium conditions: (1) equal energy dissipation per unit volume of water, and (2) equal energy dissipation per unit surface area. For model (1) the expected value is m = 0.67 and for model (2) the expected value is m = 0.4. The coefficient, a, depends on local environmental conditions and particularly on sediment fall velocity w_s (grain size) and dominant wave period, T. Although these models are theoretically strictly applicable to surf zone profiles, Dean (1977) has shown that a set of 502 actual nearshore profiles from North America exhibit close fit to the model

$$h = a\ x^{0.67} \qquad (2)$$

We compared the nearshore profile off Eastern Beach to both of Dean's models (1) and (2) above. The inner part of the profile (h ≤ 15 metres) shows good fit to either

$$h = 0.287\ x^{0.67} \qquad (3)$$

or

$$h = 1.233\ x^{0.4} \qquad (4)$$
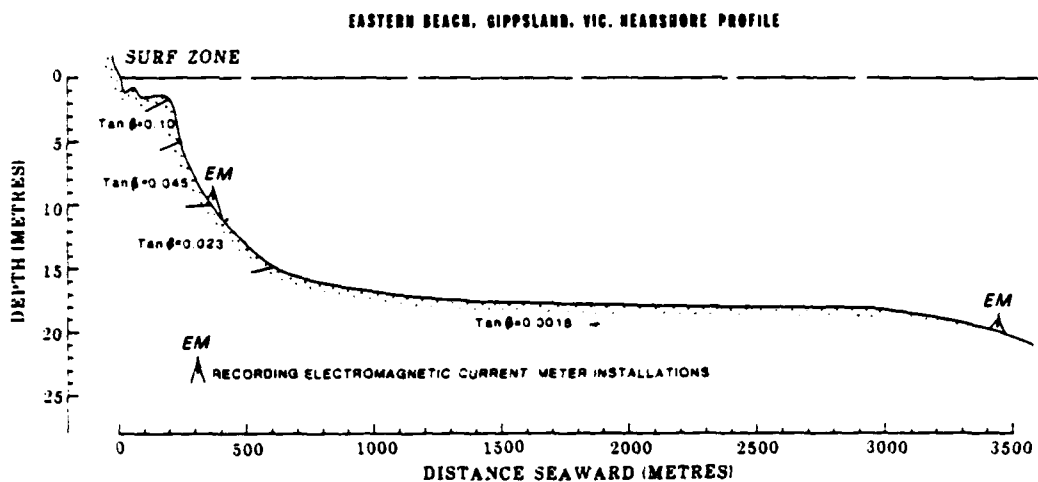
Figure 11. The nearshore profile off Eastern Beach based on surveys in May, 1981. Locations of current meter installations are indicated.
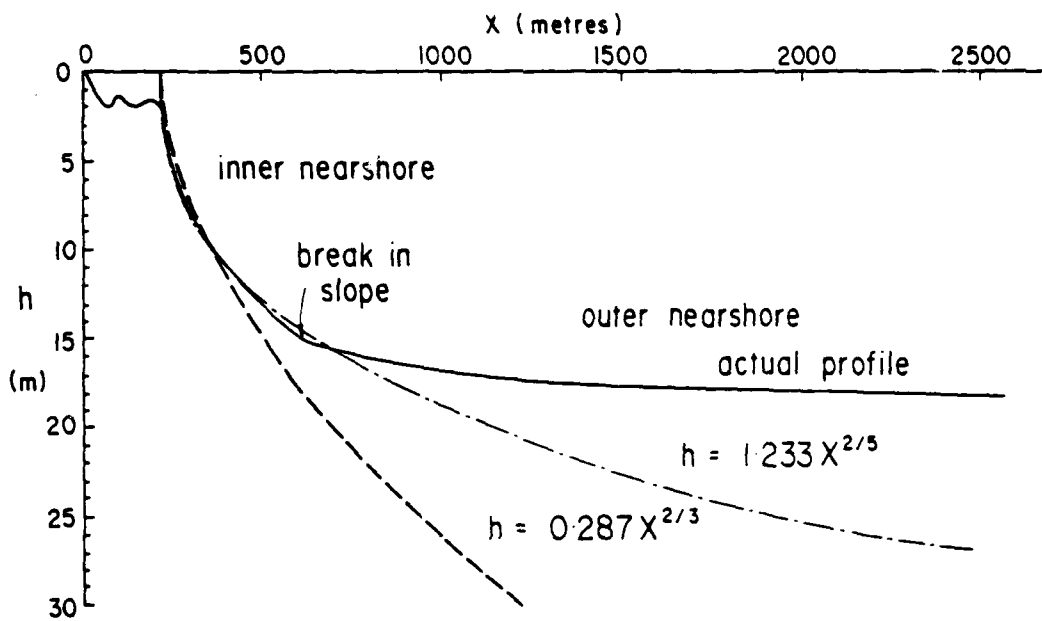
Figure 12. Comparison of the observed nearshore profile with two "equilibrium" forms (Dean, 1977). Note the abrupt divergence at h = 15m.

but the latter model (equation 4) gives the best fit. Seaward of
h = 15 metres the observed profile diverges appreciably from both
forms as illustrated by Figure 12. This suggests that the outer
nearshore plain is morphodynamically discontinuous from the inner
nearshore profile. It appears that the outer nearshore plain
is a planation surface composed of pre-Holocene sediments, the upper
layers of which are highly active today but are not in active shore-
normal exchange with the inner nearshore.

The distribution of surface sediment characteristics across the
nearshore profile (Table 1) also reveals an abrupt and dramatic change
in sediment size just seaward of the 15 metre contour and supports the
suggestion that the flat outer segment of the nearshore zone is morpho-
dynamically distinct from the inner nearshore. From the 10 metre con-
tour shoreward, the mean grain size remains roughly constant at about
0.3-0.4mm (1.7-1.3∅). Seaward of 15 metres depth grain size increases
appreciably to over 0.65mm at 17.5 metres and over 0.8 mm at 20 metres
(Table 1). The material seaward of 15 metres is also heavily iron
stained and numerous whole shells and cobbles are scattered over the
bed.

Diver observations at 20 metres and at 10 metres revealed large,
symmetrical wave-generated ripples at both positions and on two
separate occasions. The ripples had heights of 10 centimetres, lengths
(between crests) of 60 centimetres and were very sharp crested. The
coarsest material (cobbles and whole shells) accumulated in ripple
troughs. The large ripples and coarse sediment of the outer nearshore
plain in combination produced a very rough surface.

TABLE 1

NEARSHORE SAND SIZES

Sample	Depth	Mean diameter (total sample)		Mean diameter (sand fraction only)		Percent $CaCO_3$	Comments
	metres	$\emptyset$	mm	$\emptyset$	mm		
0	0	1.13	0.45	1.13	0.45	5.0	Beach face
1	2	1.39	0.38	1.43	0.37	3.0	Surf zone
2	3	1.43	0.37	1.48	0.36	2.14	Rip bay
3	3	1.67	0.31	1.72	0.30	2.24	Outer "Plateau"
4	10	1.87	0.27	1.86	0.27	5.66	Cobbles
5	10	1.38	0.39	1.36	0.39	3.50	present
6	10	1.34	0.40	1.34	0.40	4.16	with some
7	15	0.84	0.56	1.13	0.45	6.5	whole shells
8	17.5	-0.16	1.11	0.63	0.65	5.56	Cobbles present with whole shells
9	20	0.02	0.98	0.23	0.85	6.36	"
10	20	0.28	0.82	0.32	0.80	4.4	"
11	20	0.05	0.97	0.36	0.78	6.94	"

Observed nearshore currents

The duration of our field observations at 20 metres and at 10 metres was limited by instrument malfunction. The truncation of record length at the inner (10 m) station (and possibly the outer station as well) appears to have been caused by the passage of a strong gale. In any event, we obtained records of five 15-minute bursts (5 hours) from 20 metres and 35 bursts (35 hours) from 10 metres and the data from these records are good. From spectral and statistical analyses of each burst we can draw some worthwhile - albeit tentative - inferences about the magnitudes and directions of benthic transports due to tides and waves. The locations of the h = 20 metres and h = 10 metres current meter installations are indicated in Figure 11. In both cases the sensors were located at 1 metre above the bed.

Table 2 summarizes the important current statistics associated with each burst. The corresponding deep water tide level, η_t, as observed from the Kingfish B offshore oil and gas field (Fig. 2) is also indicated. The mean speeds and directions are the time-averaged drifts of each burst. The variance σ_v^2 of speed, V, for each burst has been computed from the instantaneous (2 second intervals) values in a burst. The root - mean-squared speeds V_{rms} were computed from

$$V_{rms} = <V^2>^{\frac{1}{2}} \tag{5}$$

(where the brackets denote time averaging over a burst).

The time-averaged means of the instantaneous speeds cubed $<V^3>$ are also given.

The instantaneous velocities, $\vec{V}$, were segregated into their shore normal, u (positive onshore) and shore parallel, v (positive toward west) components. The corresponding values of $<u>$, u_{rms}, $<u^3>$, $<v>$, v_{rms}, and $<v^3>$ are presented. The values of $<V>$, $<u>$ and $<v>$ reflect the contributions of tidal and wind driven currents while V_{rms}, $<V^3>$, u_{rms}, $<u^3>$, v_{rms}, and $<v^3>$ indicate the magnitudes of oscillatory flows due to incident waves (T = 3 - 30 secs) and infragravity oscillations (T = 30 - 300 secs).

The most prominent features of the net flows $<V>$, $<u>$, $<v>$ were the strong dominance of the shore parallel, $<v>$, components (the ratio $<|v|>/<|u|>$ averaged 2.3 at h = 20m and 3.5 at h = 10m) and the periodic reversals with the phase of the semidiurnal tide. These tendencies are evident from the stick diagram and progressive vector diagram for $\vec{V}$ at h = 10m (Fig. 13) and from the time series plots of $<u>$ and $<v>$ (Fig. 14). From Table 2, currents can be seen

Table 2

Current statistics for 15 minute bursts from h = 20m and h = 10m off Eastern Beach

Time	Burst	tide η+	⟨V⟩ m sec⁻¹	Direction degrees	σ^2_V m²sec⁻²	V_{rms} m sec⁻²	V_{max} m sec⁻¹	⟨v'²⟩ m³sec⁻³	Shore Normal Component (→onshore)			Shore Parallel Component (+ W)		
									⟨u⟩ m sec⁻¹	u_{rms} m sec⁻¹	⟨u'²⟩ m³sec⁻³	⟨v⟩ m sec⁻¹	v_{rms} m sec⁻¹	⟨v'²⟩ m sec⁻³
Outer h=20m 6 May '81														
1300	1	0.2	0.0945	270.85	0.1138	0.00412	0.459	0.00234	+0.025	0.061	+0.000358	+0.078	0.096	+1.00140
1400	2	0.1	0.0433	291.12	0.0638	0.00220	0.247		+0.004	0.047		+0.004	0.043	
1500	3	0.0	0.0620	37.7	0.0771	0.00211	0.247	0.000703	+0.020	0.056	+0.000208	-0.028	0.053	-0.000258
1600	4	-0.1(L)	0.100	48.41	0.1118	0.00251	0.482	0.00199	+0.033	0.065	+0.000341	-0.072	0.091	-0.001271
1700	5	-0.1(L)	0.120	51.59	0.1311	0.00287	0.376	0.00298	+0.036	0.071	+0.000414	-0.092	0.110	-0.00200
Inner h=10m 6 May '81														
1334	1	0.2	0.043	278.59	0.0744	0.00368	0.282	0.000925	+0.0058	0.051	+0.000048	+0.012	0.054	+0.000174
1434	2	0.1	0.0416	95.55	0.0399	0.00315	0.388	0.00082	-0.0043	0.0463	-0.000121	-0.0103	0.052	-0.000207
1534	3	0.0	0.0670	98.75	0.0978	0.00507	0.388	0.001803	-0.012	0.0632	-0.000225	-0.0256	0.075	-0.000349
1634	4	-0.1(L)	0.0745	90.21	0.1001	0.00446	0.353	0.001728	-0.013	0.0652	-0.000273	-0.0434	0.076	-0.000631
1734	5	-0.1(L)	0.0803	98.29	0.1085	0.00532	0.3412	0.002157	-0.019	0.0707	-0.000388	-0.011	0.0823	-0.000701
1834	6	0.1	0.0672	82.59	0.0921	0.00397	0.3647	0.001412	-0.007	0.0611	-0.000188	-0.010	0.069	-0.000498
1934	7	0.3	0.0576	95.05	0.0906	0.00488	0.3647	0.001569	-0.0075	0.0599	-0.000194	-0.018	0.067	-0.000355
2034	8	0.5	0.0414	116.89	0.0715	0.00339	0.3059	0.000852	-0.0119	0.0487	-0.000187	-0.012	0.052	-0.000160
2134	9	0.9	0.0471	142.65	0.0759	0.00353	0.3647	0.000964	-0.0025	0.0630	+0.000081	-0.0009	0.051	+0.000048
2234	10	0.9(H)	0.0485	252.74	0.0786	0.00382	0.3412	0.001055	-0.0000	0.0539	+0.000048	+0.009	0.057	+0.000140
2334	11	0.9	0.0454	246.41	0.0718	0.00309	0.3647	0.000811	-0.00142	0.0492	-0.0000141	+0.012	0.052	+0.000115
7 May '81														
0034	12	0.8	0.0490	241.65	0.0770	0.00353	0.4118	0.000964	-0.0011	0.0520	+0.0000225	+0.006	0.057	+0.000103
0134	13	0.4	0.0476	123.31	0.0794	0.00403	0.3647	0.001148	-0.0065	0.0544	-0.000087	-0.005	0.058	-0.000136
0234	14	0.2	0.0504	113.28	0.0813	0.00407	0.3647	0.001161	-0.009	0.0542	-0.0001482	-0.0104	0.0606	-0.000219
0334	15	-0.1	0.0657	108.81	0.1021	0.00611	0.4471	0.00221	-0.0155	0.0685	-0.000378	-0.0215	0.0757	-0.000176
0434	16	-0.3	0.0692	106.76	0.1031	0.00585	0.4588	0.00216	-0.0185	0.0685	-0.000395	-0.0276	0.077	-0.000529
0534	17	-0.4(L)	0.0579	88.23	0.0661	0.00411	0.3412	0.00126	-0.005	0.0676	-0.000110	-0.0187	0.0644	-0.000204
0634	18		0.0571	106.51	0.0893	0.00471	0.3647	0.00144	-0.008	0.0617	-0.000225	-0.0126	0.0645	-0.000207
0734	19		0.0489	158.41	0.0807	0.00411	0.3647	0.00112	-0.0045	0.0572	-0.0000201	-0.0004	0.0569	+0.0000564
0834	20		0.0529	255.35	0.0605	0.00368	0.2708	0.000997	-0.0004	0.0580	+3.0000384	+0.0114	0.0548	-0.0000907
0934	21		0.0718	272.69	0.0997	0.00477	0.3765	0.00180	+0.0145	0.0712	+0.000421	+0.0405	0.0698	+0.000657
1034	22		0.0945	273.0	0.1222	0.00599	0.4235	0.00307	+0.0222	0.0882	+0.000845	+0.0608	0.0445	+0.000936
1134	23	(H)	0.1107	270.33	0.1408	0.00756	0.4471	0.00453	+0.0193	0.1020	+0.000644	+0.0618	0.0971	+0.001247
1234	24		0.0837	275.47	0.1098	0.00484	0.3412	0.00208	+0.0206	0.0788	+0.000536	+0.050	0.0751	+0.000626
1334	25		0.0562	279.82	0.0859	0.00421	0.5059	0.00144	+0.0106	0.0632	+0.000113	+0.021	0.0581	+0.000108
1434	26		0.0454	134.09	0.0775	0.00395	0.3647	0.00108	-0.005	0.0569	-0.000121	-0.0025	0.0527	-0.0000568
1534	27		0.0667	103.87	0.0857	0.00413	0.3647	0.00125	-0.0169	0.0909	+0.000299	-0.0283	0.0601	-0.000349
1634	28		0.1279	65.6	0.1502	0.00620	0.5059	0.00474	+0.0137	0.0786	+0.000136	-0.1057	0.1279	-0.003125
1734	29	0.0(L)	0.1710	63.95	0.1970	0.00858	0.5177	0.01030	+0.0226	0.0909	+0.00059	-0.1418	0.1699	-0.007049
1834	30	0.0	0.1824	66.84	0.2062	0.00927	0.5294	0.01133	+0.0163	0.1069	+0.0000361	-0.1508	0.1763	-0.007428
1934	31	0.2	0.1112	71.57	0.1382	0.00672	0.3765	0.00401	+0.0021	0.0833	+0.000207	-0.084	0.1103	-0.002183
2034	32	0.4	0.0715	65.46	0.0997	0.00483	0.3294	0.00171	+0.005	0.0726	+0.000127	-0.037	0.0683	-0.0005497
2134	33	0.7	0.0451	110.87	0.0766	0.00384	0.3647	0.00105	-0.0012	0.0631	-0.000126	-0.005	0.043	-0.0000164
2234	34	0.9	0.0655	256.06	0.1052	0.00678	0.4235	0.00252	+0.0003	0.084	+0.000046	+0.007	0.0634	+0.000109
2334	35	0.9(H)	0.0282	277.86	0.0596	0.00276	0.2471	0.000655	+0.004	0.0464	-0.0000037	+0.009	0.0374	+0.000063

HOURS

6/5/81 ─ 1334

─ 0034

7/5/81 ─ 1234

─ 2234

ONSHORE N

17°

INITIAL TIME : 1334 6/5/81

0·10 m/s
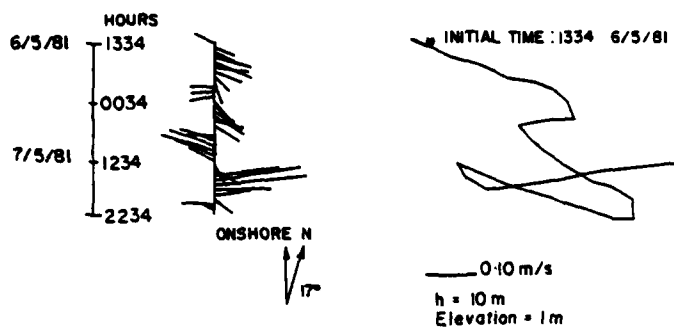
h = 10 m
Elevation = 1 m

Figure 13.   Vector "stick" diagram and progressive vector diagram
of burst-averaged benthic currents at h = 10m.   Tidal
reversals are apparent.

m/s

0·20

0·15

0·10

0·05

0

-0·05

-0·10

-0·15

-0·20

Speed

<u>

<v>

N = 35
BURST MEAN
VALUES

h = 10m
Elevation = 1m

1334   0034   1234   2334   HRS
6TH MAY 1981   7TH   MAY 1981

(a)

ONSHORE N

17°

─ 10%

h =   10m
Elevation = 1m

(b)
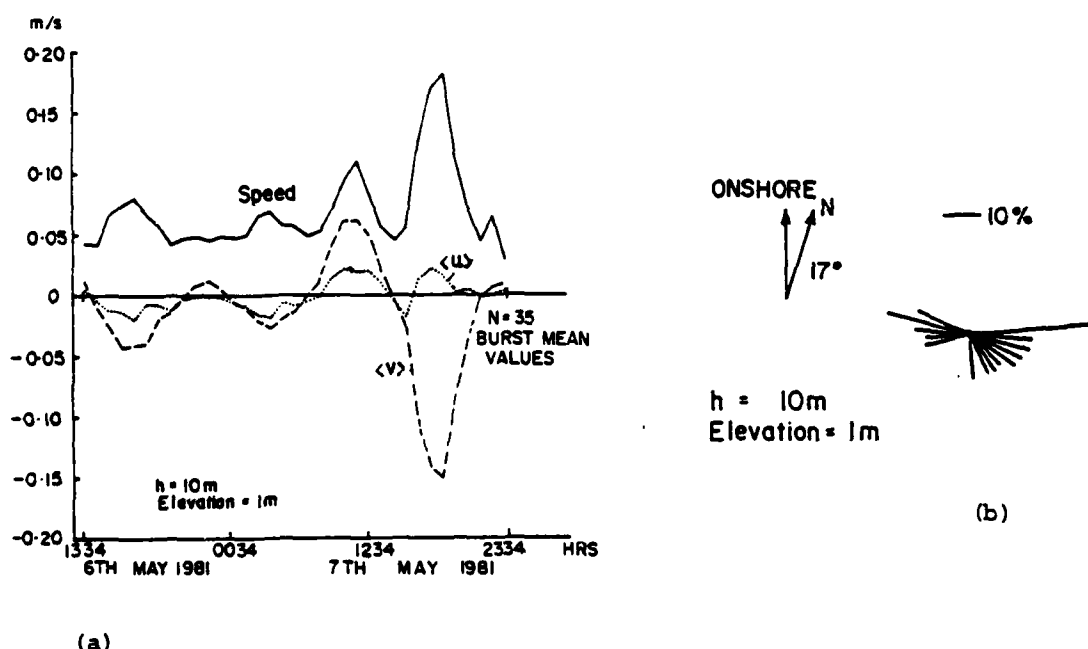
Figure 14.   (a) Time series plots of burst-averaged absolute current
speed, and the shore-normal, <u>, and shore-parallel,<v>,
components of benthic currents at h = 10m; (b) current rose.

to be roughly in phase with tidal elevation, η_t. Consistent with the model of a long wave, progressive along shore from east to west (that is, from the Tasman Sea into Bass Strait; Easton, 1970) currents set roughly toward the west at high tide and roughly toward the east at low tide. The rotational change in direction involves brief periods of relatively weak onshore-offshore transport.

For the frictionless case, the tidal current speed V is given by linear long wave theory

$$V = a \left(\frac{g}{h}\right)^{\frac{1}{2}} \cos \omega t \tag{6}$$

where a is amplitude, g is acceleration of gravity, ω is radian frequency ($2\pi/T$, T is period - in this case 12.42 hours) and t is time. For the tidal amplitudes of 0.5m - 0.65m which prevailed at the time of the observations, the frictionless velocity maxima would have been approximately 0.45m sec^{-1} at h = 20 m and 0.64 m sec^{-1} at h = 10m. However, one expects rather thick (on order of 10 m) turbulent boundary layers for tidal currents (e.g. Komar, 1976) and since the currents were observed at 1 metre above the bed in the lower part of the boundary layer, considerable frictional retardation is expected. It is thus understandable that observed currents were slower than the frictionless model predicts. In addition to the bottom boundary layer it also appears that a fairly wide lateral nearshore boundary layer exists to impede tidal currents with increasing proximity to the surf zone. This is suggested by the fact that during the five hour period that the 20 m current meter was operational, mean current speeds were about 25 percent weaker at 10 m than at 20 m (Table 2). A similar shoreward retardation of longshore tidal currents is described from a macrotidal environment by Wright et. al. (in press).

An examination of Figures 13 and 14 and Table 2 reveals that the easterly-setting currents associated with the low tide phase are consistently stronger than the westerly flows which prevail at high tide. The dominance of easterly flows is particularly obvious from the current rose shown in Figure 14b and the progressive vector diagram shown in Figure 13. The apparent asymmetry of tidal currents and the resultant net west-to-east transport probably reflects, at least in part, the regional circulation and wind-driven transport (see discussion in Fandry, 1982). The pronounced increase in the low-tide easterly flows and corresponding decrease in high-tide westerly flows evident in the last 10 bursts from h = 10 m (1434 hrs - 2334 hrs on 7 May; Table 2, Figs. 13 and 14) were related to southwesterly winds which were intensifying over this period. Since westerly and southwesterly winds are dominant for the region, we may infer that the observed net currents are typical, at least in terms of direction, of those which prevail over most of the year.

It is apparent, from the V_{rms} and maximum speed values shown in Table 2 that the instantaneous velocities within a burst, reflecting the contributions of wave and infragravity oscillations, dominate over the burst-averaged speeds and hence probably play the dominant roles in agitating nearshore sediments. Stick diagrams of instantaneous velocities for a typical pair of bursts and time series plots of the associated instantaneous u and v components at h = 20 m and h = 10 m are shown in Figure 15a-c. Histograms indicating the frequency of occurrence of different speed classes within bursts are shown in Figure 16a and b and corresponding power spectra are shown in Figure 17 a and b. The effects of the waves, causing bidirectional current oscillations, are readily apparent from Figure 15 as the spectra (Fig. 17) indicate, the dominant energy is in the swell wave band (0.07 - 0.1 hz). Our observations as well as routine observations
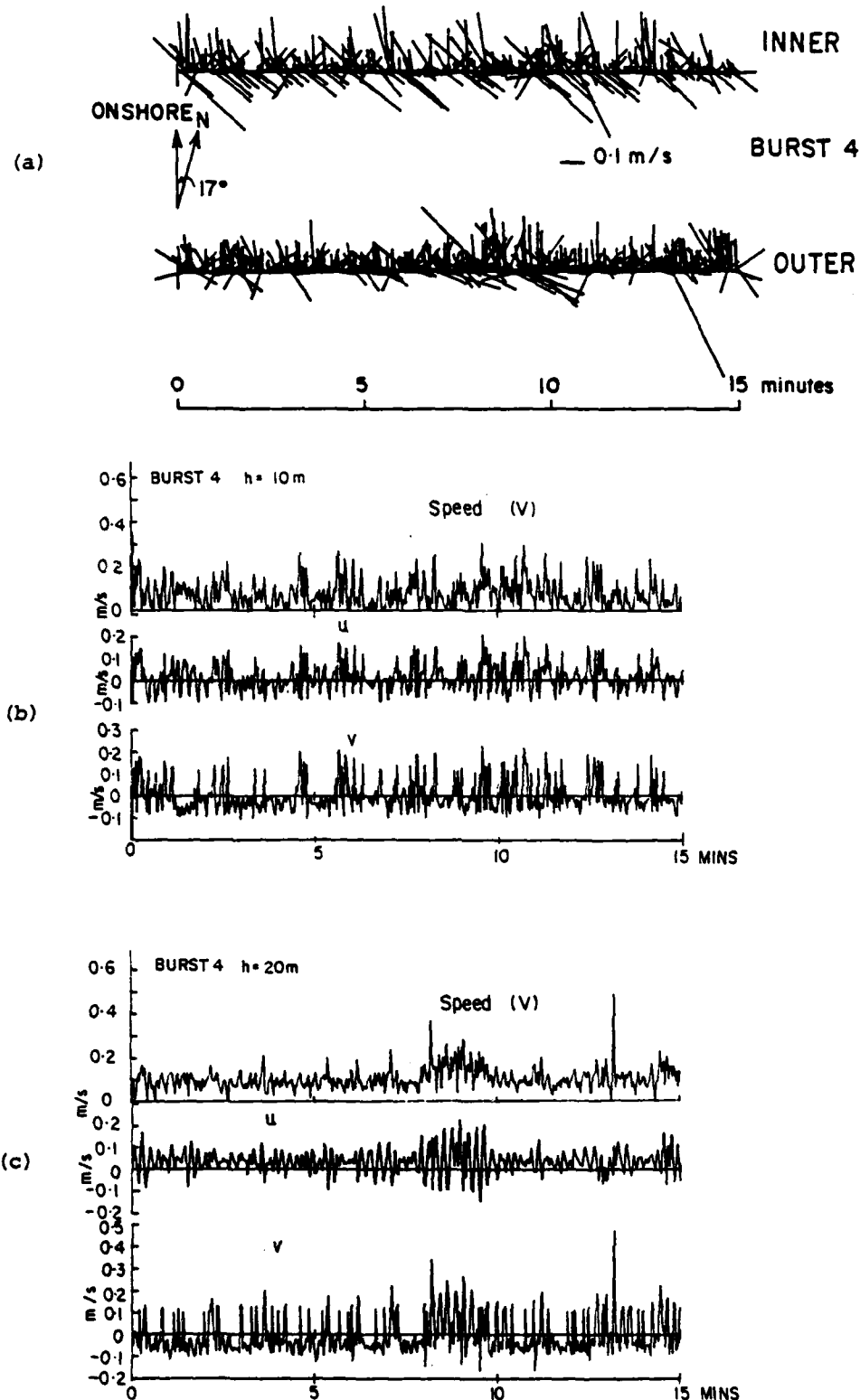
Figure 15. Instantaneous benthic currents within a 15 minute burst:
(a) instantaneous vectors at inner (h= 10m) and outer
(h = 20m) stations (b) and (c) time series of speed, u,
and v at h = 10m and h = 20m.
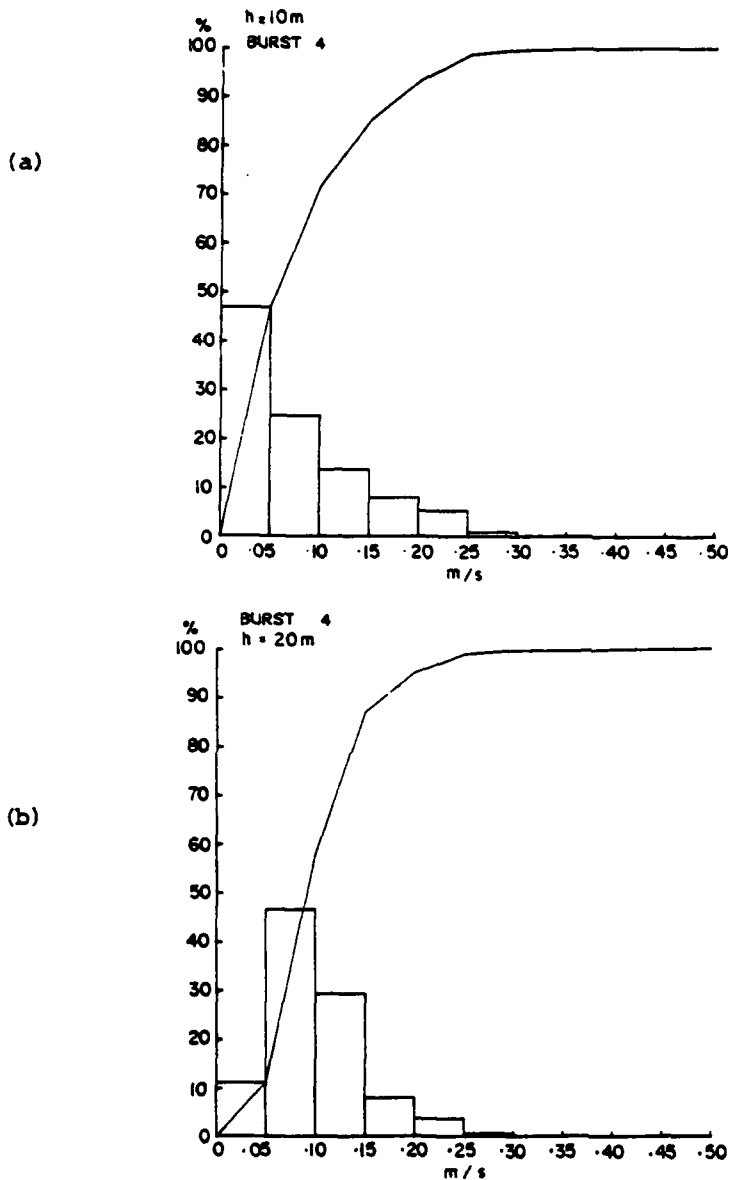
Figure 16. Frequency distributions of instantaneous benthic current speeds, burst 4 (a) h = 10m (b) h = 20m.
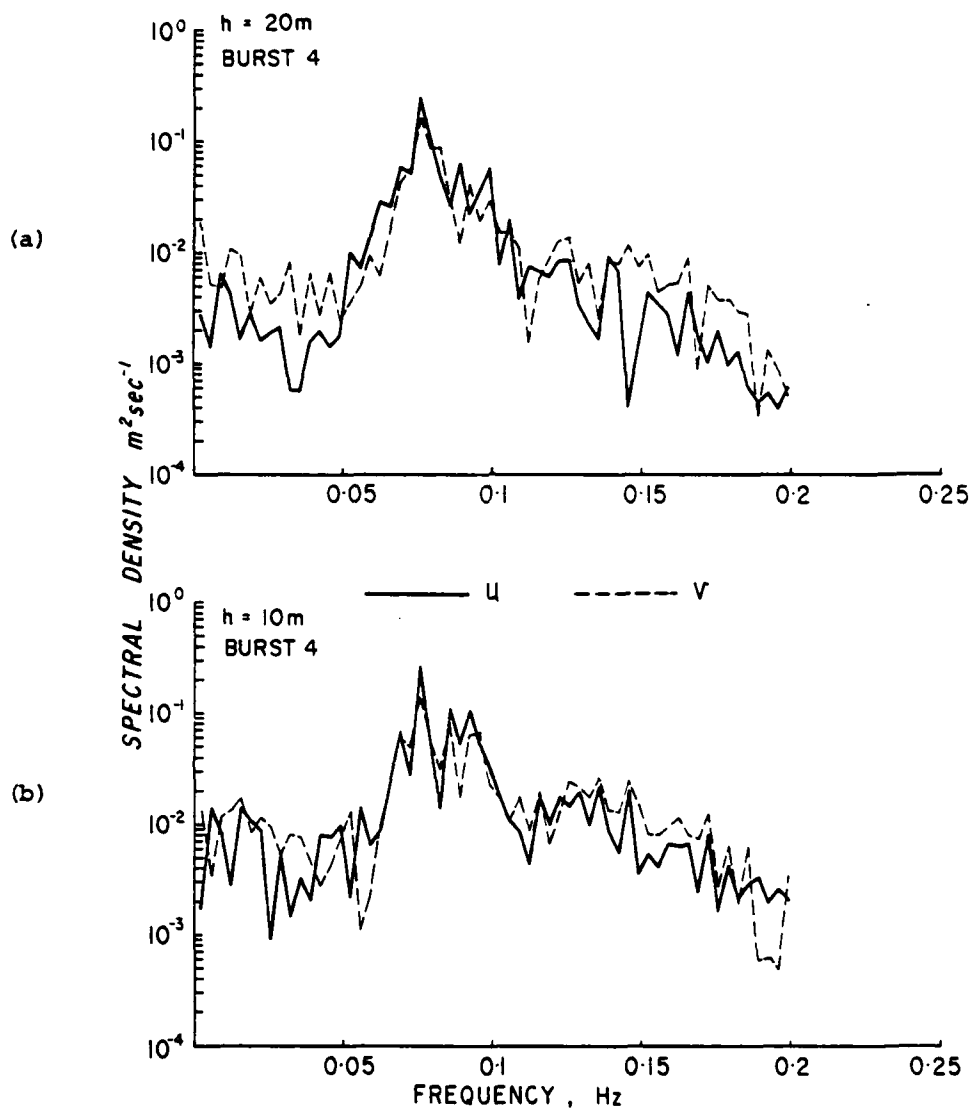
Figure 17.   Power spectra of u and v computed from time series
from burst 4 (12 degrees of freedom) (a) h = 20m
(b) h = 10m.

by the Victoria Department of Public Works at Lakes Entrance indicated
that the dominant swell during the period the currents were measured
arrived at roughly 45^0 to the trend of the coast. Hence both u and
v components are significant. However, the interaction of the oblique
wave oscillations with shore parallel net tidal currents, apparently
has the effect of causing the forward (wave crests) portion of the
orbital excursion to be deflected more onshore while the reverse flows
(wave troughs) are deflected more alongshore. This effect is con-
spicuous in Figure 15a.

To illustrate the effects of southwesterly gales on near-bottom
oscillatory currents, it is interesting to compare the results from
burst 26, recorded shortly before the passage of a gale with the re-
sults from burst 30, obtained after the gale had become fully estab-
lished. Figure 18 a-c shows the stick diagrams and associated u and
v time series from the two bursts at h = 10m; Figure 19 a and b shows
the corresponding frequency histograms of speeds and Figure 20 a and
b shows the comparative power spectra. From Figures 18 and 19 an app-
reciable strengthening of oscillatory flows following the onset of the
gale is obvious. Most importantly, the gale apparently produced strength-
ened onshore transport and easterly transport. The spectra show that
the gale caused a substantial broadening of the bandwidth of wave os-
cillations.

From spectral analyses of the instantaneous u and v components
in each burst (e.g. Figs. 17 and 20), it is possible to determine the
dominant periods of the waves as well as the characteristic magnitudes
of the bottom velocities. It is also possible to segregate the in-
fragravity oscillations from the incident waves and to estimate their
corresponding velocity amplitudes.
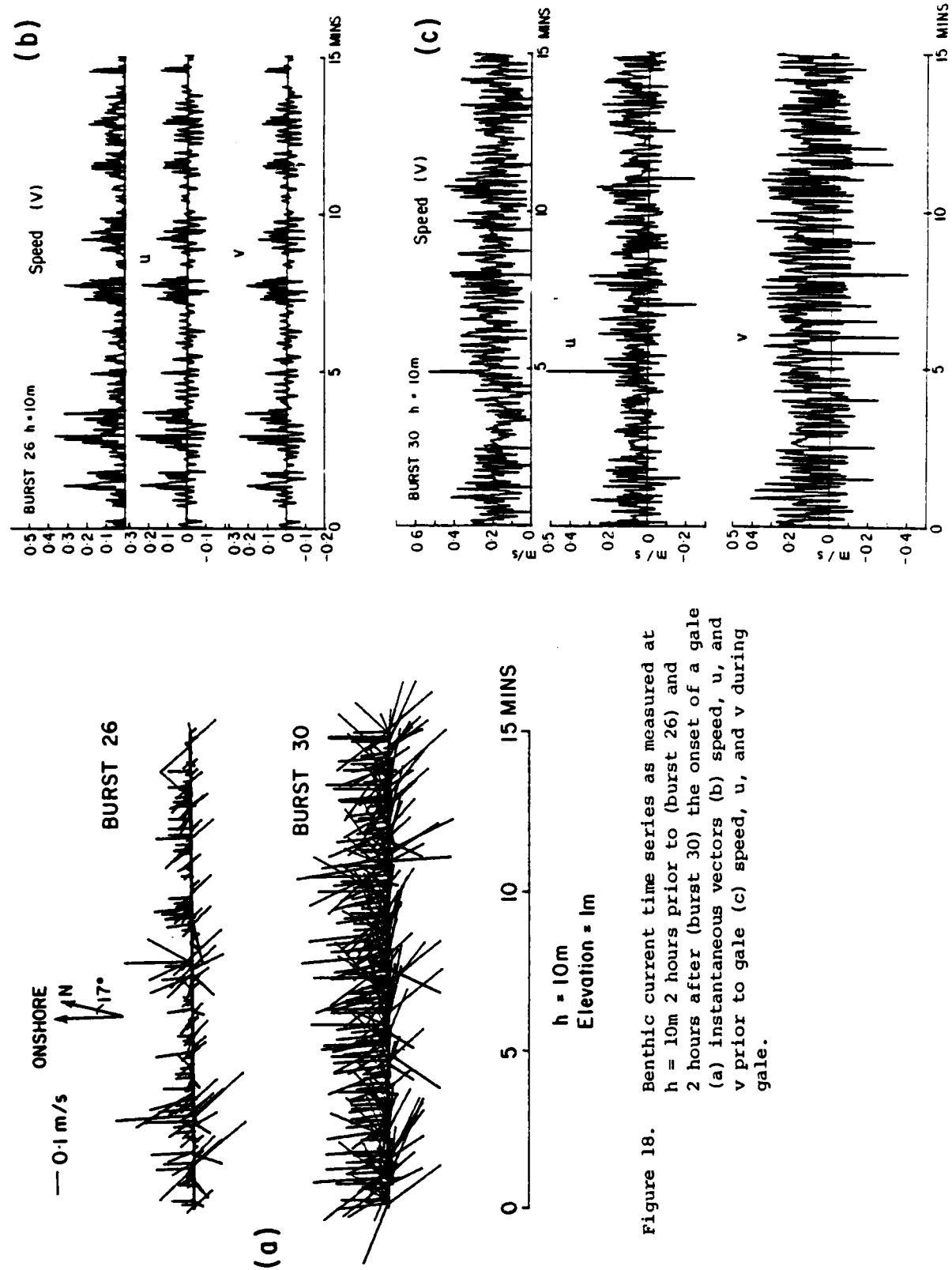
Figure 18.   Benthic current time series as measured at
h = 10m 2 hours prior to (burst 26) and
2 hours after (burst 30) the onset of a gale
(a) instantaneous vectors (b) speed, u, and
v prior to gale (c) speed, u, and v during
gale.
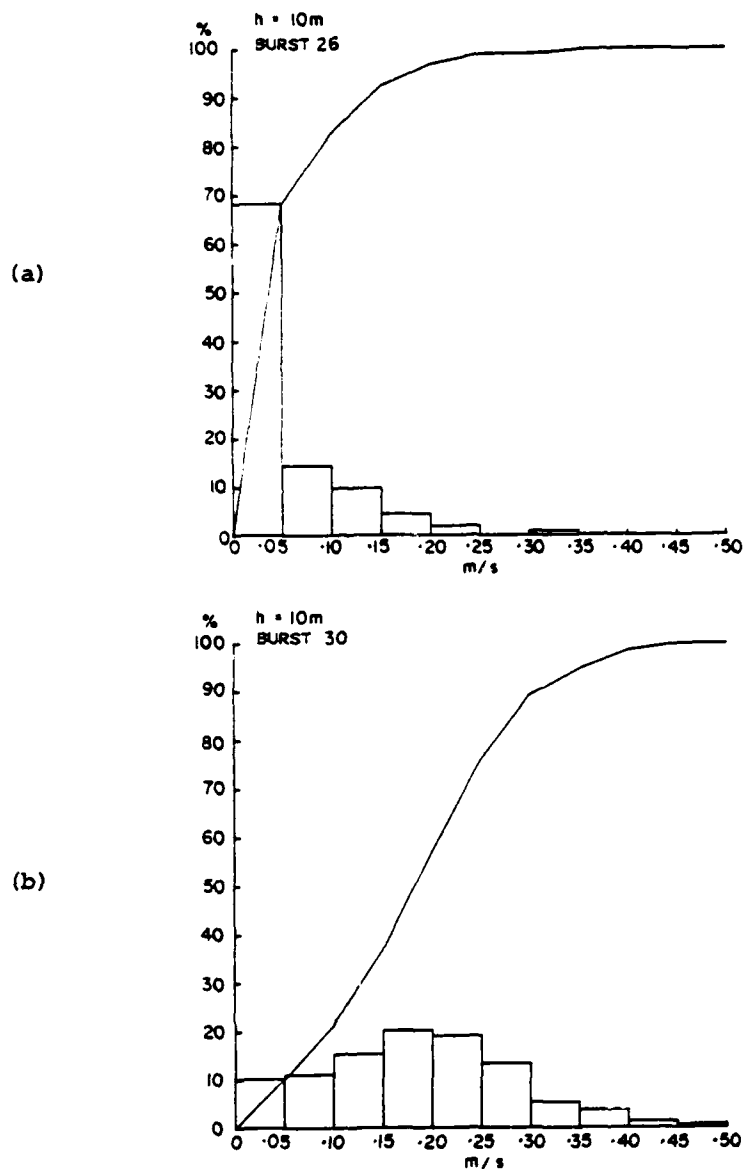
Figure 19.   Frequency distributions of instantaneous benthic
current speeds before (a) and during (b) a gale.
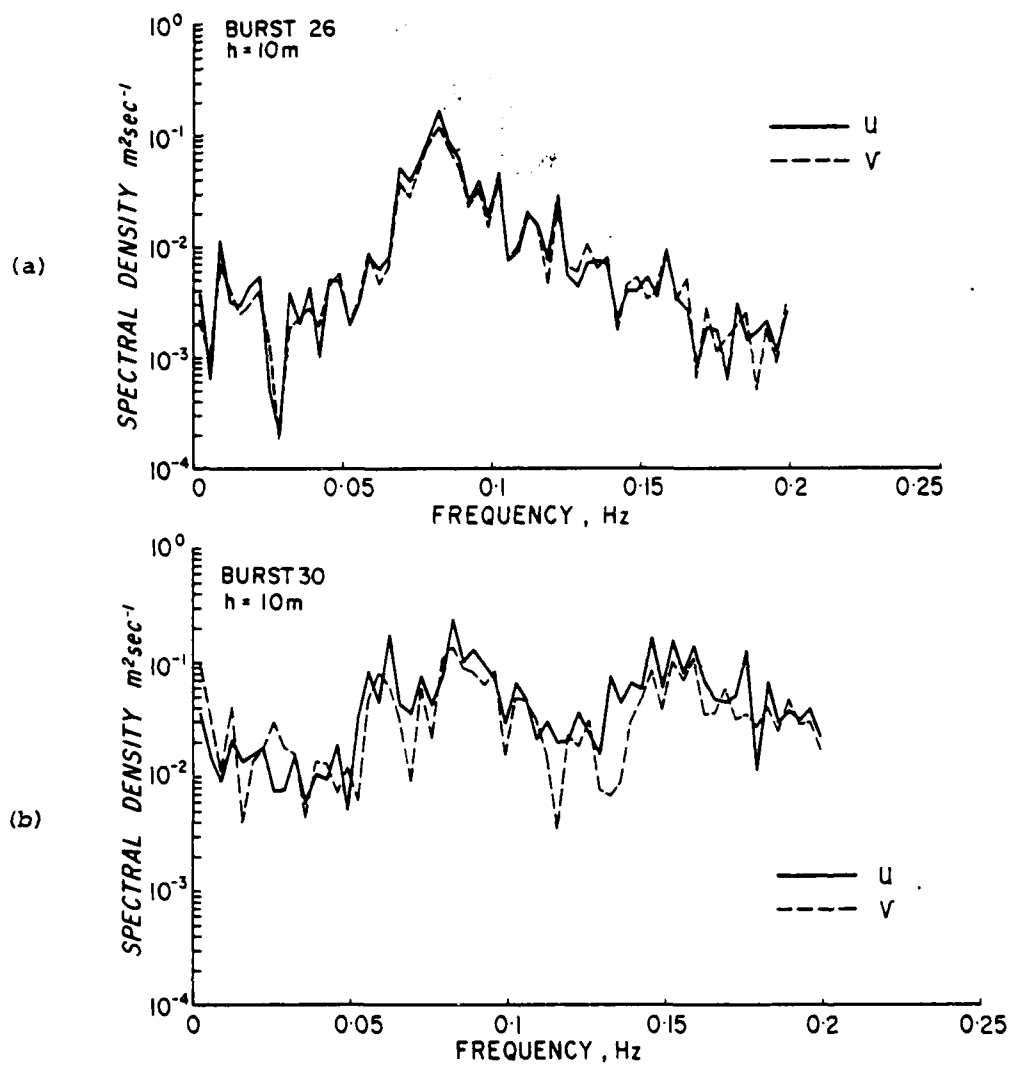
Figure 20.   Power spectra of benthic currents, u and v,
              before (a) and during (b) a gale.

The peak periods, T_p, of the incident waves are the periods at which the spectral density (variance per hertz) maxima occur. The velocity amplitudes u_s and v_s corresponding to the "significant" incident waves are estimated from the total variances σ_u^2 and σ_v^2 of u and v in the frequency band 0.033 - 0.25 hz (T = 4 - 30 secs) from

$$u_s = 2\sigma_u \text{ and } v_s = 2\sigma_v \quad ,$$

(7)

$$(4s < T < 30s)$$

The amplitudes of the infragravity oscillations are similarly estimated from the total variance corresponding to periods greater than 30 seconds. Since the root mean squared values (u_{rms}, v_{rms}) are defined as

$$u_{rms} = \sqrt{2}\,\sigma_u, \; v_{rms} = \sqrt{2}\,\sigma_u \tag{8}$$

u_s and v_s are related to u_{rms} and v_{rms}

by

$$u_s = \sqrt{2}\,u_{rms}, \quad v_s = \sqrt{2}\,v_{rms} \tag{9}$$

The total velocity amplitude, V_s, is thus

$$V_s = (u_s^2 + v_s^2)^{\frac{1}{2}} \tag{10}$$

Knowing the velocity amplitude, V_s, wave period, T_p, and local depth, h, we can estimate the significant wave heights H_s from the observed currents by using linear wave theory

$$H_s = V_s \; T_p \; \sinh \; kh/\pi \tag{11}$$

where k is the wave number $(2\pi/L$, where L is wave length) which is related to the radian frequency ω $(= 2\pi/T_p)$ by the dispersion relation

$$k = \omega^2/g \; \tanh \; kh \tag{12}$$

or for deep water

$$k_\infty = \omega^2/g \tag{13}$$

and kh may be approximated from the explicit expression following Nielsen (in press)

$$kh = \sqrt{k_\infty h} \; [1 + \tfrac{1}{6} k_\infty h + \tfrac{11}{360} (k_\infty h)^2] \tag{14}$$

The energy density, E, corresponding to the waves of height, H_s, is

$$E = \tfrac{1}{16} \rho \; g \; H_s^2 \tag{15}$$

(ρ is water density) and the energy flux, P, is

$$P = E \; C_g \tag{16}$$

where C_g is group velocity which is related to phase speed, $C = \omega/k$, by

$$C_g = C \frac{1}{2} (1 + \frac{2kh}{\sinh 2kh}) \tag{17}$$

Table 3 lists observed T_p, u_s, v_s and V_s values together with estimated H_s and P. Deep water wave conditions, H_∞, T_∞, as recorded from Kingfish B are also presented. The components u_{in}, v_{in}, V_{in} and estimated infragravity height, H_{in} were computed from the variance in the infragravity band (30s < T < 300s). From the last column in Table 3 it can be seen that infragravity oscillations over the nearshore zone were roughly 20% to 30% as high as the incident waves. The column labeled ζ indicates the peakedness of the wave oscillatory currents; it is given by

$$\zeta = \frac{<|v|^3>}{(V_{rms})^3} \tag{18}$$

For a pure sinusoid $\zeta \cong 1.20$; larger values express the irregularity of the waves, due either to shallow water deformation, local wind effects or both. This parameter will be deployed later in the discussion of wave modification.

The information and discussion just presented support the following general conclusions regarding the benthic flow field of the nearshore zone:

(1) The strongest flows are the oscillatory currents related to the shoaling wind waves and swell.

(2) Shore parallel reversing tidal currents are second in importance to the oscillatory wave-induced flows in contributing to the nearshore current regime. Flows toward the east accompanying the low tide phase tend to exceed flows toward the west which accompany the high tide phase.

(3) Over the observation period, there was a net transport toward the east.

Table 3

Wave statistics for each burst from h = 20m and h = 10m; see text for explanation

Burst No.	Time	H_∞ (m)	T_∞ sec	T_p sec	u_s m sec⁻¹	v_s m sec⁻¹	ζ	V_s m sec⁻¹	V_{rms} m sec⁻¹	H_s m	P watts m⁻¹	u_{in} m sec⁻¹	v_{in} m sec⁻¹	V_{in} m sec⁻¹	H_{in} m	$H_{ir/s}$
					Incident waves (T = 3 - 30 sec)							**Infragravity (T = 30 - 300 sec)**				
outer h = 20m 6/5/81																
1	1100	1.4	8.0	13.2	0.108	0.107	1.58	0.152	0.108	0.514	1,798	0.025	0.029	0.0383	0.110	0.21
2	1300	1.7	9.5	12.9	0.091	0.082	1.55	0.122	0.086	0.416	1,167	0.023	0.023	0.0325	0.093	0.22
3	1500	2.0	10.0	13.2	0.103	0.088	1.53	0.135	0.095	0.467	1,421	0.018	0.020	0.0269	0.077	0.17
4	1600	1.7	8.8	13.2	0.111	0.116	1.42	0.153	0.109	0.517	1,819	0.019	0.031	0.0364	0.104	0.20
5	1700	1.9	8.3	13.2	0.119	0.116	1.32	0.166	0.118	0.561	2,142	0.023	0.035	0.0418	0.120	0.21
inner h = 10m																
1	1334	1.4	8.0	13.9	0.098	0.100	2.24	0.140	0.100	0.304	504	0.019	0.025	0.0315	0.064	0.21
2	1434	1.7	9.5	13.9, 12.2	0.088	0.097	2.40	0.131	0.093	0.284	440	0.021	0.026	0.0334	0.067	0.22
6/5/81																
3	1534	2.0	10.0	12.7	0.120	0.133	1.92	0.179	0.127	0.395	832	0.025	0.037	0.0446	0.090	0.23
4	1634	1.7	8.8	13.9	0.122	0.116	1.72	0.168	0.119	0.368	730	0.030	0.037	0.0476	0.096	0.26
5	1734	1.9	8.3	13.2	0.131	0.135	1.69	0.188	0.133	0.412	916	0.030	0.039	0.0492	0.099	0.24
6	1834	1.7	7.8	11.7, 12.7	0.115	0.100	1.81	0.152	0.108	0.338	595	0.031	0.045	0.0545	0.110	0.32
7	1934	1.9	7.8	13.2	0.115	0.124	2.12	0.169	0.120	0.370	738	0.025	0.032	0.0406	0.082	0.22
8	2034	2.0	7.3	13.9	0.091	0.097	2.??	0.133	0.094	0.289	484	0.021	0.021	0.030	0.060	0.21
9	2134	1.7	8.0	13.2	0.102	0.103	2.20	0.145	0.103	0.317	542	0.020	0.026	0.033	0.066	0.21
10	2234	1.9	7.9	13.2	0.105	0.107	2.17	0.150	0.106	0.328	580	0.019	0.026	0.0322	0.065	0.20
11	2334	1.6	7.7	12.2	0.095	0.094	2.19	0.134	0.095	0.298	468	0.017	0.030	0.0345	0.070	0.23
7/5/81																
12	0034	1.5	8.2	13.2	0.100	0.108	2.11	0.147	0.104	0.322	559	0.019	0.026	0.0322	0.065	0.20
13	0134	1.6	8.6	13.9	0.104	0.110	2.29	0.151	0.107	0.328	587	0.023	0.025	0.034	0.069	0.21
14	0234	1.5	8.0	13.2	0.104	0.115	2.16	0.155	0.110	0.339	620	0.020	0.027	0.034	0.068	0.20
15	0334	1.6	9.0	12.7	0.128	0.136	2.08	0.187	0.132	0.412	905	0.033	0.040	0.0519	0.105	0.25
16	0434	1.7	9.0	12.7	0.127	0.136	1.98	0.186	0.132	0.410	896	0.030	0.039	0.0492	0.099	0.24
17	0534	1.6	8.3	13.7	0.111	0.118	1.95	0.162	0.115	0.355	672	0.020	0.026	0.033	0.066	0.19
18	0634	No Data		12.7	0.119	0.121	2.02	0.168	0.119	0.370	730	0.024	0.029	0.038	0.076	0.21
19	0734	No Data		11.7	0.111	0.109	2.13	0.156	0.111	0.350	638	0.018	0.022	0.028	0.057	0.16
20	0834	No Data		13.2	0.114	0.100	1.91	0.152	0.108	0.333	598	0.024	0.032	0.040	0.081	0.24
21	0934	No Data		11.7	0.133	0.103	1.82	0.168	0.119	0.376	736	0.035	0.039	0.052	0.106	0.28
22	1034	No Data		12.2	0.163	0.102	1.68	0.192	0.136	0.426	957	0.040	0.050	0.064	0.129	0.30
23	1134	No Data		12.7	0.192	0.136	1.62	0.235	0.167	0.518	1,431	0.045	0.055	0.071	0.144	0.28
24	1234	No Data		13.2	0.146	0.101	1.62	0.178	0.126	0.390	820	0.033	0.044	0.055	0.111	0.28
25	1334	No Data		12.7	0.119	0.101	2.27	0.156	0.111	0.344	631	0.028	0.034	0.044	0.089	0.26
26	1434	No Data		12.2	0.110	0.102	2.32	0.150	0.106	0.333	584	0.022	0.019	0.029	0.059	0.18
27	1534	No Data		11.7	0.112	0.098	1.99	0.149	0.106	0.334	581	0.029	0.036	0.046	0.093	0.28
28	1634	No Data		12.2	0.141	0.122	1.40	0.186	0.132	0.413	899	0.049	0.068	0.084	0.169	0.41
29	1734	2.3	5.2	12.2	0.185	0.164	1.35	0.247	0.175	0.549	1,589	0.040	0.078	0.088	1.177	0.32
30	1834	2.4	5.3	12.2	0.201	0.167	1.29	0.261	0.185	0.580	1,773	0.046	0.062	0.077	0.154	0.27
31	1934	2.7	5.6	13.2	0.156	0.122	1.52	0.198	0.140	0.433	1,011	0.045	0.070	0.083	0.168	0.39
32	2034	2.3	5.4	16.0	0.137	0.104	1.73	0.172	0.122	0.367	751	0.036	0.044	0.057	0.114	0.31
33	2134	2.4	5.6	15.1	0.121	0.079	2.14	0.144	0.102	0.309	532	0.025	0.026	0.036	0.073	0.24
34	2234	2.3	5.6	15.2	0.161	0.119	2.16	0.200	0.142	0.429	1,026	0.031	0.031	0.044	0.089	0.21
35	2334	2.3	5.9	13.9	0.087	0.067	2.62	0.109	0.077	0.237	306	0.022	0.022	0.031	0.063	0.27

(4) Quasi-oscillatory flows at infragravity frequencies are of
tertiary importance.

Implications for sediment transport

In order for benthic flows to cause sediment transport, the
shear stresses, τ associated with these flows must overcome the
stabilizing force of gravity on the sediment particles. An im-
portant parameter for expressing the shear stress relative to the
immersed weight of the particle is the dimensionless Shields para-
meter θ (Shields, 1936; Komar 1976) given by

$$\theta = \tau / (\rho_s - \rho) \, g \, D_s \tag{19}$$

where ρ_s and ρ are respectively sediment and water densities and D_s
is sediment particle diameter. For wave induced oscillatory flows
the shear stress is

$$\tau = \tfrac{1}{2} \rho f_w V_o^2 = \tfrac{1}{2} \rho f_w (a_s \omega)^2 \tag{20}$$

where f_w is a friction factor, V_o is orbital velocity maximum and
a_s is orbital semi-excursion length at the bed

$$a_s = H/(2 \sinh kh) \tag{21}$$

Historically (and conventionally) the friction factor, f_w, has been
assumed constant with a value around 0.02 (e.g. Bretschneider and
Reid, 1954). However, measurements by Carstens et. al. (1969) and
Lofquist (1980) have shown that f_w can have a large range of values
(up to 0.3) depending on the length scale of bed roughness, λ,
relative to the orbital semi-excursion a_s (see appendix B for dis-

cussion). Swart (1974) gives

$$f_w = \exp [5.213 \, (\lambda/a_s)^{.194} - 5.977] \qquad (22)$$

For a <u>fixed</u> (immobile), unrippled bed the roughness length is about

$$\lambda = 2.5 \, D_s \qquad (23)$$

(Nielsen, in press) which, for $D_s \sim 1$ mm ($\lambda = .0025$ m) and $a_s = 0.20$m ($H = .5$m, $T = 10$ sec, $h = 20$ m) the friction factor, estimated from equation (22) would have a "conventional" value on the order of 0.02. For initiation of sediment motion by waves, it is normal to use the skin friction Shields parameter, θ', obtained by substituting (20) into (19) and using (23) for roughness (e.g. Nielsen 1979).

Numerous studies of the critical or threshold value, θ_c, which must be exceeded before sediment transport can be initiated suggest that the critical values are about $\theta = 0.04 - 0.06$ for sand transport by both steady and oscillatory flows over smooth beds (Sternberg, 1972; Komar, 1976; Komar and Miller, 1975) over rippled beds, the critical value may be as low as $\theta_c \sim 0.03$.

For steady or quasi-steady flows (e.g. tidal currents), Sternberg (1972) found that the drag coefficient, relating current speed, $<V>_{100}$ at 1 metre above the bed to shear stress, τ, has a mean value of 3.1×10^{-3} or in other words for steady (non-wave) currents

$$\tau \cong 3.1 \times 10^{-3} \, \rho <V>^2 \qquad (24)$$

Substituting observed burst-averaged current speeds, $<V>$, (Table 2) into the above relationship for τ, using observed sediment sizes (Table 1) and assuming $\rho_s = 2650$ kg m^{-3} we estimate the associated

θ values for the swiftest observed net currents (0.18 m sec^{-1}) to be

$$\theta = 0.032 \qquad\qquad (25)$$

for $D_s = 0.2$ mm and $\theta = 0.008$ for $D_s = 0.8$ mm. Both values are subcritical and it may be inferred that, if we accept Sternberg's (1972) estimate of the drag coefficient, the observed non-wave-induced flows are unable to initiate significant nearshore sand transport.

As concluded previously, the oscillatory velocities, V_s, due to the waves are dominant over the nearshore profile and we may expect these motions to play the dominant role in agitating nearshore sediments. We will evaluate the likelihood of sediment being entrained by waves using the semi-empirical relationships proposed by Komar and Miller (1975). Komar and Miller (1975) used a Shields-type criterion or mobility number of the form

$$\Psi = \frac{\rho \, V_o^2}{(\rho_s - \rho) \, g \, D_s} \qquad\qquad (26)$$

where V_o is maximum orbital velocity (approximated in our case by V_s). They found that for turbulent boundary layers on an <u>unrippled</u> bed the critical value, Ψ_c, necessary to initiate motion is

$$\Psi_c = 0.46\pi \, (d_0/D_s)^{\frac{1}{4}} \qquad\qquad (27)$$

where d_0 is the bottom water particle excursion length, $d_0 = 2a_s$ (eg. 21).

On the basis of the above criterion, Ψ_c, bottom orbital velocities of 0.18 m sec^{-1} would be sufficient to move the finer fractions ($D_s = 0.2$ mm). This velocity was exceeded by nearly half

of the observed V_s values shown in Table 3. We can estimate that
10 second waves would require a local height of 0.7 m at h = 20 m
and 0.42 m at h = 10 m in order for the associated orbital velocities
to exceed 0.18 m sec^{-1}. For the much coarser mean grain sizes of
0.8 mm at h = 20 m and 0.4 mm at h = 10 m the respective "threshold"
velocities" would be 0.33 m sec^{-1} and 0.25 m sec^{-1}; the corresponding
"threshold" wave heights (T = 10 sec) are H - 1.3 m at h = 20 m and
H = 0.58 m at h = 10 m. The Ψ_c criterion as expressed by equation
27 assumes a smooth bed. The nearshore bed off Eastern Beach was
observed to be extremely rough with sharp crested wave ripples 10
centimetres high. Over a rippled bed sediment entrainment should take
place at lower orbital velocities. Diver observations confirmed that
oscillatory motions were entraining sediment clouds over ripples.

We conclude that waves are probably able to agitate nearshore
sediments shoreward of the 20 metre contour for most of the time.
However, agitation of sediments by oscillatory currents does not
necessarily imply any net transport. We are concerned now with
inferring the likely direction of net nearshore transport. We will
not attempt to estimate the absolute rates of transport because the
data are insufficient to allow this.

Many recent studies of nearshore sediment transport attempt to
model the transport rate, q, in terms of modified forms of Bagnold's
(1963) energetics approach (e.g. Sternberg, 1972; Seymour, 1980;
Bailard, 1981; Bailard and Inman, 1981). This approach considers q
to be proportional to the bed "fluid power" that is

$$q \propto \tau V \qquad (28)$$

This approach has been applied most often to bedload transport, q_b,
although Bailard (1981) has proposed a "total load" version. If the

net tidal and wind driven currents operated alone without wave effects,
then these currents would be the source of the shear stresses and we
would expect

$$q_b \quad \propto \quad <v^3> \tag{29}$$

However, we have shown that waves are the dominant source of
bed shear stress. Prediction of net sediment transport by a com-
bination of waves and currents is a very complicated matter and at
present there is no model in existence which at the same time is
both theoretically based and in agreement with experimental evidence.

As early as 1963, Inman and Bowen (1963) showed that the net
sediment transport under a combination of waves and currents will just
as often be against the net current as with it. This means that no
transport model by which the net transport is proportional to the net
flow will be in general agreement with the empirical evidence.

More such evidence has since been obtained by many detailed
flume experiments at the Technical University in Delft; see van de
Graaff (1980). This effect is due to the fact that the transport con-
tribution Q_n from oscillatory velocity and concentration components
U_n and C_n will often dominate over the contribution of the steady com-
ponents, Q_o

$$Q_o = \int_o^h \bar{C}(z)<u>(z) \, dz \tag{30}$$

This dominance is due to the fact that the oscillatory velocity com-
ponents will have a much thinner boundary layer than the steady flow,
and will thus penetrate to the lowest elevations, where the concen-
trations are largest.

The direction of

$$Q_n = \frac{1}{T} \int_{t}^{t+T} dt \int_{o}^{h} C_n (z,t) \, U_n (z,t) \, dz \qquad (31)$$

will depend on the phase relations between the simple harmonics $C_n (z,t)$ and $U_n (z,t)$ and as yet there is no model which is capable of predicting these phase relations on theoretical grounds.

The model presented by Nielsen et. al. (1978) and Nielsen (1979) predicts these phase relations and predicts net sediment fluxes that are in agreement with the Dutch measurements, with appropriate choice of parameters. However, this model is based on the diffusion equation and recent empirical and theoretical work shows that the entrainment of sand by a wave dominated flow is not a diffusion process (Nielsen in prep.).

In the direction perpendicular to the wave motion the problem is not so complex because there are no oscillatory velocity components and therefore the transport is given reasonably by

$$Q_y = \int_{o}^{h} \bar{c} \, (z) \, <V> \, (z) \quad dz \qquad (32)$$

Even here however $\bar{c}$ will be determined by the combined shear stress from the waves and currents and there is at present no theory which gives a satisfactory description of the boundary layer structure for combinations of waves and currents. The existing models e.g. Madsen and Grant 1979 all assume a constant or linearly increasing eddy viscosity which is in clear disagreement with the eddy viscosity measurements referred to by Lundgren (1972) and with the velocity fluctuation measurements by Nakato et. al. (1977) and Macdonald (1977). The latter two both found that the intensity of vertical velocity fluctuations decreased exponentially with the distance from a rippled bed,

and such exponentially decreasing velocity fluctuations are not very likely to correspond to a constant or linearly increasing eddy viscosity.

The key to a consistent theoretical description of wave and wave/current boundary layers over rippled beds seems to be the consideration of the fact that both suspended sand and turbulence originate at the bed and move upward by a rhythmic convective process. The nature of this process is indicated by the measurements of Nakato et. al. (1977) and Macdonald (1977) who found that both suspended sediment and turbulence are exponentially distributed with identical vertical length scales.

In the absence of good theories for the boundary layer structure of the combined flow we are forced to use the very simple assumption that the concentrations $c(z)$ are determined by the waves alone. This assumption seems to be reasonably well justified under most conditions even in the presence of quite strong currents (e.g. longshore currents as discussed in the next section).

We, therefore, can draw no conclusions as to shore-normal transport. We can, however, make some inferences at least concerning the direction of shore-parallel transport if we regard the process as involving entrainment of sediment by wave induced oscillatory currents, V_s, and net advection of the entrained sediment taking place in response to the net time averaged longshore current $<v>$. An energetics form for the superimposition of wave shear stress and steady currents is given by Seymour (1980) for the case of interacting waves and tidal currents. Seymour (1980) suggests that

$$q_b \ \propto \ << v^3>> + <<v><v_s^2>> \tag{33}$$

(The second set of brackets denotes time averaging over all bursts).

Seaward of the surf zone, the effect of wave oscillations over a rippled bed is to suspend sediment in vortices above the bed and there is considerable field and laboratory evidence that sediment transport by unbroken waves over a rippled bed takes place largely in intermittent suspension (Nielsen, 1979; in press). If the concentration of suspended sediment near the bed is C_s then the alongshore suspended load transport rate q_s will be

$$q_s \quad \propto \quad <v> \; C_s \qquad (34)$$

Field observations of suspended sediment concentration profiles measured under waves (Nielsen and Green, in press; Nielsen, 1979, see discussion of surf zone transport later in this report) indicate that C_s is roughly proportional to the cube of the Shields parameter and, hence, to the sixth power of the wave orbital velocity, that is

$$C_s \quad \propto \quad \theta'^3 \quad \propto \quad \tau^3 \quad \propto \quad v_s^6 \qquad (35)$$

We may therefore consider that

$$q_s \quad \propto \quad <v> \; v_s^6$$

Table 4 lists the observed values of all of the sediment transport indices just described, time averaged over the 35 hour observation period at h = 10 m. All shore parallel indices are negative indicating a net transport toward the east.

Table 4: Indices of relative shore-parallel sediment transport rate at h = 10 m.

	$\ll V^3 \gg$ $m^3 sec^{-3}$	$\ll V\, V_s^2 \gg$ $m^3 sec^{-3}$	$\ll V^3 \gg + \ll V\, V_s^2 \gg$ $m^3\ sec^{-3}$	$\ll V\, V_s^6 \gg$ $m^7 sec^{-7}$
Shore-Parallel (V)	$-.6 \times 10^{-3}$	$-.73 \times 10^{-3}$	$-.133 \times 10^{-2}$	$-.23 \times 10^{-5}$

v positive toward west (alongshore)

During the experiment period, the easterly setting flows dominated over the westerly setting flows. Naturally, we cannot assume, on the basis of a short sample, that this is always the case. We can, however, be reasonably confident of one important conclusion: tidal currents set to the east at low tide. As emphasized by Seymour (1980) and subsequently by Wright (in press), low tide flows are likely to transport more sediment than high tide flows of equal magnitude because wave-induced shear stresses at the bed will be greater at low tide when depth and, hence sinh kh, are reduced. The evidence at hand suggests that net sediment transport over the nearshore profile is toward the east.

Nearshore modifications of waves

From the point of view of the surf zone processes to be considered in the following section, the modifications experienced by the incident waves as they cross the nearshore zone between deep water and the break point are of considerable importance. The most important modifications include (1) shoaling; (2) refraction; and

(3) dissipation by bed friction.   Local wind shear can also produce
appreciable modification. Considering wave height variations due to
those processes, wave height, H, at any given position and depth re-
lative to deepwater wave height, H_∞ is

$$\frac{H}{H_\infty} = K_s \, K_r \, K_f \qquad (36)$$

where K_s, K_r K_f are respectively the shoaling, refraction and friction
coefficients.

The shoaling coefficient, K_s is

$$K_s = \sqrt{\frac{C_{g\infty}}{C_g}} = \sqrt{\frac{0.5 \, C_\infty}{nC}} \qquad (37)$$

where $n = \frac{1}{2}[1 + \frac{2kh}{\sinh 2kh}]$ and, for the case of straight, parallel depth
contours (a condition approximately met at the field site) the re-
fraction coefficient is

$$K_r = \sqrt{\frac{\cos \alpha_\infty}{\cos \alpha}} \qquad (38)$$

where α and α_∞ are the local and deepwater angles of wave incidence
which vary in accordance with Snell's law

$$\frac{C}{\sin \alpha} = constant \qquad (39)$$

Using the explicit formulae developed by Nielsen (in press)   we can
approximate K_s and K_r from

$$K_s = (8\pi h/L_\infty)^{-\frac{1}{4}} \exp(\pi h/2L_\infty) \qquad (40)$$

and

$$K_r = \sqrt{\cos\alpha_\infty} \; [1-2\pi h/L_\infty \; (1-h/L_\infty)^2 \; \sin^2\alpha_\infty]^{-\frac{1}{4}} \qquad (41)$$

where the deepwater wave length, L_∞ is

$$L_\infty = gT^2/2\pi \qquad (42)$$

If we could imagine the incident waves to be unaffected by friction (which we cannot) then we could expect the "modal" deepwater waves of $H_\infty = 3$ m, $T = 8.5$ sec, $\alpha_\infty = 45^0$ (SW) to break at an angle of 16.8^0 with a breaker height of slightly less than 3 m corresponding to $K_s = 1.15$ and $K_r = 0.86$.

As suggested earlier, the effects of frictional dissipation over the wide, rough nearshore bed are probably large. Whereas the effects of refraction and shoaling alone involve no change in energy flux, P, frictional dissipation results in a loss of energy flux at a rate

$$\frac{d\,P}{d\,s} = -\overline{\tau V} \approx -\frac{1}{2}\rho f_w \; \overline{|v^3|} = -\frac{1}{2}\rho f_w \; \zeta(V_{rms})^3 = -\frac{1}{4\sqrt{2}} \rho f_w \zeta v_o^3 \qquad (43)$$

where s is horizontal distance along the direction of wave propogation, V is the instantaneous bottom orbital velocity and V_o is the maximum bottom orbital velocity

$$V_o = \frac{\pi H}{T \sinh kh} \qquad (44)$$

In our preceding discussion of sediment transport, we estimated f_w from equation (22) using a roughness length of $\lambda = 2.5 \; D_s$ for purposes of calculating the skin friction Shields parameter θ', appropriate to the grains. However, in order to estimate frictional dissipation, we must consider the total combined roughness for mobile (as

opposed to fixed) beds and the presence of the ripples. The roughness λ, and consequently f_w, are considerably increased over mobile rippled beds. On the basis of several sets of available data (e.g. Carstens et. al. 1968; Lofquist 1980), we find the best empirical fit for λ as a function of ripple dimensions and grain size to be

$$\lambda = 8\eta_r^2/L_r + 190\sqrt{\theta' - .05}\ D_s \qquad (45)$$

where η_r is ripple height, L_r is ripple chord length (spacing between ripple crests), θ' is the skin friction Shields parameter. The rationale behind this expression is explained in Appendix B. Using observed ripple dimensions off Eastern Beach $\eta_r = 0.10$ m, $L_r = 0.6$ m, λ is found to be about 0.13 m under low wave energy ($H \approx 0.5$ m) when θ', and hence the moving sand contributions are small. Under larger waves, when θ' at $h = 20$ m is on the order of 0.20 for the coarser fractions and up to 0.80 for the finer fractions, the moving sand contribution would increase λ to the order of 0.20m. Substituting our new roughness estimates into Swart's (1974) formula (eg. 22) we obtain estimates of f_w ranging from $f_w = 0.18$ to 0.31; a typical rippled bed value is $f_w = 0.25$ which we will assume to be roughly constant over the nearshore profile.

Since f_w probably has a large value of ~ 0.25 and since the modal southwesterly waves have a large initial angle of incidence ($\alpha_\infty \sim 45^0$) and hence must travel large distances over the low gradient nearshore profile, considerable loss of energy must take place before the waves reach the break point. To estimate the likely breaker heights corresponding to the modal deepwater waves we must consider the combined effects of refraction, shoaling, and friction. We can do this by computing changes over consecutive segments of the profile. If h_1 and h_2 are depths at the seaward and landward

ends of a segment and H_1 and H_2 are the corresponding heights
then we can approximate the ratio H_2/H_1 from

$$\frac{H_2}{H_1} = \frac{\sqrt{\dfrac{C_{g1} \cos \alpha_1}{C_{g2} \cos \alpha_2}}}{1 + \dfrac{k_\infty f_w H_1 \zeta}{8\sqrt{2} \dfrac{dh}{dx}} \sqrt{\dfrac{C_{g1} \cos \alpha_1}{C_\infty}} \, I} \tag{46}$$

where subscripts 1 and 2 denote the values at deeper and shallower
ends of the segment, the subscript ∞ denotes the deepwater value,
dh/dx is bed slope, ζ is the peakedness function (eq. 18) which in
our case is about 2.05 (on average) and the integral I is

$$I = \int_{k_\infty h_1}^{k_\infty h_2} \frac{C_\infty^{1.5}}{C_g^{1.5} \sinh^3 kh} (\cos \alpha)^{-2.5} \, d \, k_\infty h \tag{47}$$

This integral can be approximated by

$$I = \frac{4}{5}(k_\infty h_1)^{-1.25}\left[1 - \left(\frac{h_1}{h_2}\right)^{1.25}\right] + (1-4\delta)(k_\infty h_1)^{-.25}\left[\left(\frac{h_1}{h_2}\right)^{0.25} - 1\right]$$

$$+ \ (\frac{4}{3}\mu - \frac{6}{360}\frac{1}{3} - \frac{1}{3}\delta)(k_\infty h_1)^{.75}\left[\left(\frac{h_1}{h_2}\right)^{-.75} - 1\right] \tag{48}$$

where

$$\delta \approx \frac{0.7 \tan^2 \alpha_1}{(1+\tan^2 \alpha_1) k_\infty h_1 (1 - \frac{1}{3} k_\infty h_1)} \tag{49}$$

and

$$\mu = \frac{4 \tan^4\alpha_1}{(1+\tan^2\alpha_1)^2 (k_\infty h_1)^2} - \frac{1}{3}\delta \qquad (50)$$

The cumulative error of the integral I can be inferred from the error on the corresponding explicit approximation to the integrand, and a detailed error analysis can be found in Nielsen (in press). For $\alpha_1 < 45^0$ the induced error on the predicted wave height will be insignificant.

Solving equation 46 for the estimated modal wave conditions across successive increments of the nearshore profile having constant gradients, using $f_w = 0.25$ and the observed ζ value of 2.05 and assuming negligible modifications seaward of h = 20 m we estimate the modal breaker height to be about 1 metre and the breaker angle would be about 9.6^0. Figure 21 shows the predicted change in heights across the profile for shoaling and refraction alone and for shoaling, refraction and friction. It is apparent from Figure 21 that most of the wave height reduction takes place over the wide, low gradient segment between h = 20 m and h = 15 m.

The predicted reduction in wave height to about one third the deepwater value before the waves break may seem, to some, to be excessive. Perhaps we have overestimated f_w? We can check this to a limited degree because, for a short period of five hours we have roughly simultaneous measurements of V_s and hence estimates of H_s from h = 20 m and h = 10 m (Table 3). From the H_s values in Table 3 we can estimate the dissipation factor, F_e, (which includes f_w plus any other dissipating effects which may be present) from
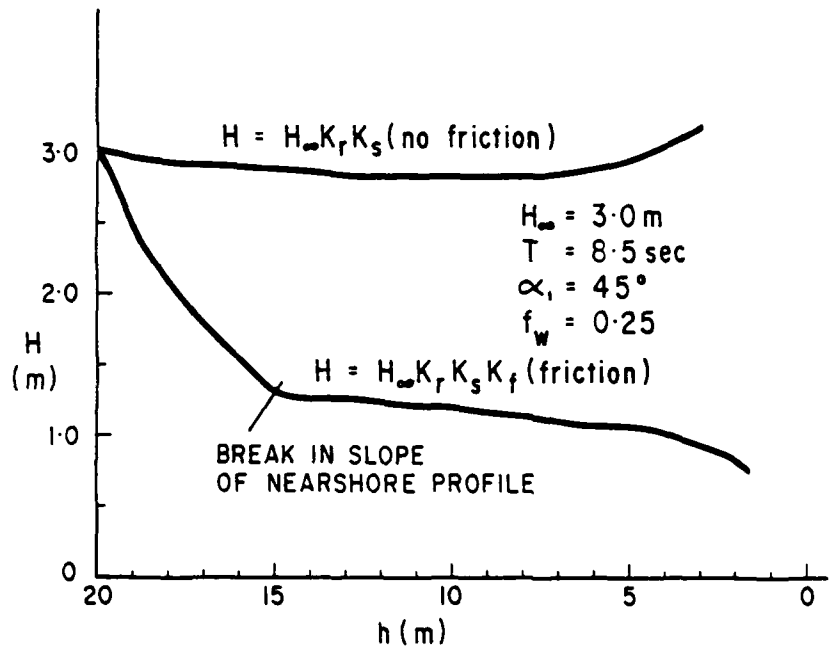
Figure 21. Variation of local wave height, H, with depth, h, as predicted for a deepwater wave with H_∞ = 3.0, T = 8.5 sec on the basis of shoaling and refraction alone and shoaling refraction and frictional dissipation over the observed nearshore profile.

$$
F_e \;=\; \frac{3\pi\,\dfrac{dh}{ds}}{k_\infty H_1 I}\;\sqrt{\frac{C_\infty}{C_{g1}}}\left[\frac{H_1}{H_2}\;\sqrt{\frac{C_{g1}}{C_{g2}}}\;-\;1\right] \tag{51}
$$

where H_1 and H_2 must be the rms values which are related to H_s by $H_{rms} = H_s/\sqrt{2}$. For irregular waves, this equation would result in overestimating F_e unless we include the observed values of ζ (instead of the "simple harmonic value" $\dfrac{8\sqrt{2}}{3\pi}$

$$
F_e \;=\; \frac{8\sqrt{2}\,\dfrac{dh}{ds}}{k_\infty H_1 \zeta I}\;\sqrt{\frac{C_\infty}{C_{g1}}}\left[\frac{H_1}{H_2}\sqrt{\frac{C_{g1}}{C_{g2}}}\;-\;1\right] \tag{52}
$$

For the observed wave conditions, the angle of incidence was at both stations close to 45° so that no refraction had taken place(since u_s and v_s were nearly equal) so $dh/ds = dh/dx \dfrac{1}{\sqrt{2}}$. For the   five hourly bursts during which both inner and outer current meters were recording simultaneously the estimates of F_e are given in Table 5.

Table 5. F_e values estimated from observed current statistics.

Burst	1	2	3	4	5	
F_e	.71	.65	.31	.59	.52	$\overline{F}_e = 0.56$

The dissipation factors obtained in this way all substantially exceed the predicted f_w value of 0.25. Some of this apparent excess dissipation is probably not real but is only a manifestation of the non-linear effects of the shoaling waves (R.T. Guza Pers. Com.; Lighthill 1978). Some may be due to extra dissipation caused by interaction between the waves and the tidal currents; and some may be due to the fact that we underestimated rather than overestimated

the friction factor, f_w.

The effects of frictional dissipation are *non-linear*; the rate of dissipation is proportional to the cube of the wave height (eq. 43). Hence the large waves will experience more attenuation than the small waves. An important question of fundamental relevance to beach and surf zone variability thus arises: how does the nearshore modification of waves by shoaling, refraction, and friction affect the annual distribution (temporal variability) of nearshore (or breaker) heights? The effects of shoaling and refraction are linear and thus only produce shifting and stretching of the distribution. The addition of frictional effects, however can be expected to cause narrowing and skewing of the wave height distribution near the break (or in shallow water) and reduce the frequency of occurrence of larger heights. *This effect is very pronounced when f_w is large and when the near-shore profile is flat.*

Equation 46 gives the wave height, H_2, at the shallow limit of the profile segment relative to the height, H_1, at the deep (offshore) limit of the segment after modification by refraction, shoaling and friction. For simplicity, we will rewrite equation 46 as

$$H_2 = G(H_1) = \frac{\psi \, H_1}{1 + \Omega \, H_1} \tag{53}$$

$$\text{where} \quad \psi = K_s K_r = \sqrt{\frac{c_{g1} \cos \alpha_1}{c_{g2} \cos \alpha_2}} \tag{54}$$

$$\text{and} \quad \Omega = \frac{f_w k_\infty \zeta}{8\sqrt{2} \frac{dh}{dx}} \sqrt{\frac{c_{g1} \cos \alpha_1}{c_\infty}} \, I \tag{55}$$

and I is given by equation 47.

Now, if the distribution of H_1 is

$$P \{H_1 \leq H\} = F_1 (H) \tag{56}$$

(where $P \{H_1 \leq H\}$ is the annual probability that H_1 is less than or equal to a given height)

and $H_2 = G(H_1)$ (57)

then the distribution of H_2 is

$$P \{H_2 \leq H\} = F_2 (H) = F_1 [G^{-1} (H)] \tag{58}$$

From (53)

$$H_1 = \frac{H_2}{\psi - \Omega H_2} \tag{59}$$

so

$$G^{-1} (H) = \frac{H}{\psi - \Omega H} \tag{60}$$

and the distribution of H_2 is

$$P \{H_2 \leq H\} = F_2 (H) = F_1 \left(\frac{H}{\psi - \Omega H}\right) \tag{61}$$

By differentiating (61) with respect to H we find the probability density of H_2,

$$p_2(H) = \frac{\psi}{(\psi - \Omega H)^2} \; p_1\left(\frac{H}{\psi - \Omega H}\right) \tag{62}$$

where p_1 and p_2 are the probability densities of heights at h_1 and h_2. The distribution of deepwater wave heights in Gippsland is broad. If H_1 (defined for $h_1 = 20$ metres) is assumed to follow a Rayleigh distribution (which it probably does not really do), then,

$$F_1(H) = 1 - \exp\left[-(H/\bar{H})^2\right] \tag{63}$$

where $\bar{H}$ is the mean height ($\bar{H} = 2$ m in our case).

Then, from (61)

$$F_2(H) = 1 - \exp\left[-\frac{H^2}{(\psi - \Omega H)^2 \bar{H}^2}\right] \tag{64}$$

and from (62) the probability density is

$$p_2(H) = \frac{\psi}{(\psi - \Omega H)^2} \; \frac{2H/\bar{H}^2}{\psi - \Omega H} \; \exp\left(-\frac{H^2}{(\psi - \Omega H)^2 \bar{H}^2}\right)$$

$$= \frac{2\psi H}{(\psi - \Omega H)^3 \; \bar{H}^2} \cdot \exp\left(-\frac{H^2}{(\psi - \Omega H)^2 \; \bar{H}^2}\right) \tag{65}$$

To obtain approximate extimates of $p_2(H)$ we use observed parameter values for the Eastern Beach case of $h_1 = 20$ m, $h_2 = 2$ m, $\bar{H} = 2$ m, $\psi = 1.4$, $\Omega = 0.59$ corresponding to the predicted f_w of. 0.25 and $\Omega = 1.32$ corresponding to the observed F_e value of 0.56.

Figure 22 shows the estimated probability density $p_1(H)$ for $h_1 = 20$ m ("deepwater") and $p_2(H)$ estimated for the "no friction" case $(f_w, \Omega) = $ (zero, zero), the "estimated dissipation case" $(f_w, \Omega) = (0.25, 0.59)$
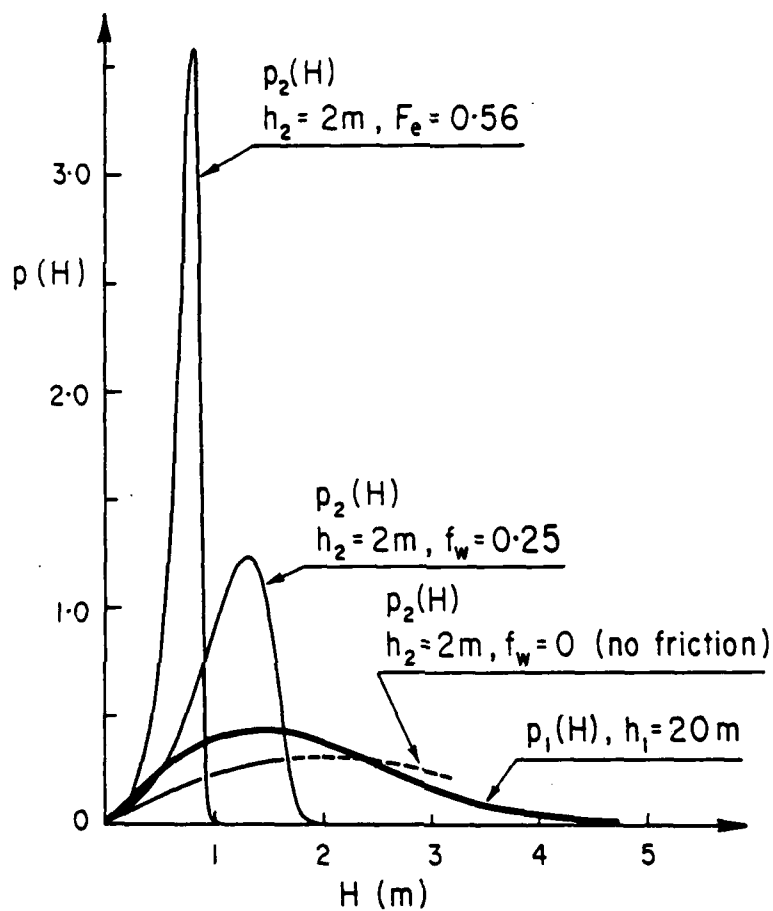
Figure 22. Probability density of deepwater wave heights, $P_1(H)$, (assuming a Rayleigh distribution) and breaker heights, $P_2(H)$ after frictional dissipation with $f_w = 0.25$ or with $F_e = 0.56$. Breaker height distribution on the basis of no dissipation is also indicated.

and the "measured dissipation case" $(f_w, \Omega) = (0.56, 1.32)$. The deep-water distribution of H_1 is very broad, the temporal variability is large and large wave heights are relatively frequent. If frictional dissipation did not operate, the distribution of breaker heights would be shifted somewhat but would remain broad with large maxima. However, a bottom friction factor, f_w of 0.25 combined with the low gradient nearshore profile substantially narrows the distribution of breaker heights and reduces the occurrence of large breakers despite the fact that much larger waves may occur offshore. For F_e values of 0.56 the distribution would be narrower still and the maximum height would rarely exceed 1 metre.

Whatever the absolute $p_2(H)$ values may really be, one qualitative point is very clear: the temporal variability of breaker height is much lower than the temporal variability of deepwater wave height and the maximum breaker height is apparently limited to about 2 metres for most of the time. This is a consequence of the rough, low-gradient near-shore profile fronting the Gippsland coast. Over steeper, narrower near-shore profiles such as that fronting the coast of New South Wales (e.g. Wright 1976) frictional attenuation is less and the variability of breaker heights is much broader. This is reflected in the stronger seasonal variability for most New South Wales beaches compared to Eastern Beach.

SURF ZONE AND BEACH PROCESSES

The surf zone and beach at Eastern Beach occupy only the innermost 200 metres of the Coastal Boundary Layer (Fig.1). However, it is within this comparatively narrow region that the previously modified waves ultimately experience their most rapid dissipation, perform work at the most rapid rate, and produce the most dramatic and rapid morphologic changes. After the incident waves break at the outer limits of the surf zone, their energy is transferred to other forms of motion including lower frequency standing waves and edge waves, longshore currents, and rip circulations.

Morphodynamic state of the surf zone and beach

Figure 23 shows the six most common morphodynamic states recognized by Wright and Short (in press). The general model shown in Figure 23 is a modified and updated version of the models originally discussed by Wright et al (1979 a and b) and Short (1979 a and b). The two extremes shown in Figure 23 a and f are respectively fully dissipative and highly reflective. Dissipative versus reflective conditions are distinguished on the basis of a surf scaling parameter proposed by Guza and Inman (1975) of the form

$$\varepsilon = a \, \omega^2/g \, \tan^2 \beta \qquad (66)$$

where a was runup amplitude (in Guza and Inman's 1975 original equation), ω is incident wave radian frequency ($\omega = 2\pi/T$, T is period) g is acceleration of gravity and β is beach or surf zone gradient. Wright et al (1979) replaced runup amplitude a with breaker amplitude, a_b to differentiate between reflective and dissipative surf zones and we follow that approach here. Guza and Inman (1975) and Guza and Bowen (1977) showed that strong reflection

DISSIPATIVE

OUTER BREAKER ZONE

TROUGH

INNER BREAKER ZONE

BEACH

NO LONGSHORE VARIABILITY

DISSIPATIVE DOMAIN

FLAT/CONCAVE BEACH FACE — LOW FREQ. SWASH BORES — SPILLING BREAKERS

$\tan\beta = 0.03$

INNER BREAKPOINT VARIABLE

WIDE NSHORE PROFILE $\tan\beta = 0.01$

OUTER BREAKPOINT MOVES SIGNIFICANTLY SEAWARD WITH HIGHER WAVES COMMONLY 100-200m WITH 2m WAVES

INTERMEDIATE
LONGSHORE BAR-TROUGH

STRAIGHT BAR → CRESCENTIC BAR WEAK RIP

BAR

TROUGH

(CUSPS MAY BE PRESENT)

REFLECTIVE DOMAIN LOW ξ_0 DISSIPATIVE DOMAIN MODERATE ξ_0

BERM (CUSPS) — SURGING BREAKERS — PLUNGING BREAKER

STEEP REFLECTIVE BEACH FACE — DEEP TROUGH / BAR

$\tan\beta = 0.05-0.20$

INTERMEDIATE
RHYTHMIC BAR AND BEACH (NORMAL OR SKEWED)

NORMAL WAVES   OBLIQUE WAVES

CRESCENTIC BAR   RIP

MEGA CUSP HORN   SCARP   MEGA CUSP EMBAYMENT

HIGH TIDE CUSPS
(CUSPS MAY OCCUR ON MEGA-CUSP HORNS)

REFLECTIVE DOMAIN   DISSIPATIVE DOMAIN
MODERATE ξ_0

MEGA CUSP HORN — SURGING BREAKER — PLUNGING BREAKER
TROUGH / BAR MIGRATION
$\tan\beta = 0.05-0.10$

LOW REF.DOM DISSIPATIVE DOMAIN MODERATE ξ_0
SCARP — MEGA CUSP EMBAYMENT — PLUNGING BREAKER — SPILLING-PLUNGING BREAKER
RIP — MEGA RIPPLES
$\tan\beta = 0.10-0.20$ $\tan\beta = 0.01$

INTERMEDIATE
TRANSVERSE BAR AND RIP (NORMAL OR SKEWED)

NORMAL WAVES   OBLIQUE WAVES

STRONG RIP

WELDED BAR   HIGH TIDE CUSPS
(CUSPS MAY OCCUR ON MEGA-CUSP HORNS)

VARIABLE ξ_0 HIGH TIDE   DISSIPATIVE DOMAIN
MODERATE ξ_0 LOW TIDE
LOW BERM — PLUNGING BREAKER — MHW — MLW
BAR

DISSIPATIVE OR REFLECTIVE DOMAIN VARIABLE DISSIPATIVE DOMAIN
RELIC SCARP — SURGING BREAKER — MODERATE ξ_0 — MHW
WIDE BEACH — RIP — MLW
$\tan\beta = 0.05$ — SPILLING-PLUNGING BREAKER

INTERMEDIATE
RIDGE-RUNNEL OR LOW TIDE TERRACE

NORMAL WAVES   OBLIQUE WAVES

MINI-RIP   RUNNEL
RIDGE   TERRACE

RUNNEL   HIGH TIDE CUSPS   SKEWED MINI-RIP

HIGH TIDE REFLECTIVE
LOW ξ_0 LOW TIDE DISSIPATIVE
MODERATE ξ_0 PLUNGING BREAKER
LOW BERM — MHW — MLW
L TERRACE

HIGH TIDE REFLECTIVE
LOW ξ_0 LOW TIDE DISSIPATIVE
MODERATE ξ_0 PLUNGING BREAKER
LOW BERM   RIDGE — MHW — MLW
RUNNEL   FLAT BAR $\tan\beta = 0.01$

REFLECTIVE

STEEP BEACH FACE   BERM CREST
CUSPS   BERM   RUNNEL

REFLECTIVE DOMAIN (HIGH & LOW TIDE)
WIDE HIGH BERM (CUSPS) LOW ξ_0 — SURGING BREAKER — MLW
RUNNEL
STEEP BEACH FACE   STEP   LINEAR LOW-GRADIENT NEARSHORE PROFILE
$\tan\beta = 0.10-0.20$ $\tan\beta = 0.01-0.02$

Figure 23.   Morphodynamic states of surf zones and beaches
(a) dissipative, (b-e) intermediate, (f) reflective.

SURF ZONE AND BEACH PROCESSES

The surf zone and beach at Eastern Beach occupy only the innermost 200 metres of the Coastal Boundary Layer (Fig.1). However, it is within this comparatively narrow region that the previously modified waves ultimately experience their most rapid dissipation, perform work at the most rapid rate, and produce the most dramatic and rapid morphologic changes. After the incident waves break at the outer limits of the surf zone, their energy is transferred to other forms of motion including lower frequency standing waves and edge waves, longshore currents, and rip circulations.

Morphodynamic state of the surf zone and beach

Figure 23 shows the six most common morphodynamic states recognized by Wright and Short (in press). The general model shown in Figure 23 is a modified and updated version of the models originally discussed by Wright et al (1979 a and b) and Short (1979 a and b). The two extremes shown in Figure 23 a and f are respectively fully dissipative and highly reflective. Dissipative versus reflective conditions are distinguished on the basis of a surf scaling parameter proposed by Guza and Inman (1975) of the form

$$\varepsilon = a \, \omega^2/g \, \tan^2 \beta \tag{66}$$

where a was runup amplitude (in Guza and Inman's 1975 original equation), ω is incident wave radian frequency ($\omega = 2\pi/T$, T is period) g is acceleration of gravity and β is beach or surf zone gradient. Wright et al (1979) replaced runup amplitude a with breaker amplitude, a_b to differentiate between reflective and dissipative surf zones and we follow that approach here. Guza and Inman (1975) and Guza and Bowen (1977) showed that strong reflection

and associated standing wave motion, particularly at subharmonic frequencies, and surging breakers with high runup prevail when $\varepsilon \leq 2.0-2.5$. Wright et al (1979 a and b) and Wright (1982) found that highly reflective natural beaches in Australia consistently exhibit ε values less than 2.5-3.0; 1.5-2.0 is typical. When $\varepsilon > 2.5$, waves begin to plunge and when $\varepsilon > 20$ spilling breakers occur (Galvin, 1972). Surf zone width and turbulent dissipation of incident wave energy increase with increasing ε. In the fully dissipative extreme, high ε values ($\varepsilon = 30-500$) prevail across the entire surf zone. Breakers are exclusively spilling and decay progressively across the flat bed to become very small by the time they reach the subaerial beach (e.g. Wright et al 1982).

Each of the intermediate states shown in Figure 23 b-e possesses both dissipative and reflective elements and ε varies appreciably either across the profile or alongshore (e.g. Wright and Short, in press). Our observations of Eastern Beach indicate that this beach typically alternates between the longshore bar-trough state (Fig.23b) and the rhythmic bar-and-beach state (Fig.23c); the modal state appears to be transitional between the two. At the beginning of the experiment period, the beach was in the longshore bar-trough state; however it quickly developed into the rhythmic bar and beach state and remained in that state for the duration of the period even though the trough narrowed.

Universally, the longshore bar-trough state is distinguished by its high bar-trough relief combined with a relatively steep beach face. Waves initially break over the bar by plunging or spilling and the bar region is moderately to highly dissipative (i.e. ε is moderate to high). In contrast to the fully dissipative extreme, however, the broken waves cease their decay after passing over the steep inner edge of the bar and reform within the deep trough. The much steeper beach face is typically reflective with respect to the partially dissipated and subsequently reformed waves and

ϵ is commonly in the vicinity of 2.0. Runup is consequently relatively high. In terms of the shore-normal segregation of a dissipative bar and reflective beach face, the rhythmic bar and beach state is similar to the bar trough state. However, rhythmic longshore undulations of the crescentic bar and the subaerial beach distinguish the rhythmic bar and beach state and maintain weak to moderate rip circulation, the rips are persistently located in embayments. Spacings between shoreline protrusions, crescentic bar horns and rips are typically on the order of 200-300 metres (Short, 1979 a and b, Wright et al 1979 a and b; Wright and Short, in press).

It is interesting to note here that, despite the pronounced temporal variability of deepwater wave conditions,a characteristic feature of the Bass Strait environment, temporal variability of the beach state is comparatively small. The beach and surf zone appear to alternate largely between two similar states. This contrasts markedly with the tendency for beaches and surf zone in New South Wales which experience dramatic temporal variations which take them through the full range of all six beach states shown in Figure 23 (Short 1979 an and b; Short and Wright 1981; Wright et al 1979 a and b; Wright and Short, in press). The comparative constancy of beach state (not necessarily of shoreline position) which characterizes the Gippsland beaches is probably due to the effects of nearshore frictional dissipation on reducing the variability of breaker height as discussed in the previous section.

Figure 24 shows the profile configuration of the beach and surf zone of Eastern Beach as it appeared in the early phases of the experiment period. Figure 25 a and b show the plan configurations near the beginning and end of the experiment. Aerial oblique and ground photographs of the study site are shown in Figure 26 a and b. Although the absolute width of the trough varied considerably over the experiment period, the main features as shown in Figure 24 remained consistent. Waves broke over the shallow bar by plunging or spilling and breaker heights were on the order 0.6 - 1.2
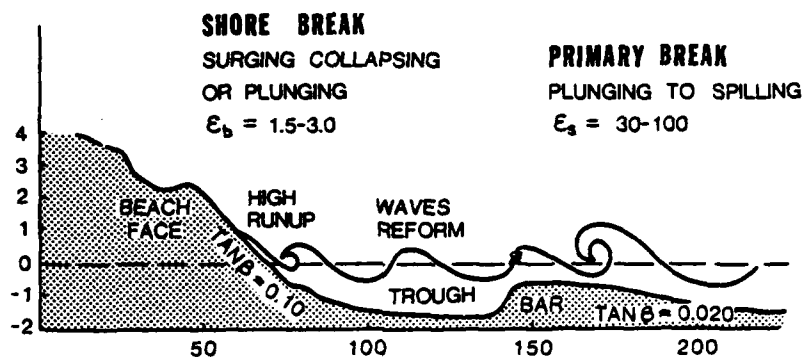
Figure 24.   Profile and major dynamic features of the Eastern
   Beach surf zone.   Based on survey of 5 May, 1981.
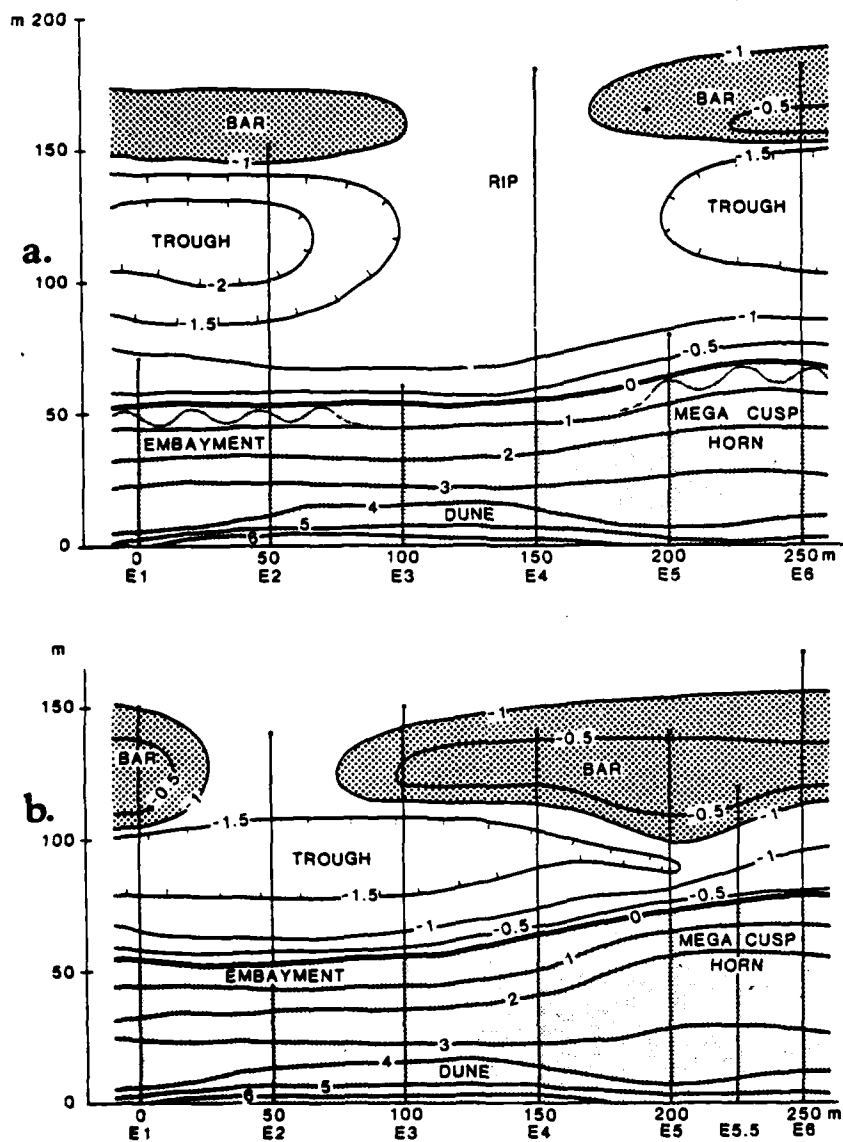
Figure 25. Plan configuration of the bar, trough and beach at the
experiment site and locations of survey lines
(a) 5 May 1981 (b) 16 May 1981.
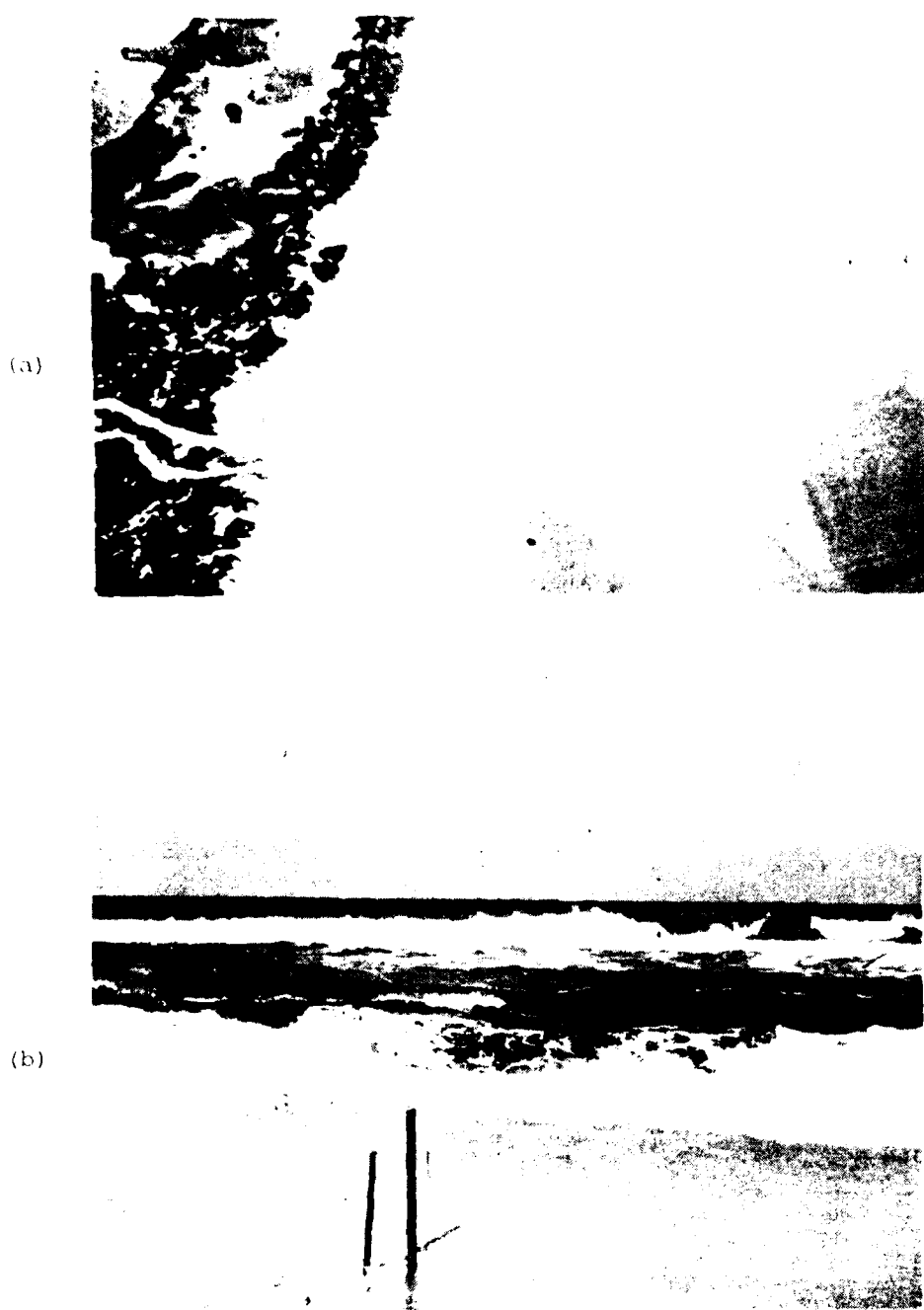
Figure 26. Aerial (a) and ground (b) views of the experiment site. The crescentic bar and associated rip pattern is apparent in (a) the outer and inner breaks are obvious in (b).

metres. The inner edge of the bar descended abruptly into the trough
which was 1.5 - 2.0 metres deep. The beach face was steep and maintained
a gradient of tan β = 0.10. Over the step at the base of the beach
there was a violent shore break (Fig.27a) followed by an explosive
surge of high runup on the beach face (Fig.27b). To distinguish the
characteristics of the outer primary break and the shore break it is
necessary to define two scaling parameters, ϵ (eq.66), an outer (or
surf) value ϵ_s computed from the primary breaker amplitude and the local
gradient of the bar crest and a beach face value, ϵ_b, computed on the
basis of the shore break amplitude and the beach gradient. These
parameters had values of ϵ_s = 30-100 and ϵ_b = 1.5-3.0 indicating, dissi-
pative and reflective conditions respectively (Fig.24).

Consistent with observations of bar-trough topographies elsewhere
(e.g. Moruya Beach, N.S.W.; Wright 1982) the profile between the upper
limit of the beach face and the inner edge of the bar conformed well to
an exponential model of the form

$$h = h_\infty (1 - e^{-\alpha x})$$

(67)

where h is local depth, x is distance seaward and h_∞ is the asymptotic
depth at which dh/dx $\sim$ 0. For the Eastern Beach case shown in Figure 24
h_∞ = 1.7m and α = 0.06. The distance from the limit of runup to the
inner edge of the bar (trough width) was about 100 metres during the
first few days of the experiment but decreased to 50 metres as the bar
migrated toward the shore.

In plan view, the beach and surf zone exhibited long crescentic
bar and beach rhythms with an average longshore wave length of 250 metres
separating shoreline protrusions, bar crescents and rips (Figs.25 and
26). Rips occupied the regions of shoreline embayments which were also
the regions of maximum trough width. In addition to the large-scale
longshore rhythms, the steep beach face exhibited beach cusps spaced

(a)

(b)

Figure 27.   A relatively high and violent shore break over the
step (a) was followed by an explosive surge of high
runup on the steep beach face (b).

at intervals of about 35 - 40 metres. These cusps were best developed
along sections fronted by the most pronounced bar-trough relief and
were poorly developed in rip bays.

Observed process signature of the surf zone

Table 6 summarizes some of the more important modes of fluid motion
which contribute to the shear stresses τ and net water transport, $\vec{V}$ in
surf zones in general. These modes of motion include: (1) oscillatory
flows corresponding directly to the incident waves; (2) oscillatory or
quasi-oscillatory flows corresponding to standing waves and edge waves
at frequencies lower than incident wave frequencies, particularly those
at subharmonic (period twice incident wave period) and infragravity
(period > 30 secs) frequencies; and (3) net circulations generated by
wave energy dissipation, specifically longshore currents, rips, and net
return flows. Our observations of different surf zones show that the
relative velocity magnitudes of these different modes of motion depend on
morphodynamic state and also vary with location within the system
(Wright 1982· Wright and Short, in press).

In highly dissipative surf zones, shoreward decay of incident
waves is consistently accompanied by shoreward growth of infragravity
standing waves. In the inner surf zone of such beaches, currents
associated with infragravity standing waves are 2 to 3 times stronger
than the orbital velocities of incident waves and are also usually
dominant over mean currents (Wright et al, 1982). On reflective beaches, incident
waves and subharmonic edge waves are strongly dominant and mean currents
and infragravity oscillations are very weak (Wright et al 1979a; Wright
1982; Wright and Short, in press). For any given set of wave conditions,
the strongest rips and associated feeder currents occur in association
with the intermediate transverse bar and rip state. It is in the presence
of the longshore-bar-trough and rhythmic bar and beach states that the
most complex process signatures prevail (Wright and Short, in press;

Wright 1982). Under these morphodynamic conditions, important roles are played by all of the modes of motion listed in Table 6.

In a succession of experimental runs, water surface, η (pressure) and horizontal currents u and v time series were recorded at different longshore and shore normal positions within the surf zone. From statistical and spectral analyses of these time series, we have estimated the velocity amplitudes corresponding to the incident waves and to sub-harmonic and infragravity standing waves, the velocities of mean currents, and the significant heights of water surface oscillations at the different frequencies. The results of these analyses from several of the more important runs are listed in Table 7 together with the positions and depths of the sensors. From an amalgamation of the data in Table 7 the process signature diagrams shown in Figures 28 and 29 have been constructed.

The example of a "process signature cross section" shown in Figure 28 is based on data from 10 May across profile 6 after the bar had migrated shoreward. The upper histograms show absolute significant heights of oscillations at incident wave (H_s), subharmonic (H_{sub}) and infragravity (H_{in}) frequencies. The lower histograms show the corresponding u and v velocity amplitudes. It is apparent from Figure 28 that motions at incident wave frequency are dominant at all locations. However, there is a shoreward growth of subharmonic and infragravity motions.

The composite plan view process signature diagram shown in Figure 29 is based on results of several runs. In this case, velocity amplitudes are shown on dimensionless scales expressed relative to the magnitudes of the bottom orbital velocities of incident waves. The general surf zone circulation pattern and the average magnitudes and directions of time-averaged currents $\vec{V}$ are also indicated. Again, the incident waves are dominant throughout the surf zone but subharmonic and infragravity oscillations become pronounced in certain regions. Specifically sub-harmonic oscillations increase in amplitude with proximity to the beach within the trough whereas the effects of the infragrav motions are

Table 6

PROCESSES WHICH CONTRIBUTE TO τ_b AND $\vec{v}$

INCIDENT WAVE ORBITAL VELOCITIES		STANDING WAVES & EDGE WAVES		NET CURRENTS AND CIRCULATION			
UNBROKEN	BROKEN	SUBHARMONIC	INFRAGRAVITY	TIDAL	LONGSHORE	RIPS	VERTICALLY SEGREGATED (e.g. RETURN FLOW)
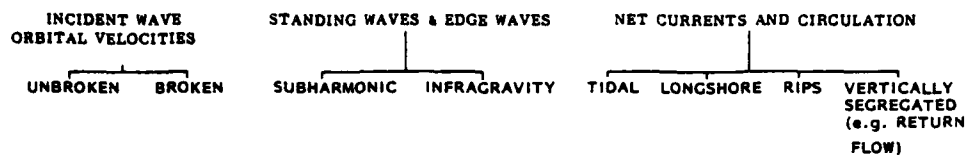
THE ABSOLUTE STRENGTHS AND RELATIVE CONTRIBUTIONS OF THESE DIFFERENT PROCESSES VARY AS FUNCTIONS OF MORPHODYNAMIC STATE AND WITH POSITION IN THE SURF ZONE.
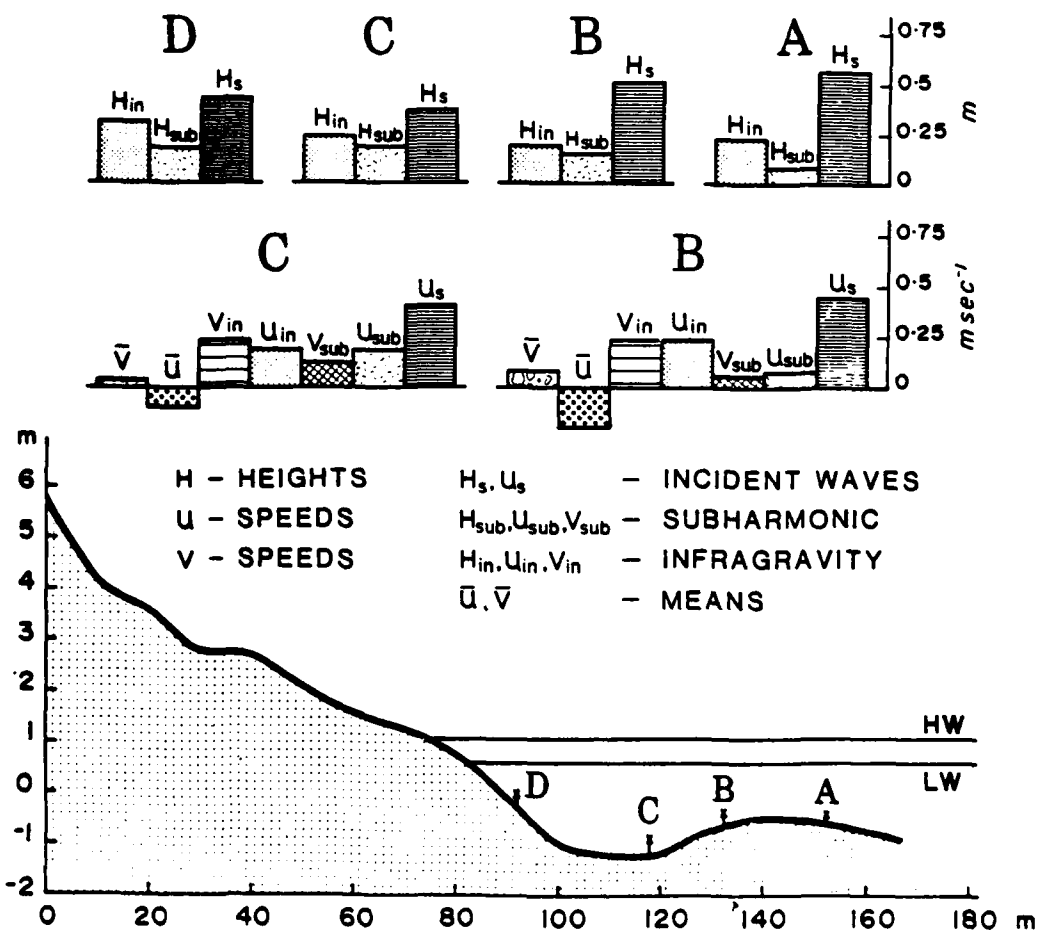

Figure 28.   Process signature cross section.
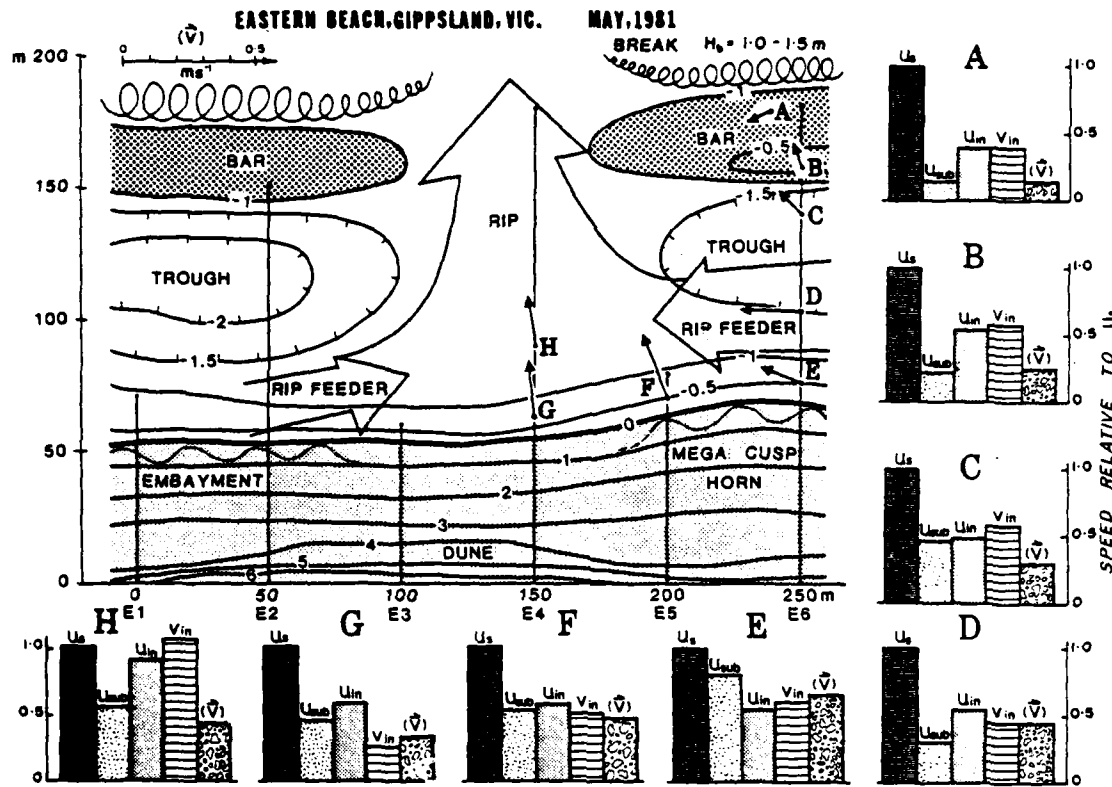
Figure 29. Composite Plan View Process signature diagram of the Eastern Beach surf zone. The bars of the graphs express the magnitudes of near bottom flows associated with different processes relative to the velocity amplitudes, u_s, of oscillations at incident wave frequency.

Table 7

Measured significant heights and velocity amplitudes of incident waves, subharmonic standing waves, infragravity standing waves, and mean currents

Run	Day May '81	Time	x (m)	h_x (m)	Pro-file No.	T_p sec	H_s m	u_s msec^{-1}	v_s msec^{-1}	H_∞ m	T_∞ sec	H_{sub} m	u_{sub} msec^{-1}	v_{sub} msec^{-1}	H_{In} m	u_{In} msec^{-1}	v_{In} msec^{-1}	$\langle U \rangle$ msec^{-1}	$\langle V \rangle$ msec^{-1}
							INCIDENT WAVES					SUBHARMONIC			INFRAGRAVITY			NET MEAN	
LE1	7	1515	17	1.0	6	12.7	0.51	0.62	0.23	2.3	5.9	0.12	0.23	0.06	0.34	0.32	0.34	-0.08	-0.13
LE1	7	1515	19	1.0	5‡	12.7	0.57	0.57	0.23	2.3	5.9	0.13	0.29	0.11	0.30	0.31	0.28	-0.24	-0.08
LE1	7	1515	16	1.0	5	13.4	0.55	0.61	0.15	2.3	5.9	0.16	0.29	0.06	0.29	0.33	0.15	-0.19	-0.08
LE3	8	1615	10	1.0	6	13.4	0.45	0.47	0.39	2.6	5.5	0.14	0.37	0.30	0.28	0.25	0.26	-0.23	-0.17
LE3	8	1615	40	2.0	6	14.2	0.61	0.35	0.68	2.6	5.5	0.21	0.19	0.41	0.33	0.31	0.36	-0.12	-0.07
LE3	8	1615	10	0.8	4	14.2	0.46	0.47	0.29	2.6	5.5	0.08	0.14	0.08	0.21	0.24	0.20	-0.09	-0.19
LE4	11	1130	115	1.4	6	13.9	0.59	-	-	2.5	5.2	0.09	-	-	0.21	-	-	-	-
LE4	11	1130	90	1.5	6	13.9	0.44	0.43	0.27	2.5	5.2	0.14	0.10	0.08	0.17	0.21	0.24	-0.13	0.02
LE4	11	1130	70	1.8	6	17.0	0.36	0.39	0.25	2.5	5.2	0.18	0.18	0.11	0.21	0.19	0.23	-0.11	-0.03
LE4	11	1130	35	1.0	6	13.3	0.45	-	-	2.5	5.2	0.15	-	-	0.26	-	-	-	-
LE5	11	1430	115	1.4	6	17.0	0.57	-	-	3.0	5.9	0.09	-	-	0.41	-	-	-	-
LE5	11	1430	90	1.5	6	17.0	0.49	0.41	0.33	3.0	5.9	0.11	0.064	0.068	0.15	0.18	0.24	-0.18	-0.30
LE5	11	1430	70	1.8	6	17.0	0.42	0.35	0.38	3.0	5.9	0.16	0.12	0.12	0.16	0.18	0.24	-0.24	-0.28
LE5	11	1430	35	1.0	6	17.0	0.52	-	0.24	3.0	5.9	0.18	-	0.11	0.20	-	0.23	-	-0.23
LE6	11	1615	115	1.4	8	14.6	0.60	-	-	3.4	6.6	0.10	-	-	0.20	-	-	-	-
LE6	11	1615	90	1.5	6	14.6	0.51	0.41	0.32	3.4	6.6	0.11	0.60	0.08	0.18	0.19	0.22	-0.20	-0.33
LE6	11	1615	70	1.8	6	14.6	0.45	0.46	0.13	3.4	6.6	0.16	0.13	0.05	0.17	0.18	0.08	-0.21	0.03
LE6	11	1615	35	1.0	6	14.6	0.52	-	0.28	3.4	6.6	0.18	-	0.11	0.20	-	0.19	-	-0.18
LE7	11	1815	90	1.5	6	16.2	0.49	0.40	0.31	3.7	6.4	0.09	0.07	0.06	0.18	0.21	0.18	-0.19	-0.27
LE7	11	1815	70	1.8	6	16.2	-	0.42	0.11	3.7	6.4	-	0.13	0.04	-	0.17	0.06	-0.19	0.02
LE7	11	1815	35	1.0	6	13.9	0.49	-	0.29	3.7	6.4	0.16	-	0.12	0.20	-	0.20	-	-0.22
LE8	11	2157	90	1.5	6	13.9	0.47	0.40	0.30	3.4	5.7	0.13	0.07	0.07	0.21	0.27	0.29	-0.17	-0.31
LE8	11	2157	35	1.0	6	13.9	0.47	-	0.28	3.4	5.7	0.27	-	0.11	0.28	-	0.27	-	-0.22
LE9	11	2326	90	1.5	6	14.6	0.52	0.42	0.33	3.1	5.6	0.12	0.07	0.06	0.23	0.26	0.27	-0.21	-0.26
LE9	11	2326	35	1.0	6	14.6	0.53	-	0.30	3.1	5.6	0.16	-	0.12	0.27	-	0.27	-	-0.25

most pronounced in the rip region. We will discuss each of the processes separately.

Incident waves and breakers

From Table 7 two important points concerning the behaviour of surf zone oscillations at incident wave frequency can be made. The first feature deserving mention is the comparative constancy of wave heights from the inner edge of the bar, across the trough to the shore break. (Fig.26b). This tendency for the waves to maintain their height after breaking and partially dissipating over the outer portion of the bar contrasts markedly with patterns observed in fully dissipative surf zones (e.g. Wright et al 1982). In low gradient dissipative surf zones, surf height decays progressively shoreward maintaining a constant height-to-depth ($\gamma = H_b/h$) ratio (Wright et al 1982). However, it is clear from Table 7 that after passing over the bar, the surf at Eastern Beach ceased to decay and, instead, experienced some subsequent shoaling over the inner margins of the trough which resulted in the shore break being somewhat higher than the waves over the inner edge of the bar (Fig.27a).

The second point is that the height of the shore break varied by only a few centimetres throughout the study period despite appreciable temporal variations in deepwater height, H_∞. Some of this reduction in shore break variation was undoubtedly due to the process of nearshore frictional "filtering" previously described. However, much of the filtering was almost certainly due to the process of partial dissipation over the bar. It would appear that this pronounced bar-trough topography is effective in limiting the heights of the waves which actually reach the beach face.

Standing waves and edge waves

The whole or partial reflection of waves from the shore produces standing waves consisting of the combination of incident and reflected waves. Depending in part on the degree to which the reflected wave is

refracted as it propagates into deep water, standing waves may be either leaky mode standing waves (e.g. Suhayda, 1974) or trapped edge waves (e.g. Eckart, 1951; Guza and Davis. 1974). In the leaky mode case, reflected energy is reradiated back to sea without being trapped inshore and, for normally incident oscillations, there is no shore-parallel motion or amplitude variation. Alternatively, reflected energy may be trapped inshore by refraction to produce edge waves which may grow through a weak resonant instability by extracting energy from incident waves (Guza and Davis, 1974).

The theory of edge waves is discussed with specific reference to beaches by Bowen and Inman (1969); Guza and Davis (1974); Ursell (1951); and Guza and Bowen (1974). Edge wave radian frequency, ω_e (=$2\pi/T_e$, where T_e is edge wave period) and alongshore wave number, k_e (=$2\pi/L_e$ where L_e is alongshore edge wave length) on a beach of constant slope β are related by Eckart's (1951) dispersion relationship,

$$\omega_e^2 = gk_e (2n + 1) \tan \beta \qquad (68)$$

where n is edge-wave mode number (n = 0,1,2,3 ...), designating the number of nodal positions (zero crossings) in the x direction (perpendicular to the shore). For the case of an exponential inshore/beach profile, Ball (1967) gives the edge wave dispersion relationship in the form,

$$\omega_e^2 = \tfrac{1}{4} g\alpha h_\infty \{(2n + 1) (\alpha^2 + 4k_e^2)^{\frac{1}{2}} - \alpha(2n^2 + 2n + 1)\} \qquad (69)$$

where α and h_∞ are defined by equation 67.

Normal to the shore, the amplitudes of both leaky mode standing waves and edge waves vary from a maximum at the shore where the first antinode occurs to zero at a succession of nodes which are separated by antinodes of progressively diminishing amplitude. The variations in amplitude normal to the shore follow the offshore dependence functions which are

(a) Leaky modes

$$F_L (x) = J_o \left[2 \left(\frac{\omega^2}{g \tan \beta} x \right)^{\frac{1}{2}} \right] \qquad (70)$$

(Suhayda, 1974) where subscript L refers to leaky mode and J_o is the zero-order Bessel function

(b) Edge waves

$$F_e(x) = \exp (-k_e x) \ Ln \ (2k_e x) \qquad (71)$$

where Ln is the Laguerre Polynomial of order n which is the same as the edge wave mode number.

For leaky mode standing waves, standing edge waves, and longshore-progressive edge waves the space and time variations of surface elevation η, and currents u and v as expressed by the single-valued velocity potential ϕ ($\eta = -\frac{1}{g} \frac{\partial \phi}{\partial t}$, $u = -\frac{\partial \phi}{\partial x}$, $v = -\frac{\partial \phi}{\partial y}$)

(a) Leaky mode

$$\phi_L = \frac{a_L g}{\omega_L} F_L (x) \sin \omega_L t \qquad (72)$$

(b) Edge wave standing in longshore direction

$$\phi_e = \frac{a_e g}{\omega_e} F_e (x) \cos k_e y \cos \omega_e t \qquad (73)$$

or

(c) Edge wave progressive alongshore

$$\phi_e = \frac{a_e g}{\omega_e} F_e (x) \sin (k_e y - \omega_e t) \qquad (74)$$

where a_L and a_e are the standing wave amplitudes at the shoreline.

The simplest edge wave model is that of the synchronous edge wave with frequency ω_e equal to the frequency ω_i of the forcing incident wind waves or swell (Bowen and Inman, 1969; Guza and Inman, 1975). The synchronous edge wave is also the highest frequency edge wave likely to occur on a beach. Although synchronous edge waves have been produced in the laboratory, they have not been shown to be important on natural beaches. Guza and Davis (1974) have shown that it is more common for edge waves with frequencies lower than ω_i to grow by a weak resonant interaction between the incident wave and two edge waves of frequencies $\omega_{e(1)}$ and $\omega_{e(2)}$ travelling in opposite directions alongshore. In this resonant triad, the conditions $\omega_{e(1)} + \omega_{e(2)} = \omega_i$ and $L_{e(1)} = L_{e(2)}$ must prevail. Guza and Davis (1974) and Guza and Bowen (1977) found that the most easily excited edge wave pair is that of subharmonic edge waves of modes n = 0,0, in which $\omega_{e(1)} = \omega_{e(2)} = \omega_i/2$. In combination, these two edge waves yield a standing subharmonic edge wave with a period equal to twice the incident wave period. Our observations of reflective beaches in Australia indicate that subharmonic edge waves are normally well developed on those beaches and that they produce cusps spaced at one-half the edge wave length (Wright et al 1979; Wright 1982; Wright and Short in press).

Subharmonic oscillations do not appear on highly dissipative beaches but large-amplitude infragravity standing waves with periods of 100-200 seconds are invariably present and dominate the inner surf zones of those beaches (Wright et al 1982; Wright 1982). Recent studies by Holman (1981) and Huntley et al (1981) suggest that these infragravity or "surf beat" oscillations are probably edge waves. Observations from intermediate topographies such as that which prevailed at Eastern Beach, typically reveal lower amplitude and higher frequency (period = 30-60 secs) infragravity standing waves as well as subharmonic oscillations near the beach (Wright et al 1979; Chappell and Wright 1979; Wright 1982).

Power spectra and cross spectra of water surface elevation, η,
and shore normal current, u, from the bar trough, and step regions of
the surf-zone are shown in Figures 30-32. Frequencies which are standing
as interpreted from phase angles of π/2 between η and u are indicated by
the horizontal bars. The spectra show dominance of energy at swell
frequency but with appreciable standing wave energy over a band encom-
passing both subharmonic and infragravity frequencies. From Table 7 the
subharmonic oscillations typically had heights of 0.10 m to 0.25 m and
associated velocity amplitudes of 0.10 m sec^{-1} up to 0.60 m sec^{-1}.
Infragravity oscillations had heights of 0.15 m to 0.40 m and velocity
amplitudes (u and v) on the order of 0.20 m sec^{-1} to 0.35 m sec^{-1}.
However, as would be expected for standing waves and for edge waves
standing alongshore, and hence exhibiting alternate nodes and antinodes,
the heights and velocity amplitudes of the infragravity and subharmonic
oscillations varied considerably with location in the surf zone as shown
in Figures 28 and 29.

The subharmonic oscillations were identified as such on the basis
of their having significant standing wave energy at frequencies close
to one half the frequency of the incident swell. These frequencies were
typically in the range of 0.038 - 0.056 hz (periods of 18 to 26 seconds).
It must be noted, however, that there was not always a clear separation
between what we refer to as subharmonic and the longer period swell or
between "subharmonic" frequencies and the higher frequency infragravity
motions. There was in fact, a broad band of standing wave energy from
0.056 hz, through to about 0.015 hz. Having expressed this caveat, we
will proceed on the assumption that the subharmonic oscillations are
edge waves since observations from other reflective and intermediate
beaches suggest that they are (Wright et al 1979; Wright 1982).

From Figure 29 the velocity amplitudes associated with subharmonic
frequencies are seen to decay seaward from a maximum above the step
indicating that these oscillations are largely confined to the vicinity

(a)

(b)
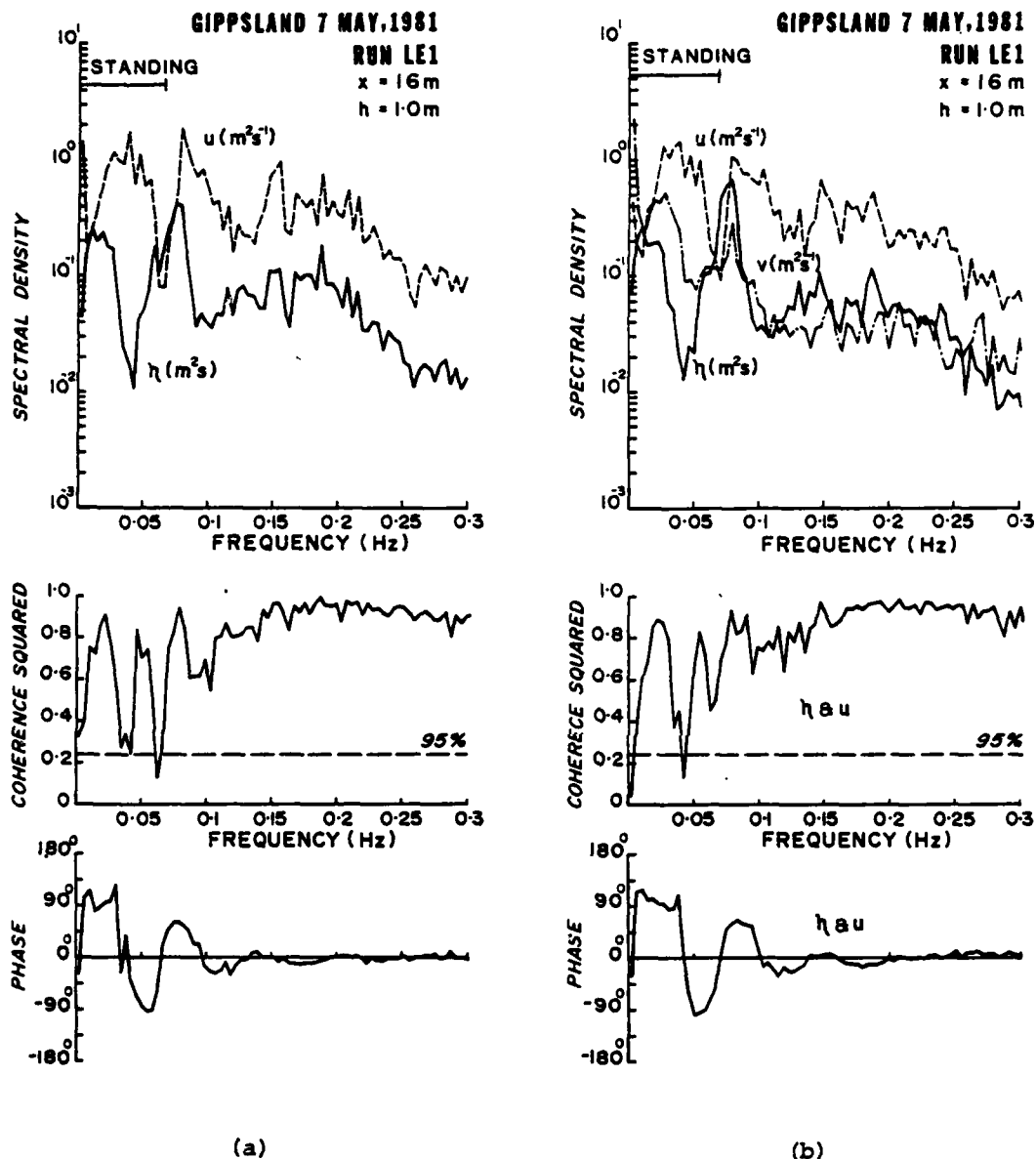
Figure 30. Power spectra and cross spectra of η, u, and v from
time series recorded from the step at the base of the
beach, on line 5(a) and 5½(b). A phase lag of 90°
indicates standing motions Δt = 1.5 sec, df = 12.

(a)

(b)
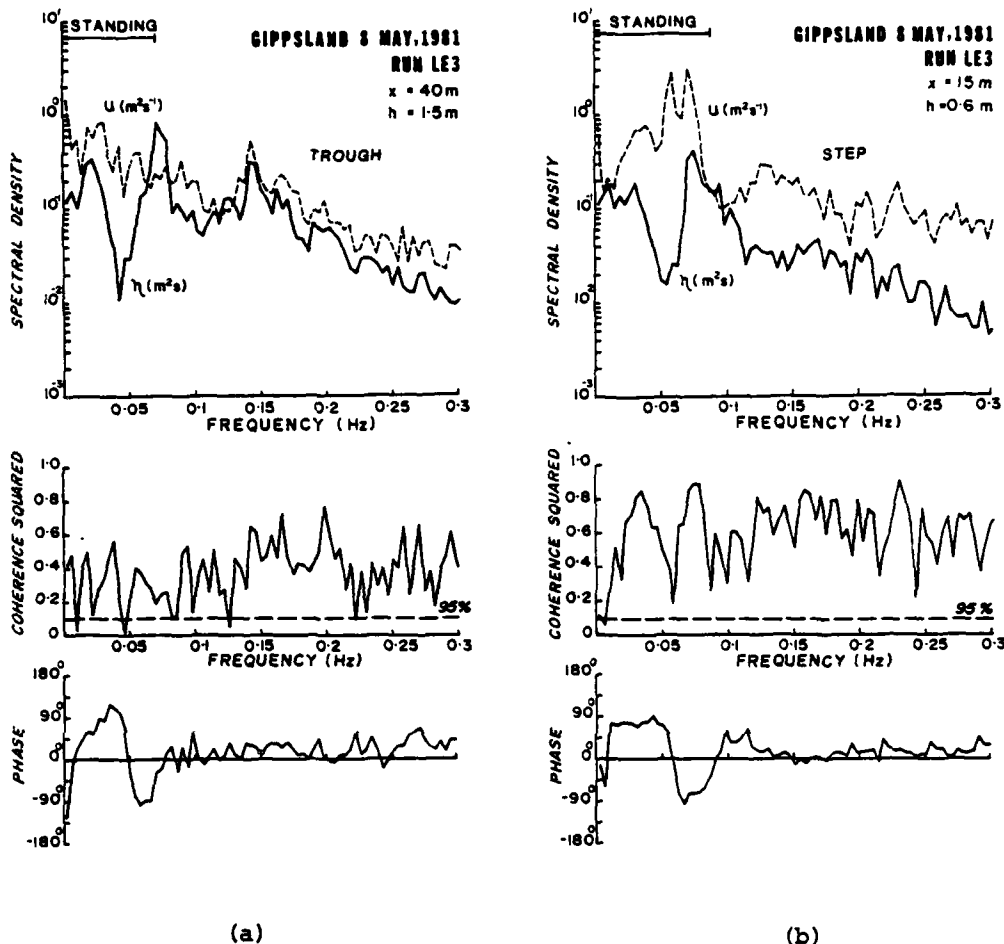
Figure 31.   Power spectra and cross spectra of η and u from time
series recorded simultaneously in the trough (a) and
over the step (b) Δt = 1.5 sec, df = 12.
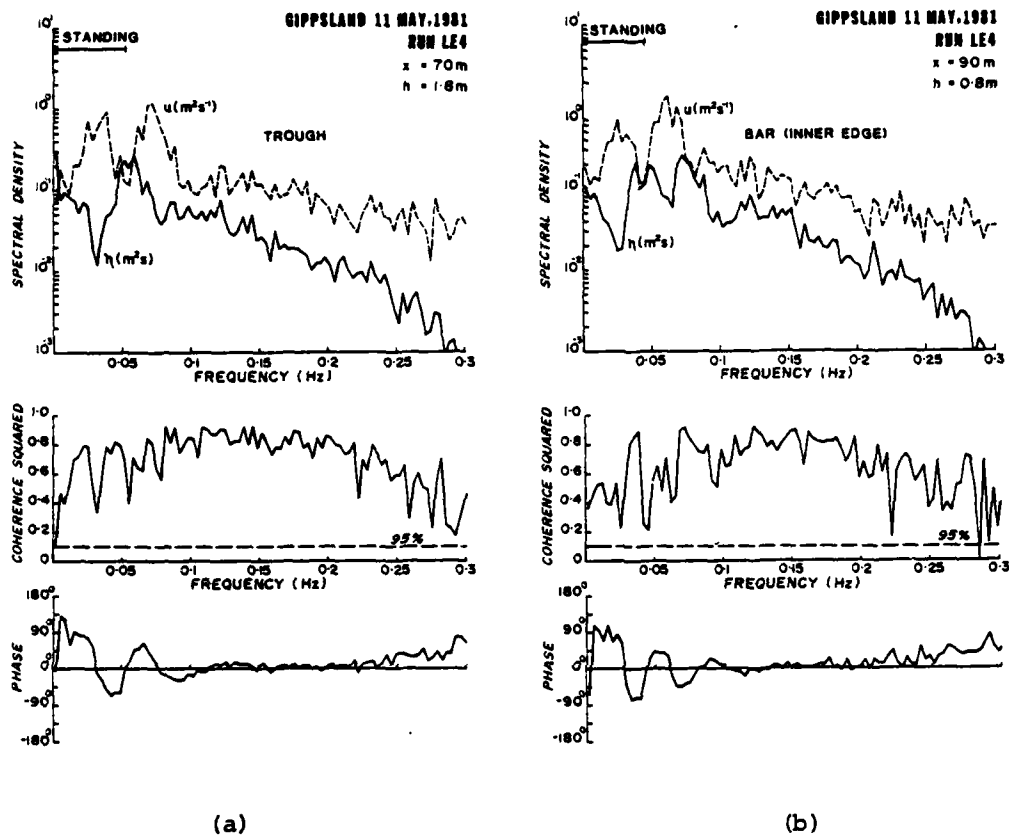
Figure 32. Power spectra and cross spectra of η and u from time series recorded simultaneously in the trough (a) and over the inner edge of the bar (b) Δt = 1.5 sec, df = 12.

of the beach face. This is roughly consistent with expectations for rule

zero edge wave which is the most probable for a reflective beach face

(Guza and Davis, 1974). For a 24 second (0.042 hz) subharmonic $n = 0$ edge

wave on the observed beach face slope of 0.10, equation 68 gives an edge

wave length of 90 metres. This is close to, but exceeds, twice the

observed cusp spacing of 35 to 40 metres. An edge wave with a period of

22 seconds would have an alongshore length of 76 metres which is very

close to twice the cusp spacing. However, Wright (1982) has found that on

reflective and bar-trough beaches where the beach face and inner surf

zone profile fits the exponential model expressed in equation 67 the

cusps spacing fits most closely to the edge wave lengths predicted on the

basis of Ball's (1967) equation (eq.69). On this basis using the observed

$\alpha = 0.06$ and $h_{\infty} = 1.7$ m a 24 second, $n = 0$ edge wave would have a length of

73 metres. Regardless of whether we use equation 68 or 69 it appears very

likely that the cusps which occurred on the reflective beach face in the

lee of the offshore bar were formed by subharmonic edge waves standing

alongshore. This is consistent with numerous observations on natural

reflective and intermediate beaches (Huntley and Bowen, 1979; Wright

et al 1979; Wright 1982) and in the laboratory (Guza and Inman 1975) that

standing subharmonic edge waves form cusps spaced at one half the edge

wave length when conditions are sufficiently reflective.

The infragravity standing waves in the Eastern Beach surf zone

occurred at much higher frequencies and were of considerably lower

amplitude than those commonly observed in highly dissipative surf zones

(e.g. Wright et al 1982). Typical periods of the infragravity oscillations

at Eastern Beach were on the order of 35-60 seconds (0.028 - 0.017 hz).

These frequencies are very similar to those observed in the presence of

bar-trough topographies elsewhere (e.g. Moruya Beach N.S.W.: Wright et al

1979; Chappell and Wright 1979; Wright 1982). These intermediate

frequency infragravity standing waves have been discussed by Chappell and

Wright (1979) and Wright (1982) who suggest that the frequencies may be

constrained or selected by the dimensions of the trough. This suggestion

has some credibility in the Eastern Beach case since the natural frequency

of the trough is estimated to be on the same order as the observed infra-

gravity frequencies.

It is tempting to suggest that the rhythmic spacings of the larger

scale surf zone features such as rips, crescentic bar "horns" and shoreline

protrusions are related to long infragravity edge waves. We presented

arguments for this in earlier papers (Wright et al 1979; Wright 1982).

Recent work by Holman and Bowen (1982) has shown how rhythmic crescentic

bar topography such as that which prevails at Eastern Beach as well as more

complex quasi-rhythmic surf zone topographies can be explained by drift

patterns related to the interactions between two edge wave modes. The

simple crescentic bar and rhythmic beach pattern like that at Eastern

Beach is considered to represent an equilibrium response to a standing

edge wave composed of two edge wave modes of the same frequency travelling

in opposite directions (Holman and Bowen, 1982). This will produce

longshore topographic periodicities with wave lengths of one half the

length of the individual component edge waves. For the observed averaged

surf zone beach gradient of about 0.03, a 60 second, mode 1 edge wave

in the Eastern Beach surf zone should, on the basis of equation 68, have

had an alongshore wave length of about 500 metres which is close to twice

the alongshore wave length of the larger scale surf zone features. Such

edge waves must extend well seaward of the bar crest.

A comparison of pressure (or η) spectra from the step, trough and

bar regions of the surf zone is shown in Figure 33. The important features

are the sharp infragravity peaks over the step and bar accompanied by an

energy trough at the same frequency in the centre of the topographic trough.

This suggests the presence of shore normal antinodes at the beach and over

the bar with the intervening node located in the trough. This is consistent

with the logical and widely held notion that troughs should be best formed

in the presence of the stronger horizontal currents of the nodal region
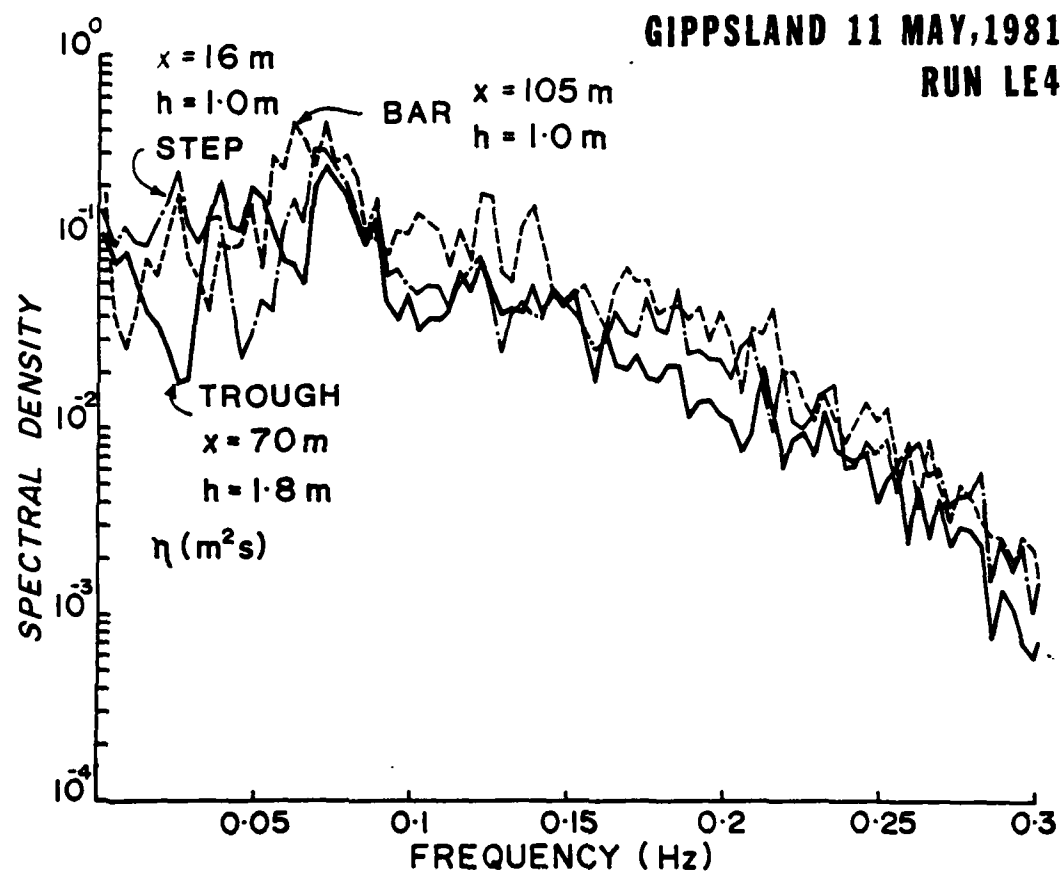
Figure 33.   Power spectra of water surface elevation, η, time series
              recorded simultaneously over the bar, in the trough and
              over the step, Δt = 1.5 sec, df = 12.   Note that infra-
              gravity peaks over the bar and over the step are
              accompanied by an energy "trough" at the same frequency
              within the topographic trough.
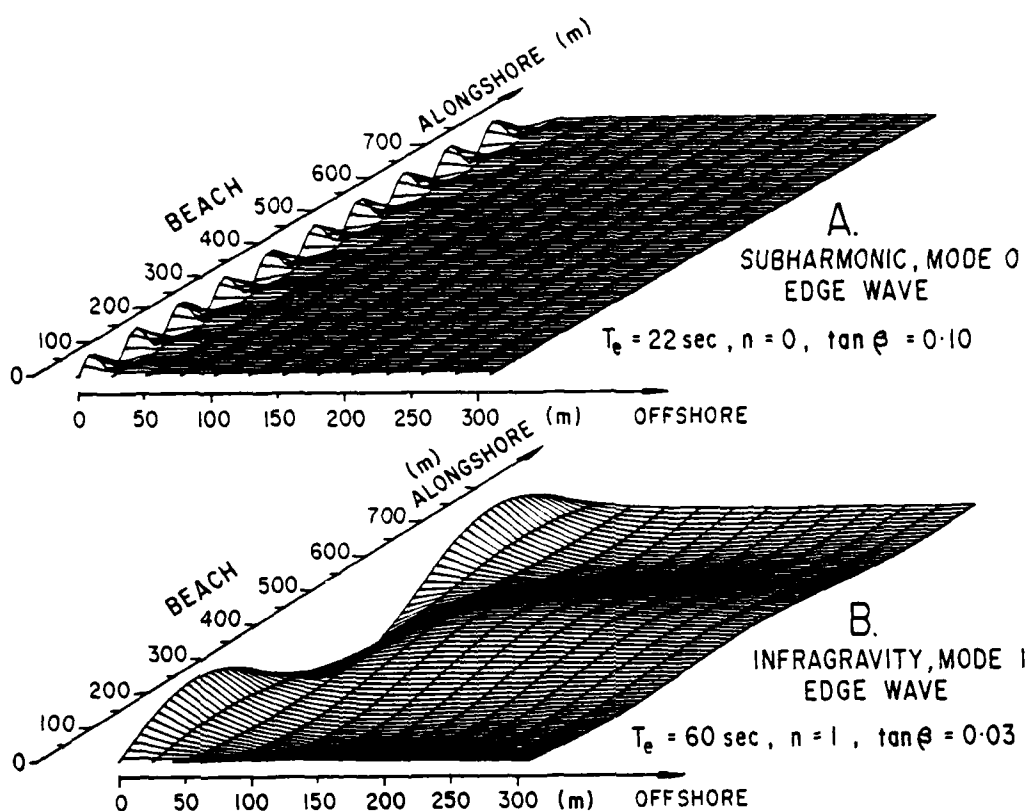
Figure 34. Instantaneous water surface topographies associated with
(a) a subharmonic, n = 0 edge wave, and (b) an infragravity,
n = 1 edge wave computed from equations (68) and (73). It
is likely that these two edge waves may coexist in the
presence of bar-trough topography.

whereas bars should accumulate beneath antinodes where drifts are weaker.
In the shore parallel dimension, both u and v components of the infra-
gravity motions intensify in the embayment region where the rip is located
(Fig.29; Table 7), suggesting that this is probably the location of the
shore parallel node. A comparison of the possible instantaneous water
surface topographies associated with the co-existing subharmonic and
infragravity edge waves is shown in Figure 34.

Surf-zone circulation and net currents

The net (time averaged) circulation features observed in the Eastern
Beach surfzone were of three general types (1) vertically segregated shore
normal drifts; (2) horizontally segregated rip circulation; and
(3) longshore currents. The vertically segregated drifts were prominent
over the bar and within the trough in regions away from rips. This form
of circulation was similar to that described for the dissipative surf zone
at Goolwa, South Australia by Wright et al (1982) and was characterized by
net onshore transport in the surface layer and net offshore transport
near the bottom. Onshore wind stress probably played in a role in main-
taining this form of circulation. ̇.e nature of this circulation is
illustrated by the results of a vertical profile of shore-normal (u)
velocity measured in the trough on profile 6 at a depth of 2.0 metres.
Figure 35 shows the time series of u, filtered with a 100 second filter
to remove wave effects, from 0.04 m 0.22 m 0.45 m and 0.91 m above the
bed. Closest to the bed, flow is seen to be exclusively offshore whereas
it is predominantly onshore on 0.91 m above the bed. Onshore transport
prevailed throughout the upper metre of the water column. As indicated
by the values of time averaged near bottom velocities ($<u>$) in Table 7,
flows below 0.30 m above the bed were seaward throughout the study period.

Since onshore transports in the upper half (or more) of the water
column were substantially stronger than seaward transports near the bed,
it may be concluded that the depth averaged transport was shoreward in

GIPPSLAND, VIC. 8 MAY, 1981
4 SHORENORMAL FLOWMETERS

I cm/min , ±0·5 m/s , 2V , 100 sec. Filter
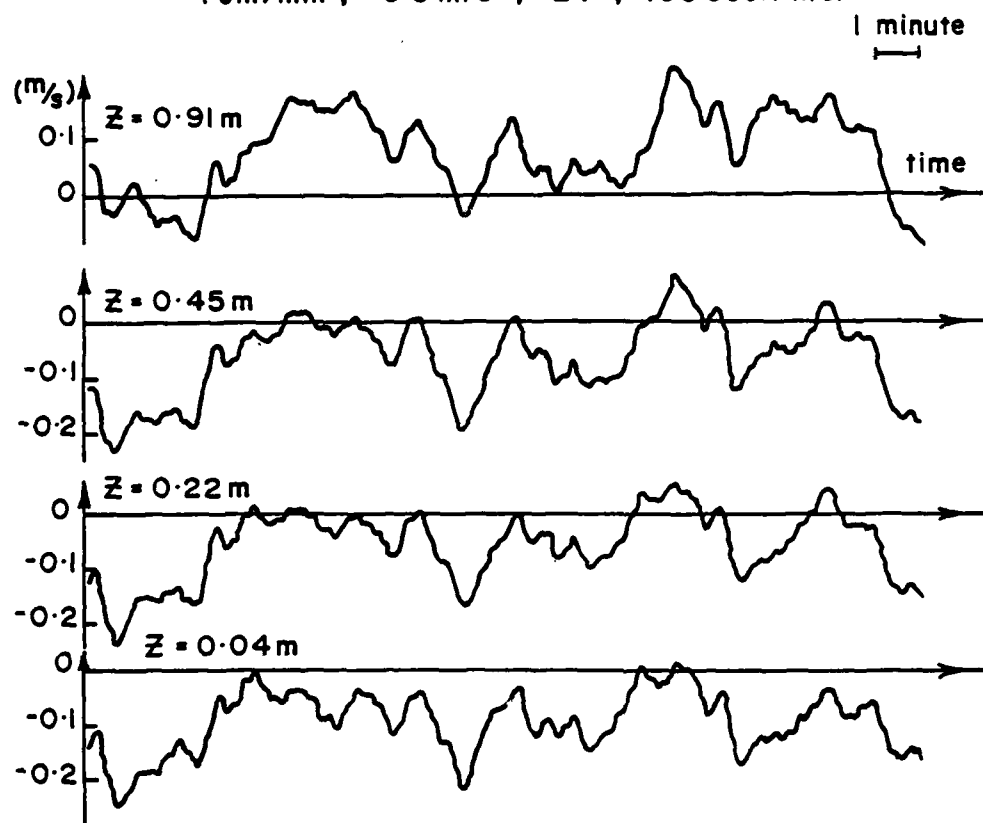
Figure 35. Shore-normal current (u) time series from 4 elevations showing vertical segregation of onshore (upper level) and offshore (lower levels) flows, an electronic filter with a 100 second time constant has been applied to remove incident waves.

the vicinity of profile 6 which was situated near a shoreline protrusion.
This excess onshore transport was accommodated by the net horizontal
circulation pattern shown in Figure 29. Water flowed alongshore within
the trough and turned offshore as a wide rip in the region of profile 4.
Within the rip, flow was seaward at all depths. Unfortunately, we were
unable to obtain a vertical velocity profile owing to the strong current
drag on the vertical mast. However, near bottom (0.20m above the bed)
velocities of up to 0.30m sec^{-1} were recorded and dye tracking of surface
flows indicated stronger surface flows. However, the observed rip
velocities were substantially weaker than those which normally occur in
association with the transverse bar and rip type of topography (Wright
and Short in press). Despite the fact that the rip was not excessively
strong, it was nevertheless effective in causing seaward bedload transport
of sand as evidenced by the presence of seaward-migrating dune bedforms.

For a few days during the experiment period, strong longshore currents
prevailed within the trough related in part to oblique wave incidence and
in part to the "feeding" of the downdrift rip. We succeeded in obtaining
vertical velocity profiles of these currents, some examples of which are
shown in Figure 36. Although longshore currents over simple topography
have been the subject of considerable attention (e.g. Komar 1975; 1976;
Longuet-Higgins, 1970a and b) there is very little field data on the nature
of longshore currents within pronounced troughs or on the vertical current
structure. Some more detailed analysis and discussion of our data is
therefore warranted.

Time averaged longshore current velocities ($<v>$) near the surface
exceeded 0.5m sec^{-1} in some runs while as close as 0.075m above the bed
(above the level of ripple troughs) velocities were still as high as
0.25m sec^{-1} (Fig.36). Although these longshore velocities were on the
same order of magnitude as the wave orbital velocities, the bottom boundary
layer was completely dominated by the waves which acted in the shore
normal direction orthogonal to the longshore currents. This is indicated

LONGSHORE VELOCITY PROFILE , MAY, 1982

EASTERN BEACH, LAKES ENTRANCE, GIPPSLAND.

△ 10 SEC FILTER, SAMPLED EVERY 6 SECS.
* 100 SEC FILTER, SAMPLE INTERVAL 1 MIN.
□ 100 SEC FILTER, SAMPLE INTERVAL 1 MIN.
x FAST, SAMPLE INTERVAL 6 SECS.
o FAST, SAMPLE INTERVAL 6 SECS.
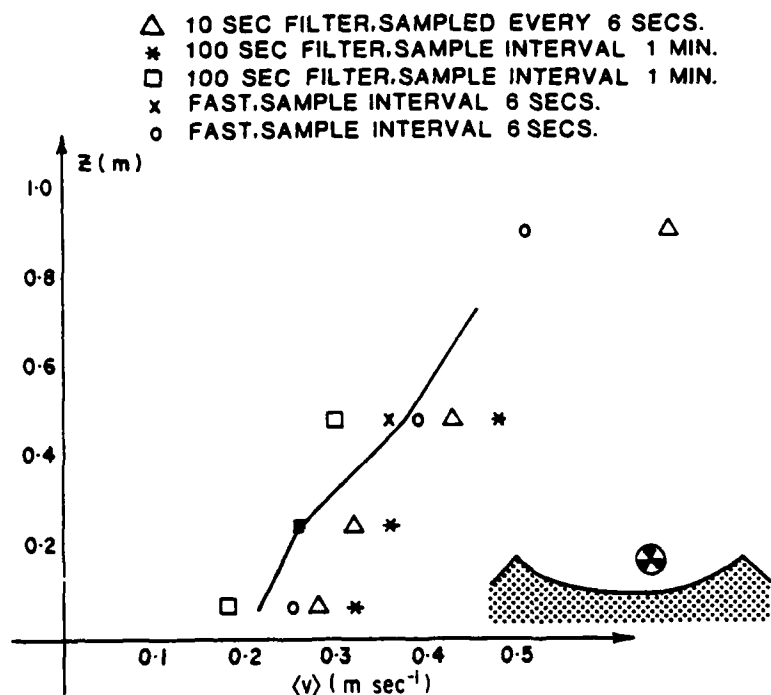
Figure 36.   Vertical profile of time-averaged longshore current
              velocity, <v>, as recorded within the trough of
              Eastern Beach in a succession of runs. The position of
              the lowest flow meter is shown.

by two lines of evidence: (1) the bed forms were fully developed, sharp-crested wave induced ripples (heights, $\eta_r \approx 0.08m$) with long crests aligned shore parallel; and (2) vertical profiles of suspended sediment concentration (discussed further in the next subsection) were perfectly exponential similar to those observed under pure wave motion and concentration magnitudes were not significantly larger than would be expected from waves alone.

On the other hand, it appears that the longshore current profiles were strongly influenced by the vortices generated by the wave oscillations over the ripples since they were not at all logarithmic (Fig.36). Between the elevations of $z = 0.07m$ and $0.30m$ above the bed, which is the domain of the vortices shed by the ripples, the longshore current velocity was nearly constant. This is understandable since the time averaged longshore shear stresses, τ must be staticly determined, as in steady flows, the velocity gradients, $d <v>/dz$, must adjust to the total eddy viscosity, ν_t, that is

$$\frac{d<v>}{dz} = \tau/\rho\nu_t \tag{75}$$

and hence be small where ν_t is large. The wave induced vortices cause a very large exchange of momentum for a given shear rate, and thus produce a large eddy viscosity. This strong effect of the vortices must be related to the fact that the axes of the vortices are oriented parallel to the direction of the longshore current. The boundary layer structure is apparently entirely different in rip currents where wave oscillations parallel the mean flow producing a "roller effect". In order to model the current flow near the bed, we will consider the mean longshore flow as a steady current which only interacts with the waves by way of the eddy viscosity, ν_t, which consists of two components ($\nu_t = \nu_w + \nu_c$): a component, ν_w attributable to the waves and a component ν_c attributable to the current.

Equation 75 relating the time average longshore velocities to shear stress then becomes

$$\rho \; (\nu_w + \nu_c) \; \frac{d<v>}{dz} = \tau \; (z) \tag{76}$$

The eddy viscosities, ν_w and ν_c are related to vertical velocity fluctuations only and are thus not vectors in the x-y plane.

We assume the distribution of shear stress to be linear

$$\tau(z) \;\; = \;\; \tau_c \; (1-z/h) \tag{77}$$

where τ_c is the longshore shear stress at the bed. The contribution of the longshore current to eddy viscosity is

$$\nu_c \;\; = \;\; C_c \; v_{*c} z (1-z/h) \tag{78}$$

where v_{*c} is the longshore friction velocity

$$v_{*c} \;\; = \;\; \sqrt{\tau/\rho} \tag{79}$$

For "pure" steady flow, the constant C_c is equal to von Karman's constant ($\kappa = 0.4$).

The wave-induced eddy viscosity ν_w can be evaluated from the empirical formula

$$\nu_w \;\; = \;\; \frac{C_w \; u_{*w} \; z}{1+1.34 (\tfrac{1}{2} f_w)^{\frac{1}{2}} \frac{z}{\delta} \exp(z/\delta)} \tag{80}$$

where f_w is the friction factor, δ is boundary layer thickness and u_w is wave friction velocity. Equation 80 was obtained by Lundgren (1972) from analyses of boundary layer measurements subsequently published by Jonsson and Carlsen (1976).

We note that ν_w is initially proportional to z but then decays exponentially with z farther from the boundary with a length scale of decay equivalent to the boundary layer thickness δ.

Exponential decay was observed by Nakato et al (1977) and MacDonald (1977) in measurements of vertical velocity fluctuations, w_{rms}, in oscillatory boundary layers (Fig.37). Their measurements also show that the vertical length scale, ℓ, of suspended sediment concentration profiles $(c(z) = C_o e^{-z/\ell}$; where C_o is concentration at the bed) are identical to those of the velocity distribution. The correspondence between w_{rms} and c is shown in Figure 37. Although we have no measurements of w_{rms}, we do have direct field measurements of c(z) (discussed further in the next subsection) obtained simultaneously with the longshore current profiles. We can use these data to obtain an estimate of the length scale, ℓ, (since c(z) showed consistent exponential decay with z) from

$$\ell = \left[- \frac{d \ln c}{dz} \right]^{-1} \approx 0.093 \text{m} \tag{81}$$

The length scale, ℓ, can then be used to replace δ in equation 80.

By replacing δ with ℓ, and inserting ν_c and ν_w as obtained from (78) and (80) into equation 76 we get

$$\frac{d\langle v \rangle}{dz} = \frac{v_{*_c}^2 (1-z/h)}{\nu_w + \nu_c} \tag{82}$$

or

$$\langle v_2 \rangle - \langle v_1 \rangle = \int_{z_1}^{z_2} \frac{v_{*_c}^2 (1-z/h)}{\nu_w + \nu_c} \, dz \tag{83}$$

where $\langle v_1 \rangle$ and $\langle v_2 \rangle$ are the longshore velocities at two elevations, z_1 and z_2 respectively. If C_w and C_c are known, equation 82 will determine v_{*_c} from any pair of measured velocities. However, we cannot consider
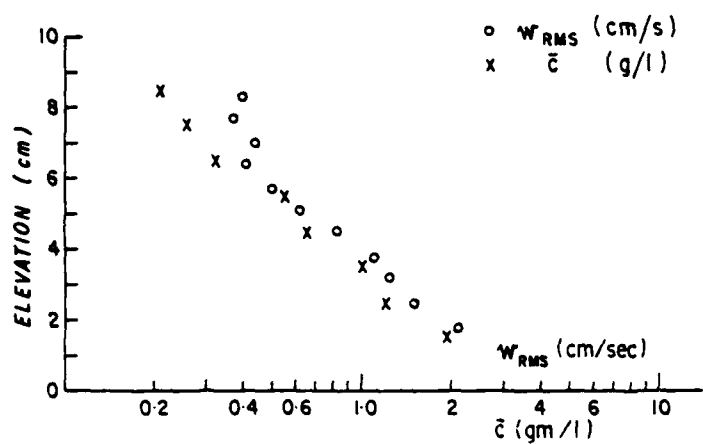
Figure 37. Vertical distribution of vertical velocity, W_{rms}, and suspended sediment concentration $\bar{c}$ after Nakato et al (1977) and MacDonald (1977). This graph indicates that $\bar{c}$, when known, provides an acceptable surrogate for W_{rms}.

$C_w = C_c = \kappa = 0.4$ since this will greatly underestimate the relative importance of ν_w and lead to a poor prediction of the velocity profile as illustrated in Figure 38. However, if we set $C_w = 0.4$ and adjust C_c and ν_{*c} a good fit is obtained for $C_c = 0.1$ and $\nu_{*c} = 0.24m\ sec^{-1}$. Alternatively, as shown in Figure 38, an equally good fit is found for the combination $C_c = 0.4$, $C_w = 7.4$ and $\nu_{*c} = 0.10m\ sec^{-1}$. The resulting profiles of ν_w, ν_c, and ν_t are shown in Figure 39.

Our available empirical basis is insufficient to permit reliable prediction of longshore current profiles. However, the qualitative implications are that wave generated vortices shed from ripples have a paramount influence on longshore current profiles. The longshore bed shear stresses corresponding to the two alternative parameter sets (C_w, C_c, and ν_{*c}) described above differ by a factor of ~17. Independent measurements of τ_c, for example by direct measurements of mean water surface slope $(d\eta/dy)$ could readily indicate which set of parameters is most appropriate.

Sediment suspension in the surf zone

The observed presence of wave-formed ripples within the trough together with the observed tendency for wave oscillations to dominate the boundary layer suggests that oscillatory flows at incident wave frequency should dominate the entrainment and suspension of sediment. As discussed previously in relation to sediment transport seaward of the surf zone, recent laboratory and field studies indicate that oscillatory flows over rippled beds cause predominantly suspended load transport (albeit close to the bed) and that suspended sediment concentrations can be modelled as functions of bottom orbital velocities $(a_s\ \omega)$, sediment fall velocity, w_s, and ripple height η_r (Nielsen et al 1978; Nielsen 1979; Neilsen and Green in press , Nielsen in preparation).
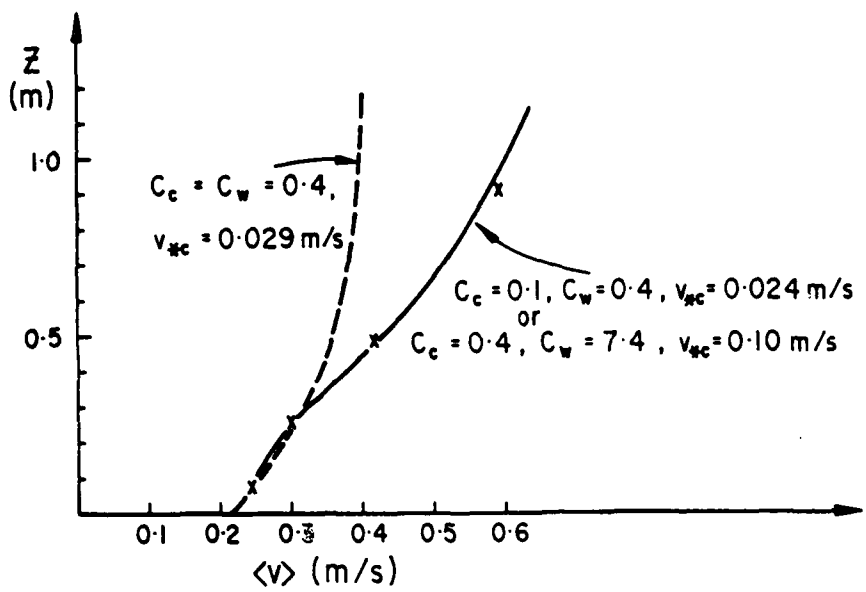
Figure 38. Predicted and observed longshore velocity profiles
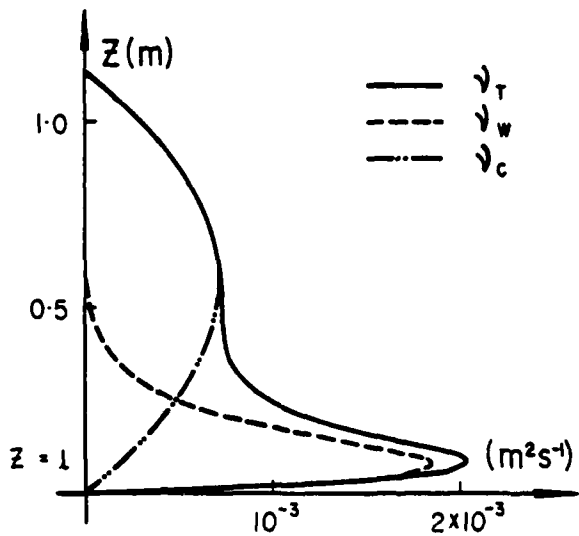
Figure 39. Vertical distribution of total (ν_t), wave induced (ν_w) and current induced (ν_c) eddy viscosity.

The conventional method of expressing suspended sediment concentration profiles is in terms of the one-dimensional diffusion equation

$$E \frac{dc}{dz} + w_s c = 0 \quad \text{or} \quad \frac{d \ln c}{dz} = - \frac{w_s}{E} \tag{84}$$

where E is diffusivity, c is suspended sediment concentration and w_s is sediment fall velocity (e.g. Nielsen 1979; Nielsen and Green in press). However, recent work by Nielsen (in preparation) suggests that a more meaningful approach is to consider c in terms of the vertical length scale, ℓ, in the form

$$C(z) = C_o \exp (-z/\ell) \tag{85}$$

where C_o is the concentration at the ripple crest level (z = 0) and ℓ is as defined by equation 81 that is

$$\ell = \left[- \frac{d \ln c}{dz} \right]^{-1} \tag{86}$$

and is related to the diffusivity by

$$\ell(z) = \frac{E(z)}{w_s} \tag{87}$$

Our change in formulation, that is from E to ℓ, is inspired by observations of concentration profiles for different sand sizes in the same flow. A set of such observations is shown in Figure 40. We see that at least the upper parts of the profiles tend to be parallel although the settling velocities vary by a factor of 7. If the entrainment process was diffusive and the diffusion equation was strictly valid, then the profile slopes should be inversely proportional to the settling velocity. This is clearly not the case. Instead, there is a strong
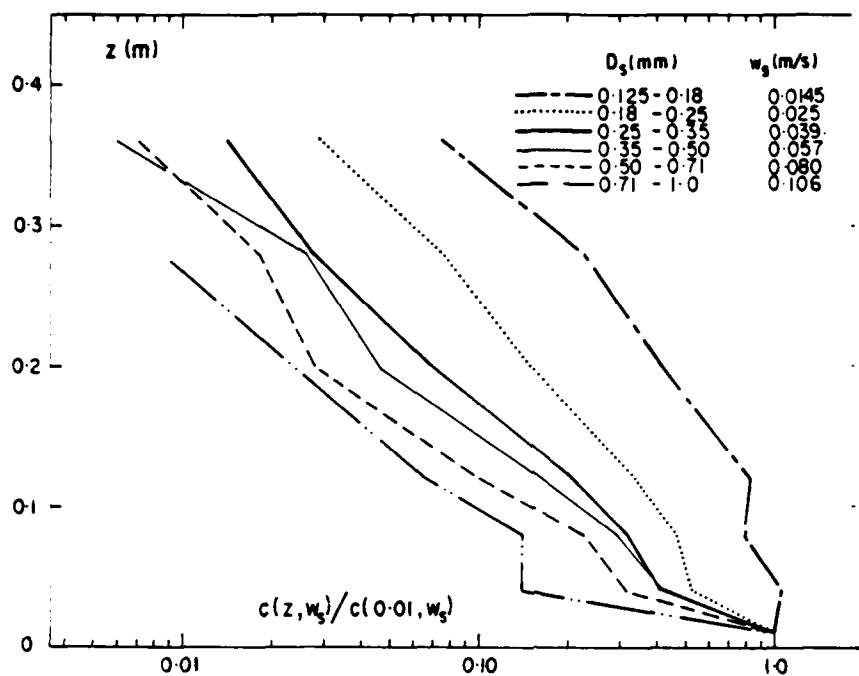
Figure 40. Vertical suspended sediment concentration profiles for
different grain sizes (from direct field measurements).
Note that despite appreciable variation in settling
velocity, w_s, the upper parts of the profiles are
parallel suggesting that the suspension of the various
sizes is related to a single length scale, ℓ.

indication that the flow, in fact, defines a single length scale, ℓ, appropriate to all grain sizes. As pointed out previously in connection with Figure 37, this same length scale also applies to the decay of vertical velocity fluctuations with elevation.

Nielsen (1979) and Nielsen and Green (in press) have shown that C_o is a function of the skin friction Shield's parameter

$$\theta' = \tau / (\rho_s - \rho) \, g D_s = \frac{\frac{1}{2} \rho f_w (a_s \omega)^2}{(\rho_s - \rho) \, g D_s} \tag{88}$$

where, as previously f_w is the friction factor, a_s is orbital semi-excursion, ω is wave radian frequency ρ_s and ρ are sediment and water densities and D_s is grain diameter. The length scale, ℓ, relative to ripple height, η_r, is a function of $(a_s \omega / w_s)$ where w_s is sediment fall velocity (Nielsen in preparation).

Using the suction device described in the methods section, we obtained 12 concentration profiles from the Eastern Beach surf zone. Examples of concentration profiles from separate runs are shown in Figure 41. The results of these measurements are strictly comparable to field results from other beaches as well as laboratory results (e.g. Nielsen and Green in press) and indicate that the concentration profiles can be reasonably modelled on the basis of suspension by waves alone. Estimates of C_o based on the Eastern Beach data together with other sets of field data indicate that C_o is well predicted from

$$C_o = .00018 \, \theta'^3 \tag{89}$$

A comparison of the predictive curve of equation 89 with field data is shown in Figure 42. Data points from the Eastern Beach surf zone are indicated and are seen to conform well to the general model.
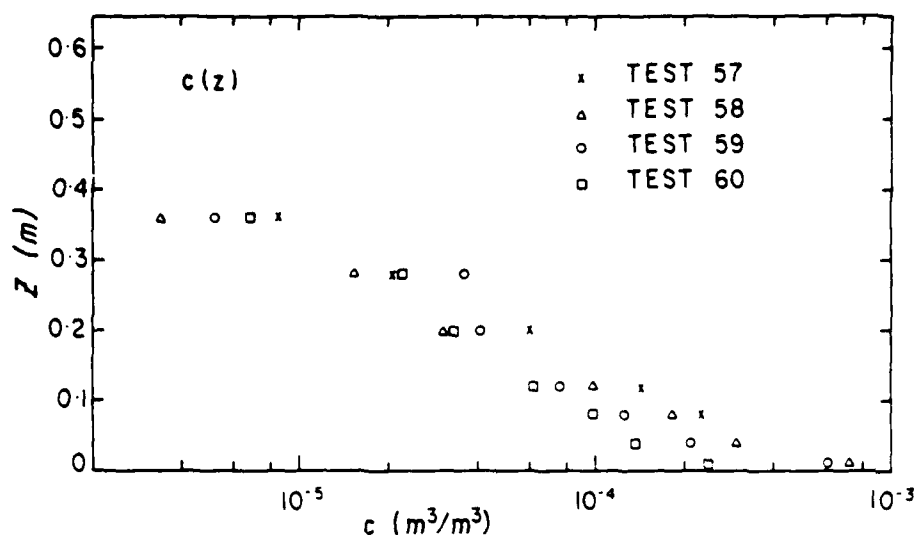
Figure 41. Suspended sediment concentration profiles from Eastern Beach.
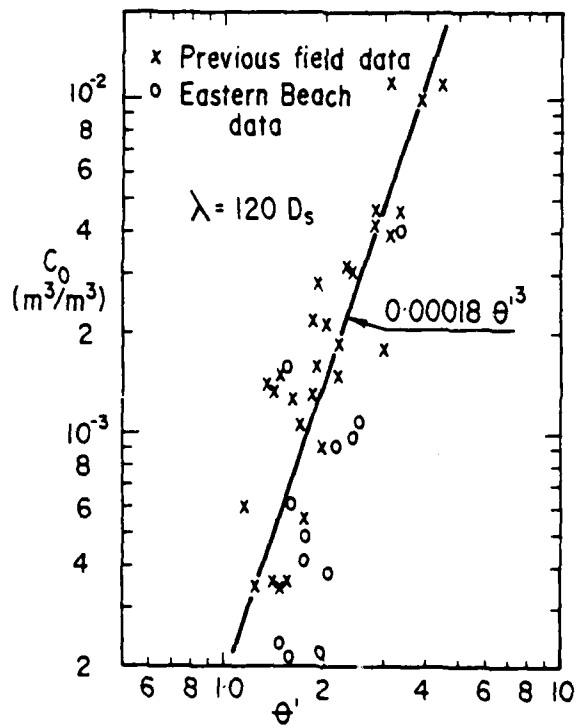
Figure 42. C_o as a function of Θ'.

The length scale, ℓ, relative to ripple height, η_r, gives the best fit to the relationship

$$\frac{\ell}{\eta_r} = 1.43 - 1.25 \exp\left[-.0011\left(\frac{a_s\omega}{w_s}\right)^3\right] \qquad (90)$$

from which we can predict ℓ if we know or can estimate ripple height, η_r. Nielsen (1981) showed that η_r is largely the function of the mobility number,

$$\Psi = \frac{\rho(a_s\omega)^2}{(\rho_s - \rho)\,gD_s} \qquad (91)$$

Available data suggests

$$\frac{\eta_r}{a_s} = \frac{0.23}{1+0.022\,\exp(\Psi/16)} \qquad (92)$$

Figure 43 shows the relationship between values of ℓ as predicted from equations 90 and 92 and values observed in the laboratory and in the Eastern Beach surf zone. Although there is appreciable scatter, the fit is reasonably good. We conclude that despite the complexity of processes in the presence of the longshore bar-trough and rhythmic bar-and-beach morphodynamic states, suspended sediment concentrations can probably be modelled in terms of entrainment by incident waves alone. More data are still needed to substantiate this.

Unfortunately, we still lack confidence in our ability to predict, quantitatively, the rate of net transfer of sediment from one region of the surf zone to another. To a degree, at least, this obviously involves superimposition of the net flow field on the suspended sediment concentration field. This is reasonable to assume for the alongshore transport where net flow acts perpendicular to wave oscillations. As was the case over the nearshore profile, longshore advection of suspended load should be
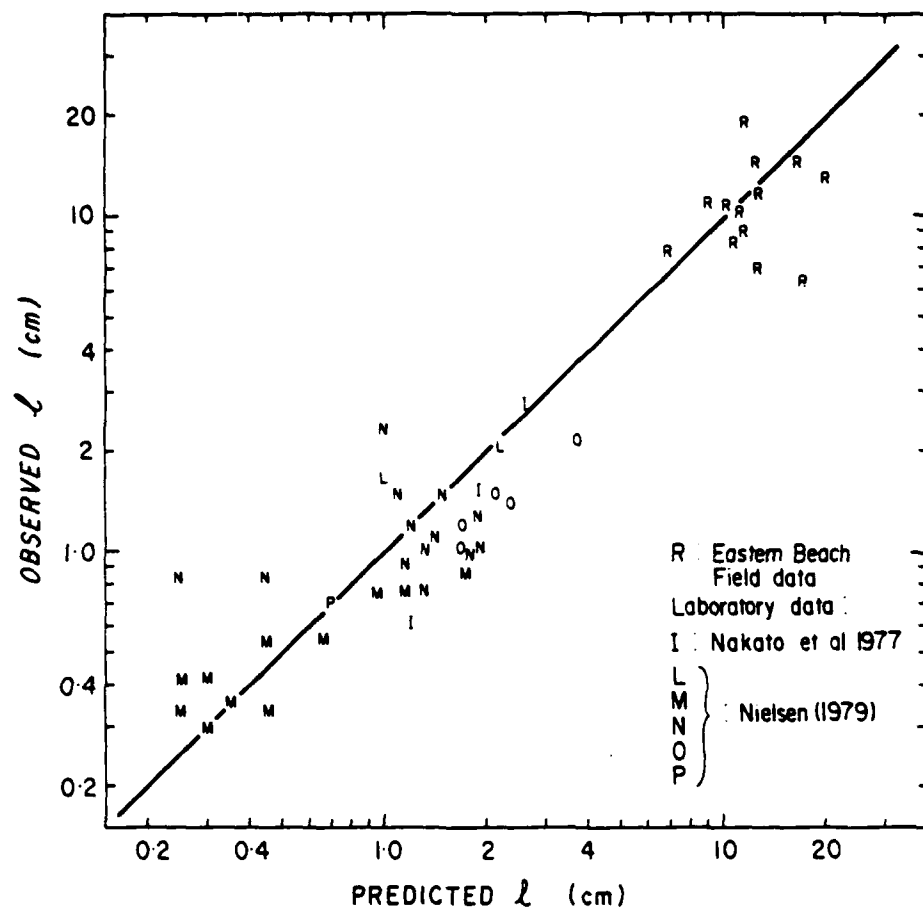
Figure 43.   Comparison between predicted and observed values of the
vertical length scale ℓ. Observations from Eastern Beach
are indicated.

$$Q_y = \int_o^h \bar{c}\,(z)\,\langle v \rangle\,(z)\,dz \qquad\qquad (93)$$

However, as explained in the discussion of nearshore processes, we cannot extend this argument to the shore-normal case where wave oscillations and net flows act parallel to each other. As we pointed out earlier, phase dependency between velocity maxima and concentration maxima can, in fact, result in sediment moving opposite to the direction of the net flow. This point is particularly well borne out by the Eastern Beach case. Although net near-bottom flow of water was exclusively seaward over the study period (e.g. Fig.35; Table 7) successive surveys (discussed in the following section) indicated a significant net onshore transport of sediment over the same period.

MORPHODYNAMIC VARIABILITY

OF THE BEACH AND SURF ZONE

Beach and surfzone morphologies, and hence, coupled sets of morphodynamic processes, represent responses to prevailing and antecedent breaker conditions in relation to the sediment composing the morphology. Variations in either breaker conditions or sediment size can be expected to produce variations in morphodynamic state and in profile configuration. Discussion of the relationships between morphodynamic state and wave conditions for specific beaches have been presented by Short (1979 a & b; 1981), Wright and Short (in press) and Wright et al (1979). Goldsmith et al (1982) have considered the relationships between changing bar-trough and crescentic bar topographies and changing wave conditions. We are concerned here with both spatial variability along the coast and temporal variability at the Eastern Beach site.

Spatial Variability

Spatial variability in morphodynamic state can be expected to result from systematic alongshore variations in breaker height (for example as a result of variations in nearshore wave modification or in exposure) or to longshore variations in sediment size, or both. Spatial variability along the Gippsland coast was assessed from aerial photos, three sets of aerial reconnaissances, and a systematic set of surveys and sediment sampling at 35 sites along the entire length of coast. The survey and sediment sampling programme was conducted in December, 1981 over a short period during which deepwater

wave conditions remained constant, eliminating possible temporal variations. The surveys extended from the foredune to the outer bar. The locations of the transects are shown in Figure 44 and the resulting profiles are shown in Figure 45. Beach states were recorded at each site.

The most pronounced spatial variability occurs in the extreme northeastern sector between Cape Howe and Cape Everard (Figure 44) owing to the combined effects of variations in coastal orientation and sheltering by headlands. Along that portion of the coast, longshore bar-trough states prevail in the most exposed localities but in sheltered areas conditions become more reflective. However, from Cape Everard southwest to Seaspray (Profile 30) beach state remains consistently in the longshore-bar-trough and rhythmic-bar-and-beach state indicating that conditions observed at the Eastern Beach site are typical of most of the coast. Between Seaspray and Reeves Beach, beach state begins to shift toward the transverse-bar and rip state as energy decreases. South of Shallow Inlet, the sheltered environment favours the prevalence of reflective states.

Despite the comparative constancy alongshore of beach state, particularly between Cape Everard and Seaspray, there are significant variations in the profiles as shown in Figure 45 . Although the general features of the profile, as discussed in the previous section, remain consistent, trough width and the slope of the inner beach face vary considerably, apparently in response to variations in local sediment size. In general the beach face is composed of medium sand ($\sim$0.39 mm), the coarsest material ($\sim$1.5 mm) comprises the step at the base of the beach face, and the bar is composed of finer ($\sim$0.32 mm) sand. However, significant coarsening of material
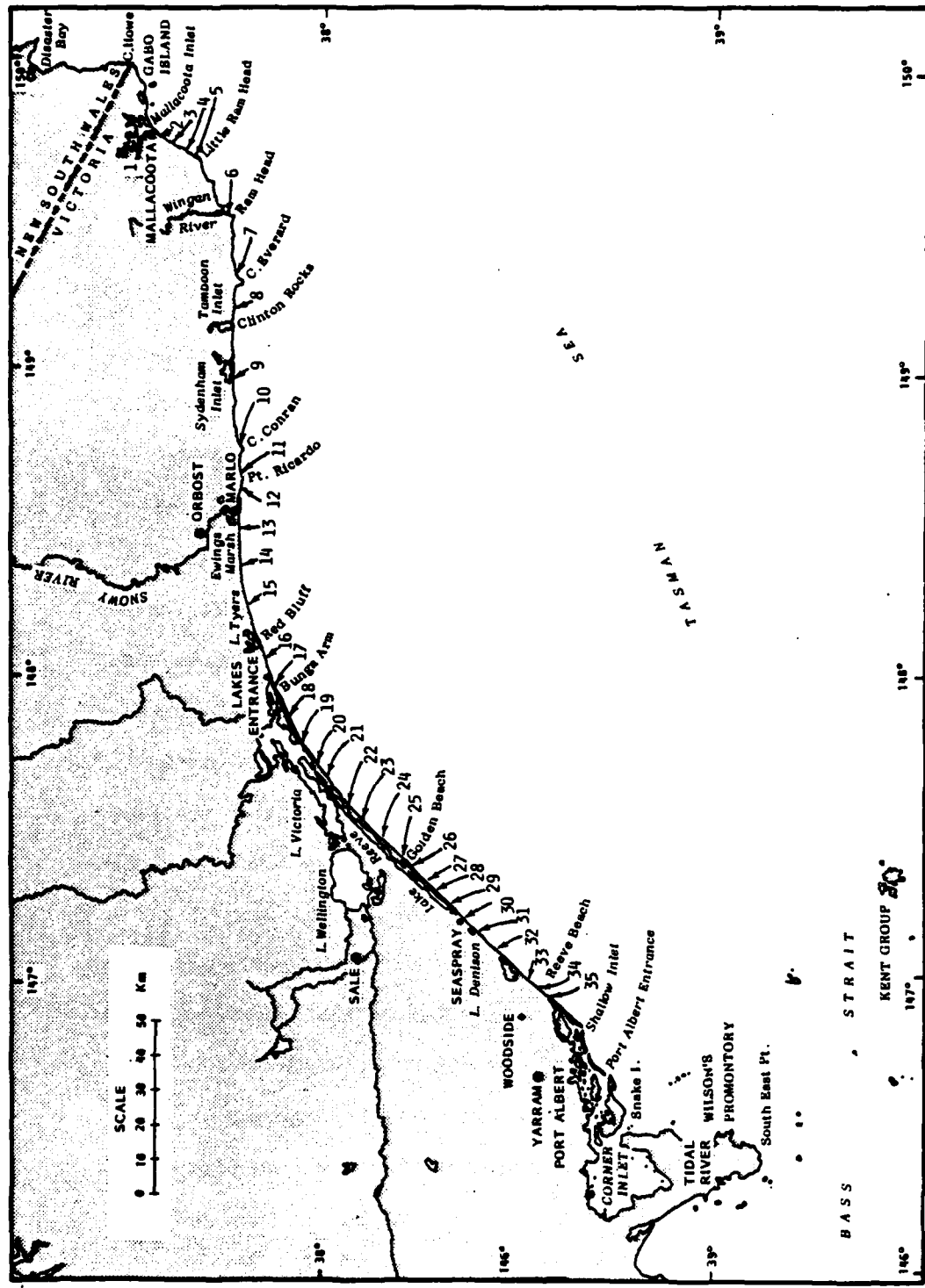
Figure 44. Locations of beach profiles and sediment samples, December, 1981.
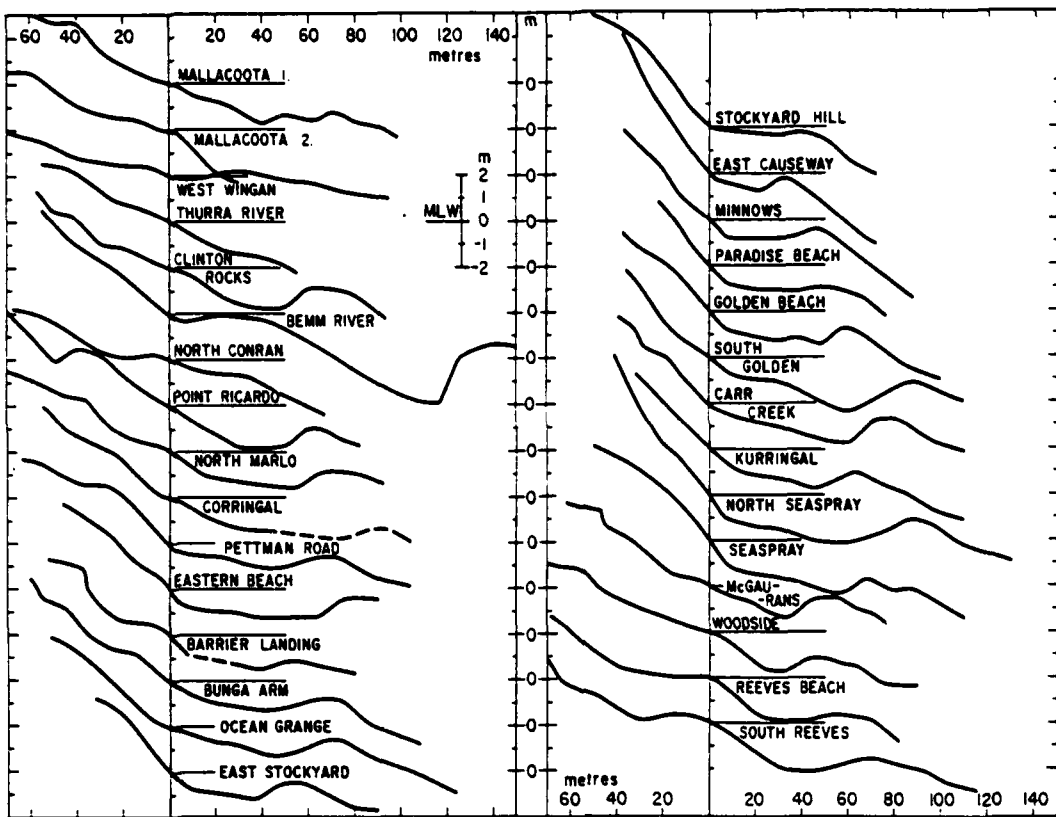
Figure 45.   Spatial variability of beach profiles, December, 1981.
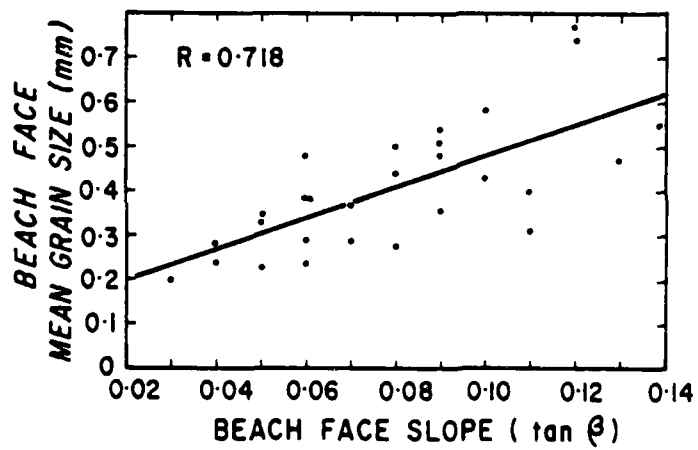
Figure 46.   Variation of beach face slope, tan β, with grain size.

in certain areas, notably between Stockyand East and Seaspray (Figure 44)
causes a narrower trough and a steeper subaerial beach. The relation-
ship between beach face slope and grain size is particularly obvious,
consistent with the observations of numerous others. This relation-
ship is shown in Figure 46.

Temporal Variability

The temporal variability of a beach expresses the temporal
variability of breaker conditions. On the New South Wales coast,
where the highly variable deepwater wave climate experiences only
minor nearshore attenuation,breaker conditions are highly variable
and, accordingly, exposed beaches experience changes which can take
them through the full range of beach states (Figure 23 ;   Short
1979; 1981; Wright et al 1979 a & b). Although the deepwater wave
climate of Bass Strait is at least as variable as that affecting
the New South Wales coast, we have shown earlier in this report that
nearshore dissipation of waves approaching the Gippsland coast
substantially reduces the temporal range of breaker conditions.
Consequently, beach states do not change through the full range, but
rather seem to alternate between the longshore-bar-trough state
under higher breaker conditions and the rhythmic-bar-and-beach state
under somewhat reduced breaker heights. Quite simply, it appears
that breakers do not reach or maintain heights large enough to cause
the beach and surf zone to become fully dissipative and they do not
remain small long enough to enable the crescentic bar to weld to the
beach face.

Despite the fact that the morphodynamic conditions tend to
remain arrested between the longshore-bar-trough and rhythmic-bar-

and-beach states, these states are among the most mobile (Short, 1981;
Wright 1981) with the result that profile changes are appreciable and
rapid. The most striking changes are associated with the onshore-
offshore migrations of the bar. Figure 47 shows a series of profiles
measured over the period 5-16 May, 1981. During an earlier phase
of this period (5-8 May) comparatively low breakers ($H_b \sim 1m$) resulted
in onshore bar migration at a rate of nearly 10 metres per day.
However, after 8 May, onshore migration slowed and halted owing to
a return to higher enegy. The associated changes as they appear in
plan view are shown in Figure 25 from which it can be seen that
longshore migration of the rip and of crescentic bar "horns" accompanied
onshore bar migration.

From Figures 25 and 47 it is evident that the greatest changes
were associated with the bar. The beach face showed much smaller
changes. Most of the beach face changes which occurred on a given
profile were actually associated with the alonghsore migration of
rhythmic features rather than with net onshore-offshore transfer of
material. The lower mobility of the beach face is probably due to
the "filtering" effects of the bar and trough system in maintaining
a relatively constant shore break amplitude.

An Atlantic Coast Analog

Although the aerial photos, aerial reconnaissances, and surveys
of Eastern Beach ocver a wide enough time frame for us to make
qualitative conclusions about the constancy of morphodynamic state
on Eastern Beach, we do not have a long enough time series of
consecutive surveys to ascertain the full extent of beach mobility.
In this regard, it is informative to make use of results from an
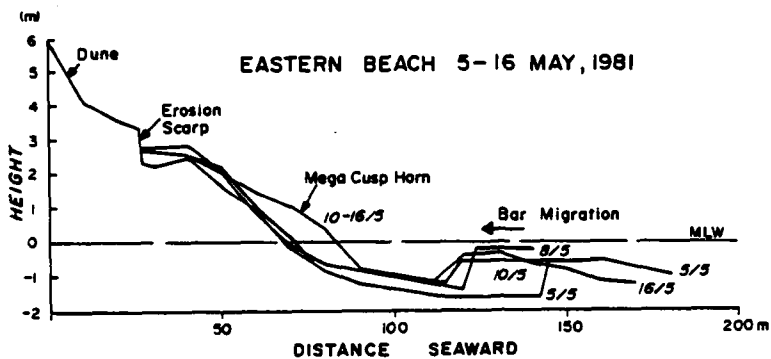
Figure 47. Temporal variations in the beach and surf zone profile at Eastern Beach, May, 1981

analogous example in a similar coastal environment elsewhere. The

analog comes from the vicinity of the U.S. Army Coastal Engineering

Research Center's Field Research Facility at Duck, North Carolina

on the Atlantic coast of North America. Using their CRAB surf-zone

survey vehicle, the Corps of Engineers carries out frequent routine

surveys of the beach and surfzone. In October-November, 1981 two

of us (L D Wright and P Nielsen) were involved in an experiment at

Duck over a period which encompassed a series of storms and were

impressed by the morphodynamic similarity to the Eastern Beach site.

Like the Gippsland coast, the North Carolina coast experiences

frequent storm waves which typically arrive at oblique angles.

Available data together with our own observations suggest that the

modal morphodynamic states at Duck are longshore-bar-trough or

rhythmic-bar-and-beach.

Figure 48 shows the sweeps of superimposed profiles on two

transects at Duck encompassing a period of 11 months and including

both high and low energy extremes. The mobility of the transects

is seen to be confined to the region above h = 8 metres and is

greatest in the region occupied by the bar; mobility of the beach

face is low. The bar is subject to rapid migrations over a horizontal

distance of 200 metres: it moves offshore during storms and onshore

under diminishing wave conditions. In contrast, the beach face

apparently advances and retreats across a zone only ∿20 metres wide.

These characteristics are especially evident from Figure 49 which

shows a typical low energy profile and a post storm profile.

Although bar positions and bar crest depths are vastly different,

the beach face shows only modest change in gradient and position.

Furthermore, it is readily apparent that the "cut" of the beach face
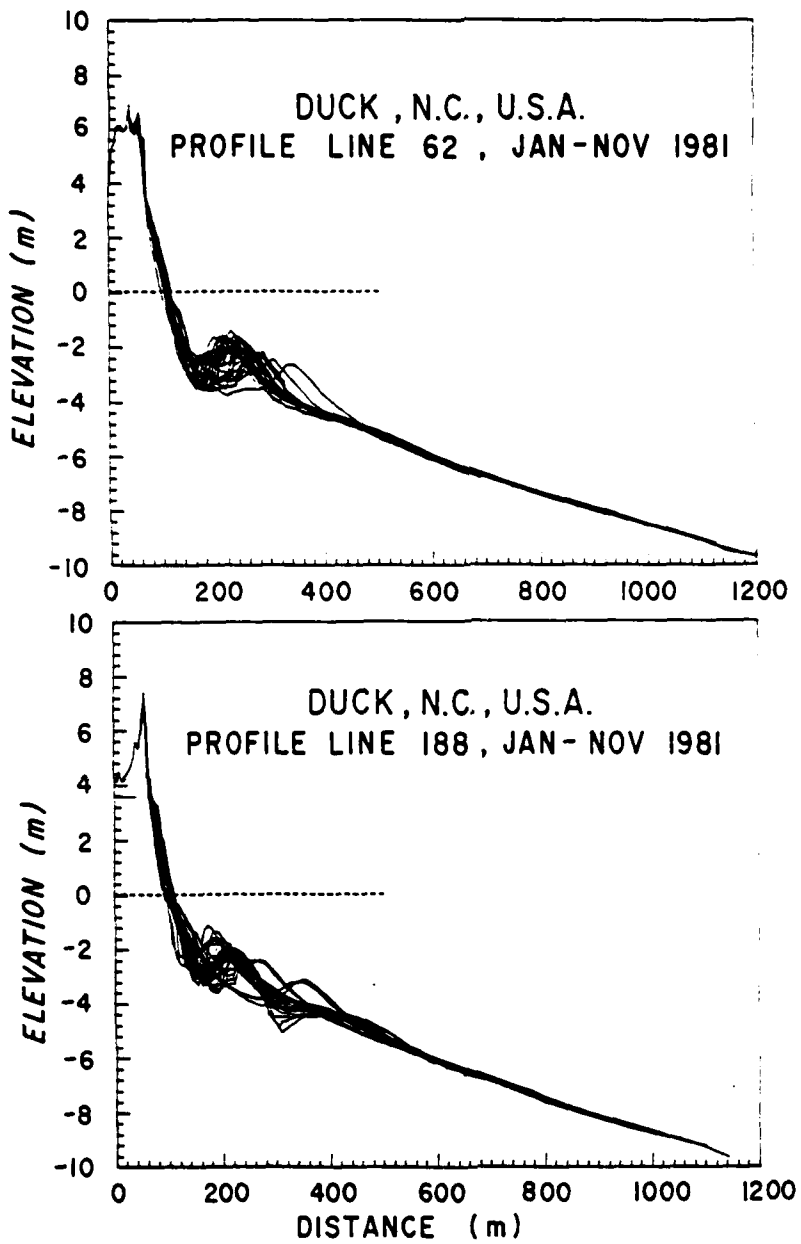
Figure 48.   Temporal variability of two beach and nearshore profiles
             at Duck, N.C. Jan-Nov. 1981. From survey data collected
             by U.S. Army Corps of Engineers, CERC, Field Research
             Facility.
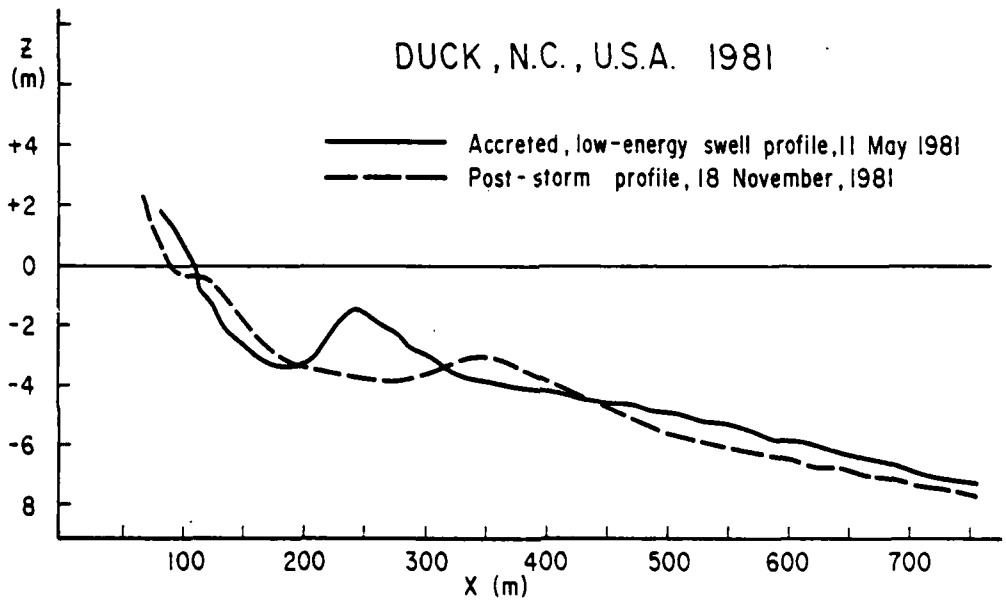
Figure 49.   Comparison of a typical low energy or "swell" profile
with a post-storm profile from Duck, N.C. 1981.

is confined to the subaerial portion above a shallow step and
is accompanied by accretion on the segment immediately below the
step. There does not appear to be significant exchange of sediment
across the trough between the beach face and the bar. An important
implication is that not only are the bar and beach face regions
dynamically discrete in terms of their dissipative versus reflective
characteristics but are also at least quasi-discrete in terms of
their mobility. The maintenance of standing wave nodes in the trough
may provide a barrier to sediment exchange.

At Duck, the sediment population was strongly bimodal with
medium sand composing the bar and coarse to very coarse sand composing
the beach; this undoubtedly influenced the modal beach state. Similar,
though less dramatic, sediment properties prevailed at Eastern Beach.
Although a bimodal sediment distribution is not a prerequisite for
longshore-bar-trough and rhythmic bar-and-beach topographies, it
certainly seems to favour the occurrence of those states.

CONCLUSIONS

In approaching coastal problems from a morphodynamic point of
view, we are concerned with the complete assemblages of depositional
forms, hydrodynamic processes, and processes of sediment redistribution;
with the patterns, sequences and extents of temporal change of those
assemblages; and with the relationships of the assemblages and their
temporal variability to environmental conditions. In the foregoing,
we have examined a Coastal Boundary Layer system in the presence of
environmental conditions characterize. by a temporally-variable deep-
water climate subject to the frequent occurrence of obliquely-in-
cident storm waves, shore parallel tidal and wind driven inner shelf
currents, and a wide, low gradient inner shelf. This combination of
environmental conditions results in the maintenance of beach and surf-
zone morphodynamic states characterized by longshore bar-trough and
rhythmic bar and beach topographies with their attendant complex suites
of fluid motions. We have attempted to illuminate some of the con-
nectivities between different components of the system and to explain
some of the physical mechanisms which cause the system to behave as it
does.

Specific conclusions and implications have already been pointed
out in the appropriate sections and subsections of this report and do
not need to be repeated here. However, it is worth highlighting some
general points of possible global relevance:

1.   Seaward of the surf zone, tidal currents may make sub-
stantial secondary contributions to the shore parallel trans-
port of sediment even in microtidal environments.

2.   Over rippled beds composed of coarse material, frictional
dissipation is probably appreciably greater than has been con-

ventionally assumed. Consequently, the configuration and roughness
of the nearshore profile play very fundamental roles in determining
breaker hight, the temporal variability of breaker heights, and
hence the modal state and mobility of the beach.

3.   Although longshore bar-trough and rhythmic bar and beach
topographies have complex process suites, incident waves remain
dominant right up to the beach face and play the major role in
suspending sediments. Incident waves also exert a pronounced in-
fluence on the structure of longshore currents by contributing
most of the eddy viscosity near the bed. Standing waves and
possible edge waves make important secondary contributions to the
net drift. Their shore normal modes may locate and even arrest
the trough position and may probide a weak barrier to the exchange
of sediments between the bar and the beach. Cusps and rhythmic
surf zone topography are probably expressions of edge waves at
different frequencies.

4.   The bars associated with longshore-bar-trough and rhythmic
bar-and-beach states exhibit high mobility characterized by rapid
and extreme onshore-offshore migrations. However, beach-face
mobility is surprisingly low and this may reflect the ability of
bar-trough readjustments to partially "absorb" changes in breaker
height and thereby reduce variations in shore-break amplitude.

ACKNOWLEDGEMENTS

REFERENCES

Bagnold, R.A., 1963. "Mechanics of marine sedimentation". In: M.N. Hill, (Ed.), "The Sea". New York, Interscience, Vol. 3, pp. 507-523.

Bailard, J.A., 1981. "An energetics total load sediment transport model for a plane sloping beach". J. Geophys. Res., Vol. 86, pp. 10,938-10,954.

Bailard, J. and Inman, D.L., 1981. "An energetics bedload model for a plane sloping beach: local transport". J. Geophys. Res., Vol. 68, pp. 2035-2043.

Ball, F.F., 1967. "Edge waves in an ocean of finite depth". Deep Sea Research, Vol. 14, pp. 79-88.

Bird, E.C.F., 1978: "The geomorphology of the Gippsland Lakes Region". Environmental Studies Series No. 186, Ministry for Conservation, Vic., 158pp.

Bowen, A.J. and Inman, D.L., 1969. "Rip currents 2: Laboratory and field observations". J. Geophys. Res., Vol 74, pp. 5479-5490.

Bradshaw, M.P., Chappell, J., Hales, R.S. and L.D. Wright, 1978. "Field monitoring and analysis of beach and inshore hydrodynamics". Proc. Aust. Coastal and Ocean Engineering Conf. 4th, (Adelaide), pp. 171-175.

Bretschneider, C.L. and Reid, R.O., 1954. "Modification of wave height due to bottom friction, percolation and refraction". Beach Erosion Board, Tech. Memo No. 45.

Carstens, M.R., Neilson, F.M. and Altinbilek, H.D., 1969. "Bed forms generated in the laboratory under oscillatory flow". Coastal Eng. Research Centre, Technical Memo 28, Washington D.C., 78 pp.

Chappell, J. and Wright, L.D., 1979. "Surf Zone resonance and coupled morphology". Proc. Int. Conf. Coastal Eng., 16th, Hamburg, pp. 1359-1377.

Dean, R.G., 1977. "Equilibrium beach profiles: U.S. Atlantic and Gulf Coasts". Department of Civil Eng., University of Delaware, Newark, Delaware, Ocean Engineering Tech. Rept. 12, 46pp.

Easton, A.K., 1970. "The tides of the continent of Australia". Horace Lamb Centre, Flinders Univ. Research Paper No. 37, 326pp.

Eckart, C., 1951. "Surface waves in water of variable depth". Scripps Inst. Oceanogr., SIO Wave Report 100, 99pp.

Fandry, C.B., 1982. "A numerical model of the wind-driven transient motion in Bass Strait". J. Geophys. Res., Vol. 87, pp. 499-517.

Franklin, E.H. and Clifton, B.B., 1971. "Halibut Field, Southeastern Australia". Am. Assoc. Petr. Geologists Bull., Vol. 55, No. 8, pp. 1262-1279.

Galvin, C.J., 1972, "Wave breaking in shallow water". In: R.E. Meyer, (Ed.), "Waves on Beaches". Academic Press, New York, N.Y., pp. 413-456.

Goldsmith, V., Bowman, D. and Kiley, K., 1982. "Sequential stage development of crescentic bars: Hahoterim Beach, Southeastern Mediterranean". J. Sed. Pet., Vol. 52, pp. 233-249.

Grant, W.D. and Madsen, O.S., 1979. "Combined wave and current interaction with a rough bottom". J. Geophys. Res., Vol. 84, No. C4, pp. 1797-1808.

Guza, R.T. and Bowen, A.J., 1977. "Resonant interactions from waves breaking on a beach" Proc. Int. Conf. Coastal Eng., 15th, pp. 560-579.

Guza, R.T. and Davis, R.E., 1974. "Excitation of edge waves by waves incident on a beach". J. Geophys. Res., Vol 79, No. 9, pp. 1285-1291.

Guza, R.T. and Inman, D.L., 1975. "Edge waves and beach cusps". J. Geophys. Res., Vol. 80, No. 21, pp. 2997-3012.

Holman, R.A., 1981. "Infragravity energy in the surf zone". J. Geophys. Res., Vol. 86, pp. 6442-6450.

Holman, R.A. and Bowen, A.J., 1982. "Bars, bumps and holes: models for the generations of complex beach topography". J. Geophys. Res., Vol. 87, pp. 457-468.

Huntley, D.A. and Bowen, A.J. 1979. "Beach cusps and edge waves". Proc. Int. Conf. Coastal Eng., 16th, Hamburg, pp. 1378-1393.

Huntley, D.A., Guza, R.T. and Thornton, E.B., 1981. "Field observations of Surf beat 1: Progressive edge waves". J. Geophys. Res., Vol 86, pp. 6451-6466.

Inman, D.L. and Bowen, A.J., 1963. "Flume experiments on sand transport by waves and currents". Proc. Int. Conf. Coastal Eng., 8th, pp. 137-150.

Jonsson, I.G. and Carlsen, N.A., 1976. "Experimental and theoretical investigations in an oscillatory (rough) turbulent boundary layer". J. Hydr. Res., Vol 14, No. 1, pp. 45-60.

Komar, P.D., 1975. "Nearshore currents: generation by obliquely incident waves and longshore variation in breaker height". In: J.R. Hails and A. Carr (Eds.), "Nearshore Sediment dynamics and Sedimentation". Wiley, N.Y., pp. 17-45.

Komar, P.D., 1976. "Beach processes and sedimentation". Prentice-Hall, Englewood, N.J., 429 pp.

Komar, P.D. and Miller, M.C., 1975. "Sediment threshold under oscillatory waves". Proc. Int. Conf. Coastal Eng., 14th, pp. 756-775.

Lighthill, J., 1978. "Waves in Fluids"Cambridge, Cambridge University Press, 504pp.

Lofquist, K.E.B., 1980. "Measurements of oscillatory drag on sand ripples." Proc. Int. Coastal Eng. Conf., 17th, Sydney, pp. 3087-3106.

Longuet-Higgins, M.S., 1970a. "Longshore currents generated by obliquely incident sea waves 1." J. Geophys. Res., Vol. 75, pp. 6778-6789.

Longuet-Higgins, M.S., 1970b. "Longshore currents generated by obliquely incident sea waves 2". J. Geophys. Res., Vol. 75, pp. 6790-6801.

Lundgren, H., 1972. "Turbulent currents in the presence of waves". Proc. Int. Conf. Coastal Eng., 11th, Vancouver, pp. 623-634.

MacDonald, T.C., 1977. "Sediment suspension and turbulence in an oscillating flume". C.E.R.C. Tech. Paper No. 77-4.

Nakato, T., Locher, F.A., Glover, J.R. and Kennedy, J.F., 1977. "Wave entrainment of sediment from rippled beds". Journ. Waterways, Harbours and Coastal Eng. Div., A.S.C.E., Vol. 103, No. WW1, pp. 83-100.

Nielsen, P., 1979. "Some basic concepts of wave sediment transport". Series Paper 20, Institute of Hydrodyanmics and Hydraulic Engineering, Tech. Univ. of Denmark, Lyngby, 160pp.

Nielsen, P., 1981. "Dyanmics and geometry of wave-generated ripples." J. Geophys. Res., Vol 86, No. C7, pp. 6467-6472.

Nielsen, P., in press; "Explicit formulae for practical wave calculations". Coastal Engineering.

Nielsen, P., in preparation. "Analytical determination of nearshore wave height variation due to refraction, friction and shoaling". Coastal Engineering.

Nielsen, P., in preparation. "Suspended sediment distributions in wave boundary layers". J. Geophys. Res.

Nielsen, P. and Cowell, P.J., 1981. "Calibration and data correction procedures for flow meters and pressure transducers used by the Coastal Studies Unit". Coastal Studies Unit Tech. Rept. 81/1, Coastal Studies Unit, University of Sydney, 33p.

Nielsen, P. and Green, M.O., in press. "Suspended sediment under waves". Jour. Waterways, Harbours and Coastal Engineering Div., A.S.C.E.

Nielsen, P., Svendsen, I.A. and Staub, C., 1978. "Onshore-offshore sediment movement on a beach." Proc. Int. Coastal Eng. Conf., 16th, Hamburg, pp. 1475-1492.

Seymour, R.J., 1980. "Longshore sediment transport by tidal currents". J. Geophys. Res., Vol. 85, pp. 1899-1904.

Shields, I.A., 1936. "Anwendung der Ahnlichkeitsmechanik und der turbulenzforschung auf die Geschiebebewegung". Mitt. Preuss. Ver. Anst., No. 26, Berlin.

Short, A.D., 1979a. "Three dimensional beach-stage model". J. Geol., Vol. 87, pp. 553-571.

Short, A.D., 1979b. "Wave power and beach stages: a global model". Proc. Int. Conf. Coastal Eng., 16th, Hamburg, pp. 1145-1162.

Short, A.D., 1981. "Beach response to variations in breaker height". Proc. Int. Conf. Coastal Eng., 17th, Sydney. pp. 1016-1035.

Short, A.D. and Wright, L.D.,1981. "Beach systems of the Sydney Region". Australian Geographer, Vol. 15, pp. 8-16.

Sonu, C.J., Pettigrew, N. and Fredericks, R.G.,1974. "Measurements of swash profile and orbital motion on the beach". In: Ocean Wave Measurement and Analysis., Am. Soc. Civ. Eng.,Vol. 1, pp. 621-634.

Spillane, K.T., Falconer, R.L. and Wright, D.S.,1972. "Deep water waves and swell state in Bass Strait" Commonwealth of Australia, Bureau of Meterology, Meteorological Summary, April, 1972, 120pp.

Sternberg, R.W., 1972. "Predicting initial motion and bed load transport of sediment particles in the shallow marine environment". In: D.J.P. Swift, P.B. Duane and O.H. Pilkey, (Eds.), "Shelf sediment transport processes and pattern". Dowden, Hutchinson, Ross, Stroudsberg, Pa., pp. 61-82.

Suhayda, J.N., 1974. "Standing waves on beaches". J. Geophys. Res., Vol. 79, pp. 3065-3071.

Swart, D.H., 1974. "Offshore sediment transport and equilibrium beach profiles". Delft Hydr. Lab.,Publication No. 131.

Ursell, F., 1952. "Edge waves on sloping beaches". Proc. Roy. Soc. Sec. A., Vol. 214, pp. 79-97.

Van de Graaff, J. and Tilmans, W.M.K.,1980. "Sand transport by waves". Proc. Int. Conf. Coastal Eng., 17th,Sydney, Ch. 70, pp. 1140-1157.

Wright, L.D., 1976. "Nearshore wave power dissipation and the coastal energy regime of the Sydney-Jervis Bay region, New South Wales; a comparison". Aust. J. Marine and Freshwater Research, Vol. 27, pp. 633-640.

Wright, L.D., 1981. "Modes of beach cut in relation to surf-zone morphodynamics". Proc. Int. Conf. Coastal Eng., 17th,Sydney. pp. 978-996.

.... .m. "H.e.i observations of long-period surf-zone
. .. . to contrasting beach morphologies".
...., Vol. 13, pp. 181-201.

.   .... "Nearshore ..... currents and sand trans-
. . .. Geo-Marine Letters.

.. .. Bradshaw, M.P. and Cowell, ..J.,
.. . .ssipative beach and
.. .. Mar. Geol., Vol. 32,

...........s of a high
.... 45, pp. 41-62.

.   ...press.
.. ..

.. .. s of beaches
.... "Handbook
. ...

..rph dynamic
.. .... Conf. Coastal

Appendix A-1: Survey Site number, location and shoreline distance
from Cape Howe (N.S.W. - Victorian border).

EASTERN VICTORIA

No.	Location	Kms
1	Bastion Point	21
2	Mallacotta (Golf Course)	24
3	Mallacotta (Airport)	27
4	Shipwreck Creek	32
5	Double Creek	35
6	West Wingan	56
7	Thurra River	77
8	Clinton Rocks	90
9	Bemm River	114
10	North Conran	130
11	Point Ricardo	142
12	North Marlo	144
13	Corringal Beach	157
14	Ewings Marsh (Beach Road	165
15	Ewings Marsh (Pettman Road)	182
16	Eastern Beach	197
17	Barrier Landing	204
18	Bunga Arm	215
19	Ocean Grange	222
20	Stockyard East	235
21	Stockyard Hill	239
22	East Causeway	246
23	"Minnows"	256
24	Paradise Beach	261
25	Golden Beach	266
26	South Golden Beach	271
27	Carr Creek	276
28	Kullingal	281
29	North Seaspray	286
30	Seaspray	292
31	Denison Creek	293
32	McGaurans Beach	302
33	Woodside Beach	318
34	Reeves Beach	323
35	South Reeves Beach	328

Appendix A-2: Frequency of occurrence of wind speed and direction at Gabo Island, Lakes Entrance and Tidal River (Source: Bureau of Meterology, Melbourne).

GABO ISLAND (1960-1981)

WIND DIRECTION	WIND SPEED (KNOTS)							
	1-5	6-10	11-20	21-30	31-40	41-50	>50	%
N	2.3	2.0	1.5	1.5	1.0	.6	.1	9.0
NE	2.0	3.0	5.0	7.5	3.1	1.1	.4	22.1
E	.4	.8	1.1	.6		.1		3.1
SE	.6	.7	.5	.3	.4			2.9
S	1.0	1.3	1.7	1.1	.8	.6	.4	7.0
SW	2.0	2.8	3.4	4.7	6.0	6.0	5.6	30.5
W	4.1	4.3	2.8	1.6	1.8	1.7	.8	17.1
NW	2.4	1.5	.4	.1				4.4
	14.8%	16.4	16.4	17.4	13.2	10.1	7.8	96.1

LAKES ENTRANCE

WIND DIRECTION								
N	1.8	3.0	2.1	.8	.2	.1		8.0
NE	1.1	1.8	2.0	.7	.3	.1		6.0
E	2.2	3.7	5.6	3.0	1.3	.8	.2	16.8
SE	1.4	4.2	3.8	1.4	.4	.3	.1	11.6
S	1.3	3.2	3.7	2.0	.8	.7	.2	11.9
SW	1.5	3.2	4.4	3.0	1.9	1.8	.6	16.4
W	1.9	3.9	3.4	2.4	1.3	1.1	.4	14.4
NW	2.8	4.1	3.2	1.4	.4	.3		12.2
	14.0%	27.1	28.2	14.7	6.6	5.2	1.5	97.3

TIDAL RIVER

WIND DIRECTION								
N	1.8	1.0	.8	.5	.2			4.4
NE	4.3	3.3	1.7	.8	.4	.2		10.7
E	3.2	3.2	1.6	1.1	.3	.3	.2	9.9
SE	1.3	.5	.3	.2	.2	.1		2.5
S	1.3	1.0	.7	.2	.1			3.3
SW	14.0	12.2	6.6	1.4	1.5		.2	36.2
W	3.7	3.2	2.4	.4	.4	.3	.5	10.7
NW	2.2	2.0	2.1	.3	.6	.4		7.6
	31.8%	26.4	16.2	4.9	3.7	1.5	.9	85.4

Appendix A-3

WIND VELOCITY

% OF OCCURRENCE

Knots	Gabo Is.	Lakes Entrance	Tidal River
0	2	3	14
1-5	15	13	32
6-10	17	27	26
11-20	17	28	16
21-30	18	15	5
31-40	13	7	4
41-50	10	5	2
> 50	8	2	1

Appendix A-4: Direction and state of swell and sea at Gabo Island (Source: Bureau of Meterology, Melbourne).

GABO ISLAND

DIRECTION OF SWELL (1973-1982)

	CALM	NE	E	SE	S	SW	W	NW	N	N/A
J	5.2	22.6	19.0	12.7	23.0	14.9	.9	-	-	1.2
F	3.4	23.7	21.2	14.1	21.3	15.4	.1	.1	-	.8
M	3.2	18.8	21.2	16.6	20.7	18.2	-	-	.1	1.2
A	3.1	13.0	17.7	14.6	28.8	21.8	-	-	-	.8
M	6.3	9.5	12.1	22.7	34.4	14.7	.1	.1	.1	.2
J	7.9	6.1	13.4	22.0	34.7	14.3	.1	.1	-	1.4
J	5.4	5.8	12.4	18.1	39.5	17.0	-	-	-	1.8
A	7.2	6.4	13.7	19.4	38.8	13.4	-	.1	.1	1.0
S	6.7	8.9	15.7	17.4	36.4	14.2	-	-	.1	.6
O	4.9	15.9	15.4	15.6	24.4	15.2	.1	-	.1	.8
N	4.4	16.9	14.2	14.9	29.9	18.7	.1	-	.1	.8
D	4.8	18.6	17.8	11.4	28.4	18.5	-	-	-	.4
Σx	62.5	166.1	193.9	199.6	360.3	196.5	1.6	.4	.5	10.9
x̄	5.2	13.8	16.2	16.6	30.0	16.4	.1	<.1	<.1	.9

STATE OF SWELL (1973-1982)

	CALM	0-2 <11	0-2 >11	2-4 <6	2-4 6-11	2-4 >11	>4 <6	>4 6-11	>4 >11	CON-FUSED
J	5.3	38.8	17.5	17.6	15.0	2.1	1.9	1.2	.3	.4
F	3.5	38.8	19.0	17.7	14.8	2.9	1.8	1.1	-	.4
M	3.3	41.5	21.0	17.1	10.7	2.7	2.1	1.3	.1	.2
A	3.0	36.1	24.5	15.3	14.3	2.5	3.1	.9	.3	-
M	6.3	36.4	19.1	11.9	19.0	3.6	5.5	3.5	.8	-
J	8.1	34.8	18.2	10.5	16.8	2.8	4.2	3.7	.7	.1
J	5.9	36.8	15.1	14.2	19.2	3.2	3.9	1.5	.2	.1
A	7.6	32.1	20.5	12.7	15.3	3.4	4.3	3.4	.6	-
S	6.9	37.1	16.2	16.7	11.6	3.1	3.2	2.4	.8	.1
O	5.0	37.9	16.5	17.9	14.8	2.2	4.0	.7	.2	.2
N	4.4	25.1	14.9	19.1	15.3	3.3	5.2	2.2	.2	.1
D	4.8	39.4	13.9	19.6	14.8	2.0	3.7	1.6	.2	.1
Σx	64.2	434.6	216.2	190.2	181.4	34.8	42.8	23.6	4.3	1.9
x̄	5.3	36.2	18.0	15.9	15.1	2.9	3.6	2.0	.4	.2

Appendix A-4: Continued

STATE OF SEA (1975-1982)

	CALM	0-.1	.1-15	.5-1.25	1.25-2.5	2.5-4	4-6	6-9	9-14	>14m
J	.2	3.9	22.5	43.2	25.0	4.8	.2	-		
F	.1	3.9	23.2	45.9	21.3	5.2	.3	-		
M	-	4.0	33.0	40.7	17.3	4.7	.4	-		
A	-	6.7	35.8	34.2	16.1	7.0	.2	-		
M	.1	7.5	36.5	30.6	14.5	8.6	2.1	.3		
J	-	5.8	37.3	30.8	16.1	8.1	1.6	-		
J	.1	4.2	41.1	27.9	15.5	10.3	.8	-		
A	.1	6.3	35.0	29.5	16.0	11.2	1.9	-		
S	-	6.1	32.6	34.2	16.2	10.2	.8	-		
O	.1	5.7	25.4	38.0	21.5	8.8	.4	-		
N	-	3.7	25.0	38.4	21.4	10.8	.7	-		
D	.1	4.7	26.0	37.5	22.3	8.8	.6	.1		
Σx	.9	59.2	373.5	430.9	223.2	98.1	9.5	.4	-	-
%	.1	4.9	31.1	35.9	18.6	8.2	.9	.03	-	-

APPENDIX B
ESTIMATION OF FRICTION FACTORS AND ROUGHNESS
PETER NIELSEN

In order to predict frictional dissipation, we must be able to estimate the friction factor f_w or f_e. In the following we use Jonsson's (1966) definition for the wave friction factor f_w

$$\tau_{max} = 1/2 \rho f_w u_{b,max}^2 \tag{B1}$$

where τ is the bed shear stress. We also define an energy dissipation factor f_e by

$$\overline{\tau u_b} = \frac{2}{3\pi} \rho f_e u_{b,max}^3 \tag{B2}$$

where $\overline{\tau u_b}$ is the time averaged energy dissipation. These two definitions lead to identical values for f_e and f_w if the near bed velocity u_b is simply sinusoidal, that is if

$$u_b(t) = u_{b,max} \sin \omega t \tag{B3}$$

and $\tau(t)$ varies as

$$\tau(t) = \tau_{max} |\sin \omega t| \sin \omega t \tag{B4}$$

Lofquist (1980) has measured the variation of $\tau(t)$ over natural wave ripples and found that it can differ considerably from $|\sin \omega t| \sin \omega t$, as shown in Figure B1.

Lofquist also derived values for f_w and f_e in accordance with
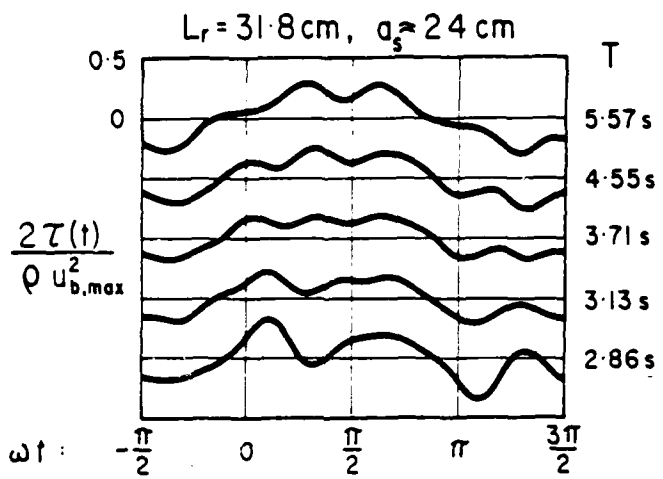
Figure B1: Variation of τ(t) for different wave periods (T), from Lofquist (1980). The corresponding free flow velocity varies as sinωt.

definitions (B1) and (B2). Figure B2 shows that f_e and f_w are generally nearly equal. The two extreme deviations correspond to tests where $\tau(t)$ has a narrow peak. The friction factor is a function of the Reynolds number $a_s u_{b,max}/\nu$ and of the roughness to semi excursion ratio λ/a_s (Jonsson 1966).

When the flow is rough turbulent as is normally the case under field conditions f_w (and f_e) depend only on a_s/λ.

Several authors (Jonsson, 1966; Kajiura, 1968; Kamphuis, 1975; and Grant and Madsen, 1982) have suggested different forms of the relation between f_w (f_e) and a_s/λ derived in analogy with steady boundary layer flow. According to Grant and Madsen (1982) this analogy seems reasonably well satisfied when a_s/λ is large ($a_s/\lambda \geq 28$) as in Jonsson and Carlsen's experiments, however the variation of $\tau(t)$ as measured by Lofquist shows that the structure of the boundary layer over large natural ripples may be very different from that of a steady boundary layer. Figure B1 shows that $\tau(t)$ has several narrow peaks and troughs that are related to the formation and release of strong ripple vortices. A boundary layer dominated by such vortices, generated right at the bed is not likely to be logarithmic. Therefore it seems not worthwhile to compare the theoretical merits of the different formulae in great detail. Instead we will use the most handy one which turns out to be Jonsson's in the explicit form given by Swart (1974):

$$f_e = \exp[5.213(\frac{\lambda}{a_s})^{0.194} - 5.977], \text{ for } \frac{\lambda}{a_s} < .63 \qquad (B5)$$

$$f_e = 0.30 \qquad\qquad \text{for } \frac{\lambda}{a_s} \geq .63 \qquad (B6)$$

$$f_w = \frac{2\,\tau_{max}}{\rho\,u^2_{b,max}}$$

$$f_e = \frac{\overline{\tau\,u_b}}{\frac{2\rho}{3\pi}\,u^3_{b,max}}$$
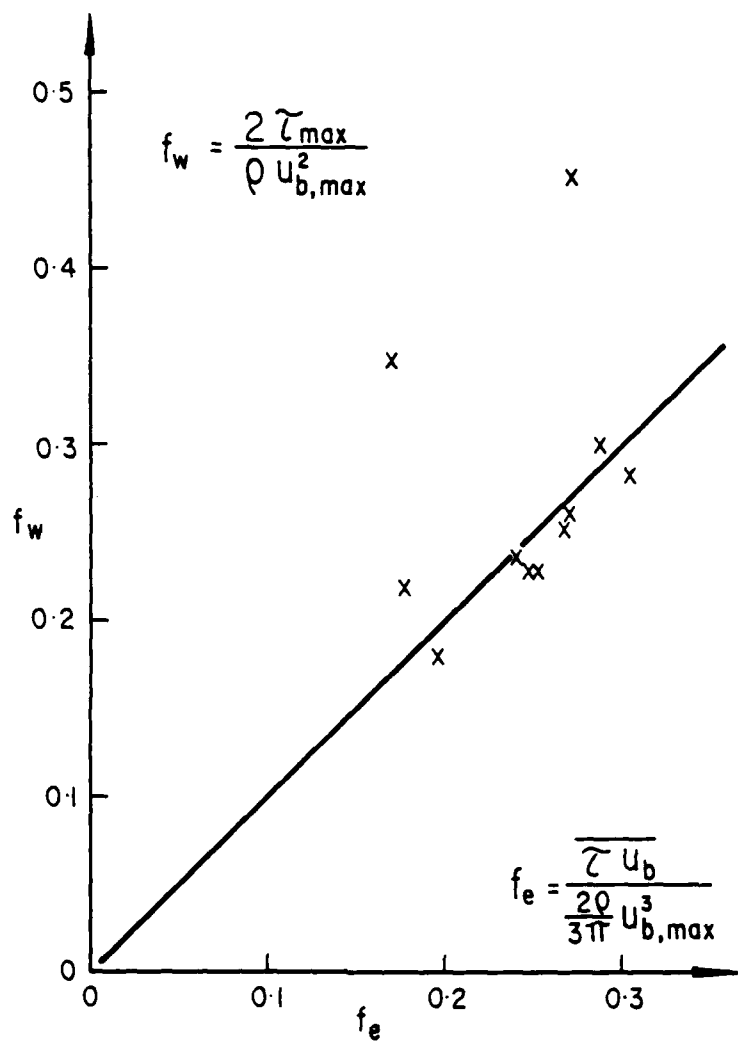
Figure B2: Comparison of measured values of f_w and f_e from Lofquist (1980). We see that f_w and f_e are generally nearly equal. The few extreme deviations stem from experiments where $\tau(t)$ has a pronounced narrow peak.

Figure B3 shows the variation of f_e with λ/a_s.

The upper limit of 0.30 is rather arbitrary (Grant and Madsen argue that it should be only 0.23), and it is traditionally based on Bagnolds observation: that f_e did not increase above 0.24 over his artificial ripples in sediment free water. However, the more recent measurements by Carstens et. al. (1969) and Lofquist (1980) using natural sand beds indicate that f_e can be 0.30 and even larger, and it is not unlikely that the presence of loose sand may lead to friction factors larger than the maximum values for fixed beds. This is supported by the observation of Nakato et. al. (1977) that the presence of loose sand enhanced the turbulence intensity by a factor 2 over ripples, all other things being equal.

The influence of moving sand on the roughness is shown in Figure B4 where we have plotted measured f_w values from Kamphuis (1975) and f_e values from Carstens et. al. (1969). Kamphuis measured the shear force on a flat bed of fixed sand grains and Carstens et. al. measured the energy dissipation over a flat bed of loose sand. We see that the friction is nearly one order of magnitude stronger over the loose sand for the same values of a_s/D_s. D_s is the mean grain diameter.

Kamphuis' fixed-bed-measurements are well predicted by equation (B5) with

$$\lambda = 2.5 \ D_s \tag{B7}$$

For the loose-sand-data the corresponding value is $\lambda \simeq 120 D_s$.

When the bed is covered by ripples or other bed forms, these will add to the friction. Following Grant and Madsen (1982) we will assume that the combined roughness from bed forms and moving sand can
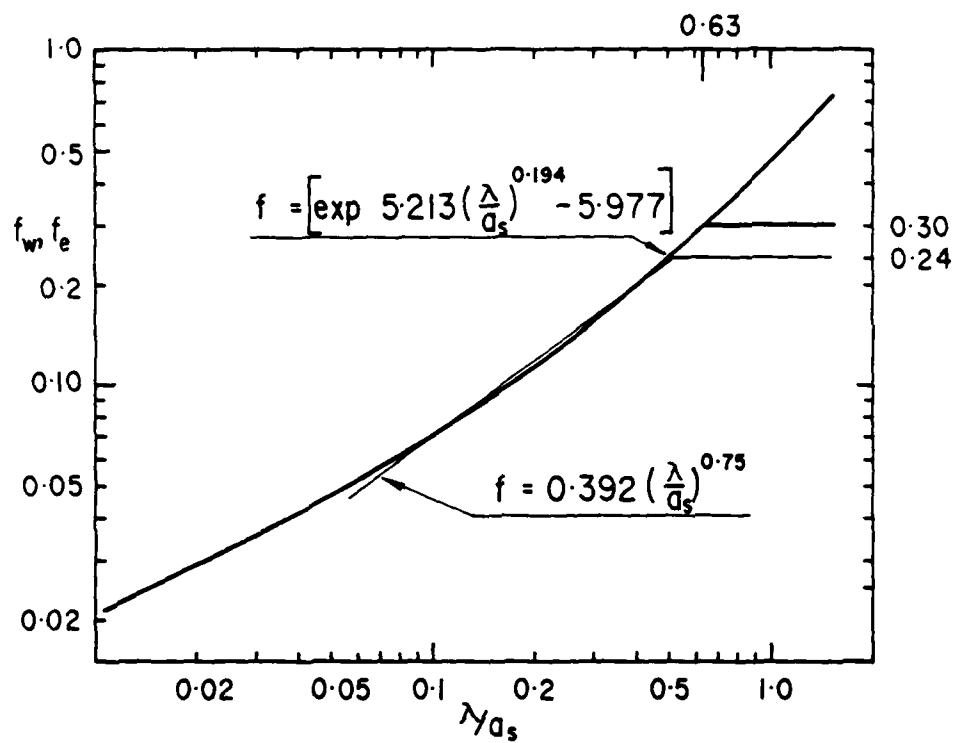
Figure B3: Variation of f_e with λ/a_s following equations (B5) and (B6) or equation (B13).
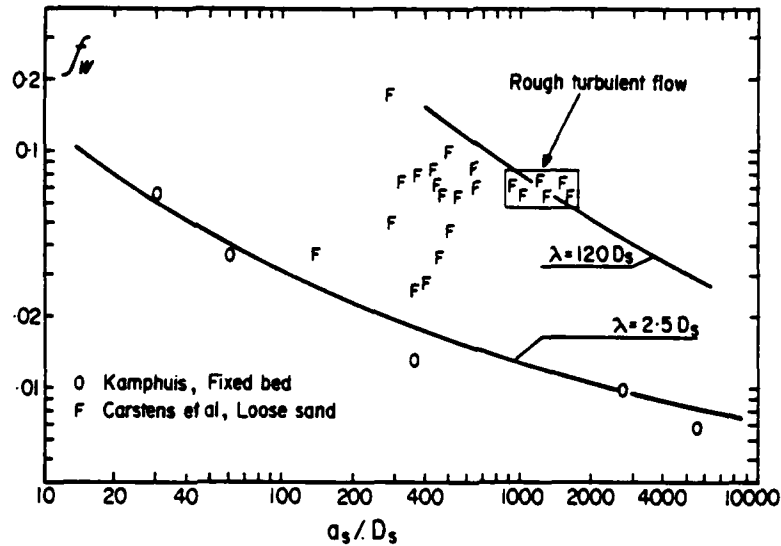
Figure B4: Friction factors measured over flat beds of fixed
and loose sand. We see that the friction is nearly
an order of magnitude stronger over loose sand than
over fixed sand for the same values of a_s/D_s. The
curves correspond to equation B5 with the shown
roughness lengths.

be described by

$$\lambda = (s + C_M)F(\theta')D_s + K\frac{\eta_r}{L_r}\eta_r \tag{B8}$$

where η_r is the ripple height , L_r the ripple length, θ' is the skin friction Shields parameter, s is the relative density of the sand (ρ_s/ρ) and C_M is the added mass coefficient for sand grains ($\simeq 0.5$). Grant and Madsen assume the value 28 for the constant K and derive

$$F(\theta') = 160 \; \theta_c \; [\sqrt{\theta'} - 0.7\sqrt{\theta_c}]^2 \tag{B9}$$

in analogy with Owen (1964) who studied sand grain saltation in air. The weak point in this analogy is that the vertical length scale of the sediment motion is derived from the idea that a sand grain which hits the bed with horizontal velocity v_i may bounce off vertically and reach a height of the order of magnitude $v_i^2/2g$. This is probably true in air where the relative density (sand to air) is of the order 2000 and inertia and gravity may dominate over the drag force, but in water where the relative particle density is a thousand times smaller a sand particle will only move a distance comparable to its own diameter before an initial upward velocity is annihilatedby the drag force. Furthermore, sand grains do not bounce off in water because of the water's cushioning effect.

However, the general form of (B8) is physically sound, so in the following we will derive an empirical formula based on (B5) and (B8). The skin friction Shields parameter θ' is calculated from

$$\theta' = \frac{\frac{1}{2} f_w u_{b,max}^2}{(s-1) g D_s} \qquad \text{(B10)}$$

where f_w is derived from (B5) with $\lambda = 2.5 D_s$. First we look for the value of the constant K. Figure B5 shows observed (via equation (B5)) values of $\lambda/(\eta_r^2/L_r)$ versus θ'. The line labelled "Bagnold" is derived from Bagnolds (1946) result

$$f_B = 0.072 \left(\frac{L_r}{a_s}\right)^{0.75} \qquad \text{(B11)}$$

which can be transformed into

$$f_e = 3.75 \left(\eta_r^2/L_r a_s\right)^{0.75} \qquad \text{(B12)}$$

if we remember that the ripple steepness in Bagnold's experiments was $\eta_r/L_r = 0.149$, and that $f_B = f_e/3$ by definition. If we force (B12) to coincide with

$$f_e = 3.92 \left(\frac{\lambda}{a_s}\right)^{0.75} \qquad \text{(B13)}$$

which is a good approximation to (B5) for $0.1 < \frac{\lambda}{a_s} < 0.5$ we find that Bagnold's result corresponds to

$$\lambda = 20.3 \frac{\eta_r}{L_r} \eta_r \qquad \text{(B14)}$$

The lines labelled "Jonsson I" and "Jonsson II" refer to the two experiments from Jonsson and Carlsen (1976) where $\lambda L_r/\eta_r^2$ was found to be 10.9
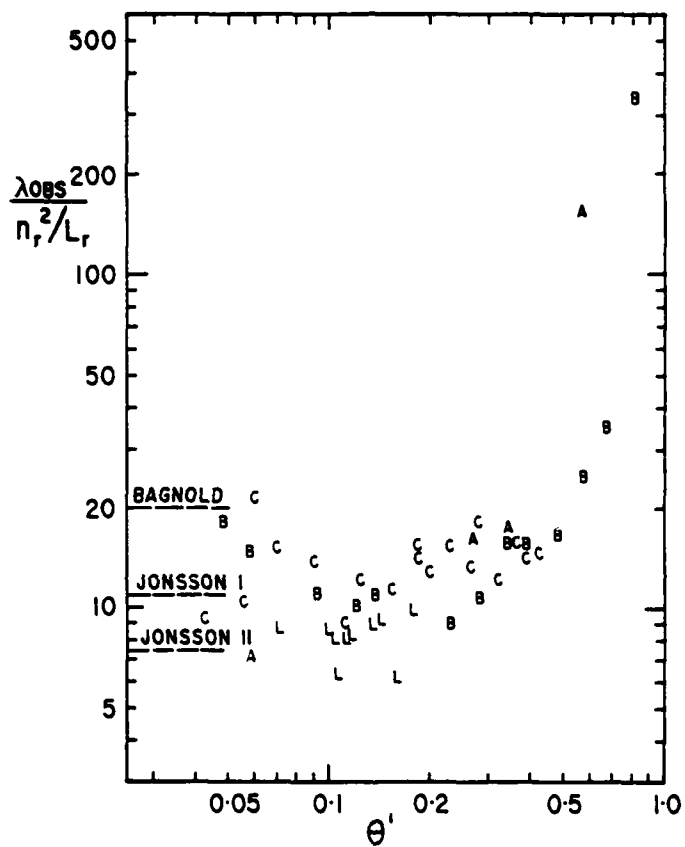
Figure B5: Observed values of $\lambda L_r/\eta_r^2$ as function of θ'. The broken lines labelled "BAGNOLD", "JONSSON I" and "JONSSON II" correspond to experiments with solid, artificial ripples.

and 7.4. As θ' approaches unity $\lambda L_r/\eta_r^2$ tends to infinity because η_r/L_r goes to zero (e.g. Nielsen 1981). The optimal value of K for natural sand ripples turns out to be approximately 8.

Figure B6 shows $(\lambda_{obs} - 8\eta_r^2/L_r)/D_s$ plotted against θ'. Again the scatter is very considerable but there seems to be no systematic deviations between different grain sizes. The flat-bed-data from Carstens et. al. conform well with the rest although they correspond to an unstable situation, from which ripples would have developed sooner or later. We see that the formula

$$(s + C_M)F(\theta') = 190\sqrt{\theta' - .05} \qquad (B15)$$

gives a fair representation of the trend while

$$(s + C_M)F(\theta') = 504[\sqrt{\theta'} - 0.16]^2 \qquad (B16)$$

which is the Grant and Madsen's formula with $C_M = 0.5$, $s = 2.65$ and $\theta_c = 0.05$ seems too steep.

We will therefore recommend the following formula for the combined roughness

$$\lambda = 8\eta_r^2/L_r + 190\sqrt{\theta' - 0.05}\, D_s \qquad (B17)$$

for quartz sand with $s \approx 2.65$, and $C_M \approx 0.5$.

Figure B7 shows a comparison between λ/a_s derived from measured f_e values by equation (B5), and values predicted by equation (B17). The
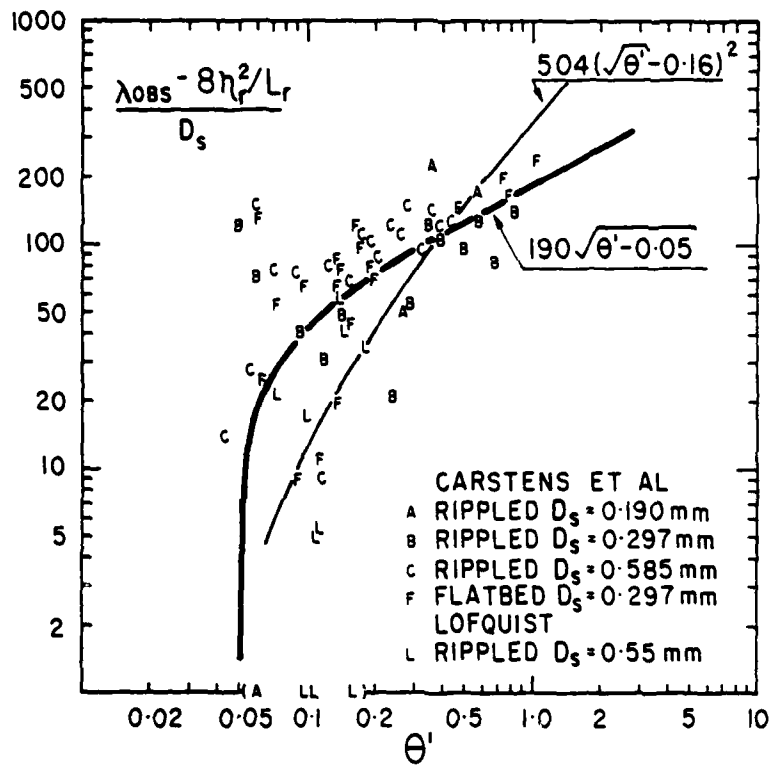
Figure B6: For the presently available data the roughness
            contribution from the moving sand can be appro-
            ximated by $\lambda_d = 190\sqrt{\theta' - .05}\, D_s$.
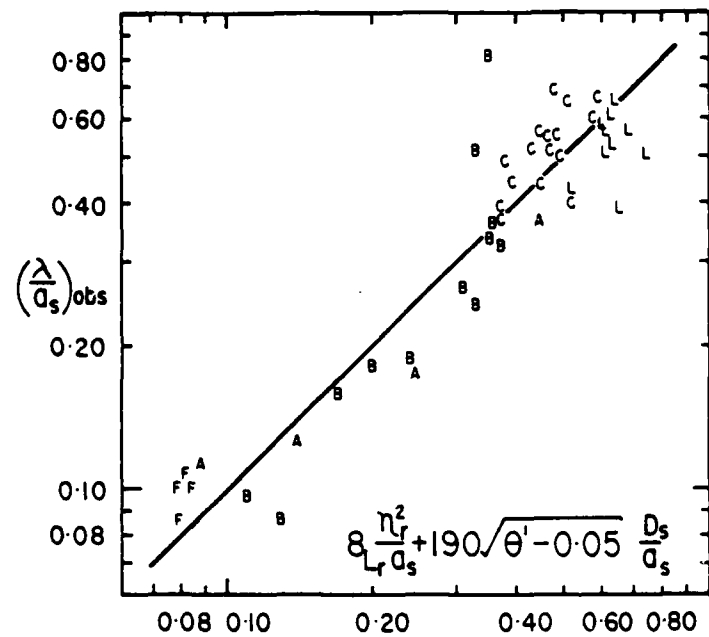
Figure B7: Comparison between predicted and measured roughness to semi excursion ratios.

agreement between measured and predicted values is acceptable and
the agreement between the corresponding f_e values will be closer be-
cause $\dfrac{1}{f_e}\dfrac{d\,f_e}{d(\lambda/a_s)}$ is considerably smaller than unity over most of
the practical range.

The only systematic trend seems to be that Carstens et. al.'s
measurements over non equilibrium flat beds given slightly larger f_e
values than measurements over stabilized rippled beds at the same θ'
values. This may mean that non equilibrium beds are rougher because
they are more active at the same values of θ'. Savage (1953) obser-
ved similarly that the friction factors were larger when the ripple
pattern was not in equilibrium with the wave conditions. Under irre-
gular field waves, the bedforms can never be in equilibrium with the
instantaneous wave conditions, so we may expect slightly larger dis-
sipation factors in the field than in laboratory experiments with
regular waves.

Figure B8 shows the roughness derived from Carstens et. al.'s
"flat-bed-data" versus the skin friction Shields parameter. We see
that the best fit for these data alone is

$$(s + C_M)\ F(\theta') \quad = \quad 230\sqrt{\theta' - 0.05} \qquad\qquad (B18)$$

which is approximately twenty percent larger than the overall best fit
given by equation (B15).

In conclusion we recommend determination of f_e (f_w) for rough
turbulent flow over natural sand beds by equation (B5) when λ/a_s <
0.63 and equation (B6) when $\lambda/a_s \geq 0.63$. The roughness length, λ, is
best estimated by equation (B17).

For prediction of the ripple geometry under field conditions, one
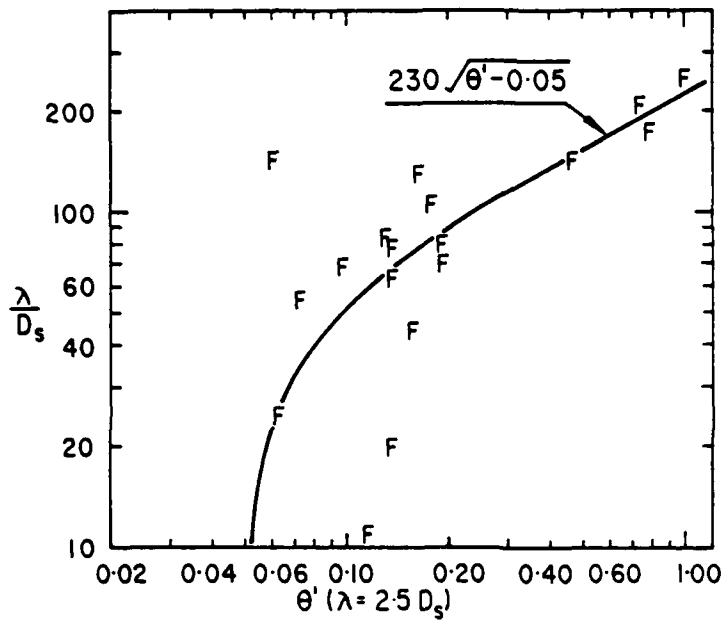
Figure B8: Roughness values derived by equation(B5) from Carstens et. al!s "flat-bed-data". Note that only four highest θ'-values correspond to fully developed rough turbulent flow according to the criteria given by Jonsson (1980).

may use

$$\eta_r/L_r = 0.342 - 0.34 \sqrt[4]{\theta'} \qquad \text{for } \theta' < 1. \tag{B19}$$

$$\eta_r/a_s = 21\left(\frac{u_{b,max}^2}{(s-1)gd}\right)^{-1.85} \tag{B20}$$

as suggested by Nielsen (1981). When $\theta' > 1$, the ripple height should be taken as zero.

LIST OF SYMBOLS

a_s	m	Water semi excursion
C_M	-	Added mass coefficient
D_s	m	Mean sand grain diameter
f_e	-	Energy dissipation factor
f_w	-	Friction factor
g	m/s^2	Acceleration of gravity
K	-	Non dimensional constant, eg (B8)
L_r	m	Ripple wave length (spacing)
s	-	Relative density of sand
u_b	m/s	Water particle velocity
τ	N/m^2	Bed shear stress
λ	m	Hydraulic roughness
η_r	m	Ripple height
ω	rad s^{-1}	Wave radian frequency
θ'	-	Skin friction Shields parameter

REFERENCES

BAGNOLD, R.A. (1964): Motion of Waves in Shallow Water: Interaction Between Waves and Sand Bottoms. Proc. Roy. Soc. London, A Vol. 187, pp. 1-15.

CARSTENS, M.R., NIELSON, F.M. and H.D. ALTINBILEK, (1969): Bed Forms Generated in the Laboratory under Oscillatory Flow, Coastal Engineering Research Centre, Technical Memo 28, Washington D.C.

GRANT, W.D. and O.S. MADSEN (1982): Movable Bed Roughness in Unsteady Oscillatory Flow. Journal of Geophysical Research, Vol. 87. pp. 469-481.

JONSSON, I.G. (1966): Wave Boundary Layers and Friction Factors. Proc. Int. Conf. Coastal Engineering, Tokyo, Chapter 10.

JONSSON, F.G. and CARLSEN, N.A. (1976): Experimental and theoretical investigations in an oscillatory (rough) turbulent boundary layer. J. Hydr. Res., Vol 14, No. 1. pp. 45-60.

KAJIURA, K. (1968): A model of the bottom boundary layer in water waves. Bull. Earthquake Res. Aust. Univ. Tokyo, 46, Chapter 5, pp. 75-123.

KAMPHUIS, J.W. (1975): Friction Factors under Oscillatory Waves. Proc. A.S.C.E. Vol 102, WW2, pp. 135-144.

LOFQUIST, K.E.B. (1980): Measurements of Oscillatory drag on sand ripples. Proc. 17th Coastal Eng. Conf. Sydney, pp. 3087-3106.

NAKATO, T., LOCHER, F.A., GLOVER, J.R. and J.F. KENNEDY (1977): Wave entrainment of sediment from rippled beds. Proc. A.S.C.E., Vol 103, No. WW1, pp. 83-100.

NIELSEN, P., (1981): Dynamics and Geometry of Wave Generated Ripples. Journal of Geophysical Research, Vol 86, No. C7, pp. 6467-6472.

OWEN, P.R. (1964): Saltation of Uniform Grains in Air. Journal of Fluid Mechanics, Vol 20, part 2, p. 225.

SAVAGE, P.R. (1953): Laboratory Study of Wave Energy Loss by Bottom Friction and Percolation. Beach Erosion Board, Tech, Memo 31.

SWART, D.H. (1974): Offshore Sediment Transport and Equilibrium Beach Profiles. Delft Hydr. Lab., Publication No. 131.

Appendix C-1: Beach-Surfzone Type along East Victorian Coast from Various Sources

DISTANCE		17.5.65		8.3.66		3.5.67		22.12.68		9.5.81		18.5.81		6.12.81	
km	survey site no.	1	0	1	0	1	0	1	0	1	0	1	0	1	0
Cape Howe to Shallow Inlet															
0-3															
3-8														RB	
8-10		TB												TB	
10-15		LT	BT											LT	RB
15-20		TB	D											TB	RB
20-25	2	TB	D											LT	
25-30	3	TB		RB										TB	
30-35		LT		RB										LT	
35-37		LT		TB	BT									TB	
37-40				TB	BT									TB	
40-45				TB	BT									TB	
45-50				TB	BT									RB	
50-55	6			TB	BT									RB	BT
55-60				TB	BT									LT	
60-65				TB	BT									RB	
65-70				LT	BT									LT	BT
70-75	7			RB	BT									RB	BT
75-77				RB	BT									TB	
77-84				LT	BT									TB	BT
84-85	8			LT	BT									TB	BT
85-90				TB	BT									RB	
90-95				TB	BT									RB	
95-100				TB	BT									LT	BT
100-105	9			LT	BT									LT	BT
105-110				LT	BT									LT	BT
110-115				LT	BT									RB	
115-118														RB	
118-120														LT	BT
120-125	10			LT	BT			RB				LT	BT	LT	BT
125-230				LT	RB			RB				R	RB	RB	
130-134				LT	RB			RB						RB	
134-135								TB							
135-140	11,12			LT	BT			BT				R	BT	RB	BT
140-145				LT	RB			BT	R			R	BT	LT	BT
145-150									R			R	BT	LT	BT
150-155				LT	BT							R	BT	LT	BT
155-160	13			LT	BT							R	BT	LT	BT
160-165												R	BT	LT	BT
165-170												R	RB	LT	RB
170-175													RB	LT	BT
175-180														LT	BT

Appendix C-1: continued

Distance	No.	17.5.65	8.3.66	3.5.67	22.12.68	9.5.81	18.5.81	6.12.81
180-185			R			RB	RB	RB
185-190			R			RB	RB	RB
190-193			RB			RB	RB	RB
193-195	15		RB			RB	RB	BT
195-200	16		TB			RB	RB	BT / LT
200-205	17		RB			RB	RB	BT / LT
205-210	18		RB			RB		BT / LT
210-215			RB	BT / R		RB	TB	BT / LT
215-220	19		BT	BT / R		RB	TB	BT / LT
220-225			BT	BT / R			TB	BT / LT
225-230	20		BT	BT / R			TB	BT / LT
230-235	21		RB	RB / R			LT	BT / LT
235-240			TB	BT			LT	BT / LT
240-245	22			BT			LT	BT / LT
245-250				BT / R			LT	BT / R
250-255	23			BT / LT			LT	BT / R
255-260	24			LT			TB	BT / R
260-265	25			LT			RB	BT / R
265-270	26			BT / LT			RB	BT / R
270-275	27			BT / TB			RB	BT / R
275-280	28			TB			RB	BT / R
280-285	29			RB			LB	BT
285-290	30			RB			LT	BT
290-295				TB			LT	BT
295-300				TB			LT	BT
300-305	32			TB			LT	BT / LT
305-310				TB			BT / LT	BT / LT
310-315				TB			BT / LT	BT / TB
315-320	33			TB			BT / LT	BT / TB
320-325	34			TB			BT / LT	BT / TB
325-330	35			BT / TB			LT	BT / TB
330-335				BT / TB			LT	
335-340							LT	
340-346							LT	

Key: D   Dissipative
BT   Longshore Bar-Trough
RB   Rhythmic Bar and Beach
TB   Transverse Bar and Rip
LT   Ridge and Channel or Low Tide Terrace
R   Reflective

See figure 23 for Beach Type Model
Blanks indicate no data
One bar type indicates single(inner)bar only, all other are
    double (inner-outer) bar systems.

Appendix C-2:   Selected Beach, foredune and bar type measurements for survey sites

LOCATION	BEACH HEIGHT[1] m	BEACH WIDTH[2] m	INCIPIENT FOREDUNE WIDTH m	INCIPIENT FOREDUNE HEIGHT[3] m	FOREDUNE HEIGHT m	BEACH TYPE INNER	BEACH TYPE OUTER[4]
2	3.17	60	50	3.25	9.10	RB	-
3	2.85	82	18	2.82	3.40	LT	-
6	3.06	85	23	3.06	8.00	RB	-
7	3.69	105	30	8.25		R	BT
8	4.47	70	>10	7.05		LT	BT
9	4.50	55	10	8.50	18.40	TB	BT
10	3.50	80	-40	-5.00	4.84	TB	-
11	3.50	60	-30	6.60	-15.00	LT	BT
12	4.40	90	25	8.60	10.15	R	BT
13	-4.70	-50	-30	7.00	28.35	RB	BT
15	3.65	60	-15	-5.00	-15.00	LT	BT
16	3.50	50	-10	6.00	-10.00	LT	BT
17	3.25	55	12	4.20	5.90	LT	BT
18	4.40	60	-15	5.40	13.00	LT	BT
19	3.90	50	15	6.30	15.00	R	BT
20	3.38	35	10	4.20	-17.00	LT	BT
21	4.89	50	20	7.00	-16.00	LT	BT
22	5.00	35	5	6.00	-13.00	LT	BT
23	4.20	35	7	4.20	-15.00	R	BT
24	2.90	20	15	-5.00	11.70	R	BT
25	3.50	40	10	4.00	15.00	R	BT
26	4.90	40	25	5.50	-15.00	R	BT
27	3.70	35	5	3.75	-12.00	R	BT
28	3.40	30	-25	-4.50	-15.00	R	BT
29	4.33	25	3	-4.50	-12.00	R	BT
30	3.75	45	-	-	-10.00	R	BT
31	3.75	65	20	3.85	7.60	LT	BT
32	3.15	75	5	3.50	6.55	TB	BT
33	2.78	70	10	4.10	9.00	TB	BT
34	3.20	70	5	-4.00	6.25	TB	BT
n	29	30	30	29	28	30	27
ȳ	3.75	57	17	5.2	12.0	LT	BR
σy	.65	20	11	1.6	5.1	-	-

Key: 1   Height of maximum swash and/or lower vegetation limit
       2   Distance from = to MSLM
       3   Maximum elevation of primary vegetation, usually spinfex or marram
       4   Beach type of inner and outer bar, see figure   for beach type model

Appendix C-3: Selected beach-surfzone morphological and sediment characteristics at survey sites

LOCATION	BEACH FACE GRADIENT	SURFZONE GRADIENT	TROUGH WIDTH m	TROUGH DEPTH m	%CARB D	%CARB BF	%CARB S	%CARB O	BEACH M_ϕ	BEACH σ_ϕ	SURFZONE M_ϕ	SURFZONE σ_ϕ	OUTER M_ϕ	OUTER σ_ϕ
1	1:16	1:20	-	-		4	9	6	2.09	.37				
2	1:15	1:39	60	.5		3	5	3	2.07	.30				
3	1:38	1:69	-	-		2	5	7	1.78	.30				
6	1:19	1:25	-	-		5	8	4	2.29	.29				
7	1:18	1:44	70	.76		1	1	6	1.59	.28	.43	.50		
8	1:12	1:63	105	2.64			5	6	1.82	.40	.92	.93		
9	1:25	1:33	-	-		4	7	7	1.84	.60				
10	1:15	1:51	60	.95		5	7	7	1.39	.49				
11	1:15	1:56	70	.60		0	1	0	1.06	.27				
12	1:12	1:52	90	.30		0	0	0	1.18	.24				
13	1:10	1:58	-	-	0	1	2	0	1.12	.31				
14	1:10	1:58	70	.40		0	3	-	1.21	.28				
15						1	1		1.13	.36	.90	.66	-	
16	1:16	1:43	55	.30		5	5	2	1.40	.27			1.70	.32
17	1:14	1:42	70	.36		3	4	-	1.45	.25	1.02	.79		
18	1:12	1:43	75	.60		7	4	2	1.01	.63				
19	1:8	1:49	55	.70		8	22	6	1.08	.51				
20	1:11	1:36	40	.10		9	28	4	.90	.82	.17[s]	.61	.96	.88
21	1:7	1:25	30	.64	3	12	30	10	.87	.56	-.19[s]	.97	.61	
22			-	-		10	23		.23	.51	.39[s]	.83		
23	1:8	1:27	50	.42		10	22	5	.38	.63	.61[s]	.60		
24	1:8	1:27	45	.19		8	19	6	.43	.47	-.62[s]	.55		
25	1:11	1:33	58	.80		8	17	10	.96	.65	.75[s]	.56		
26	1:9	1:52	90	1.45		5	12	7	1.68	.42	.80[s]	1.00	1.96	.48
27	1:11	1:55	75	.80		8	19	6	1.06	.87	.60[s]	.79		
28	1:9	1:37	60	.80		12	11	6	1.34	.95	.73[s]	.97		
29	1:9	1:44	85	1.10		8	14	6	.79	.85	.86[s]	.80		
30	1:10	1:33	65	.70	5	4	8	7	1.46	.53	.92[s]	.98		
31			-	-		4	4		.87	.65	-.38[s]			
32	1:17	1:47	55	.90		3	10	5	1.80	.31	.01	1.31		
33	1:25	1:36	50	.60		4	16		2.06	.30	.87	1.18		
34	1:18	1:36	55	.30		4	10		2.10	.35	.44	1.25		
35	1:21	1:48	70	.55		8	9	7	1.52	.91	.62	1.24		
$\bar{x}$	29	29	25	25	4	35	31	25	.35	.35	.20	.19	4	3
y	1:14	1:42	64	.70	3	5	11	5	1.33	.48	-.20	.87	1.30	.56
σy	±7	±12	17	.5	34	8	8	3	.53	.21	.66	.25		

Key: D - Dune, BF - Beach Face, S - Surfzone, O - Outer Bar Crest
M_ϕ - Mean grain diameter in phi units
σ_ϕ - Standard deviation (sorting)
%CARB - Percent Carbonate Material

Appendix C-4: Vegetation types at survey locations

LOCATION

FOREDUNE

INCIPIENT FOREDUNE

BANKSIA TEA TREE Leptospermum ACALIA Longifolia CALOCEPHALUS Brownii MARRAM Ammophila Arendria SPINIFEX Hirstus CAKILE Maritana

2 3 6 7 8 9 10 11 12 13 15 16 17 18 19 20 21 22 23 24 25 26 27 28 29 30 32 33 34 35

Key: ✓ dominant: (✓) present: +m plus marram: +s plus spinifex

REPORT DOCUMENTATION PAGE		READ INSTRUCTIONS BEFORE COMPLETING FORM
1. REPORT NUMBER	2. GOVT ACCESSION NO. AD-A119034	3. RECIPIENT'S CATALOG NUMBER
4. TITLE (and Subtitle) NEARSHORE and SURFZONE MORPHODYNAMICS of a STORM WAVE ENVIRONMENT: EASTERN BASS STRAIT, AUSTRALIA		5. TYPE OF REPORT & PERIOD COVERED TECHNICAL REPORT 81/82
		6. PERFORMING ORG. REPORT NUMBER TECH. REPT. 82/3
7. AUTHOR(s) L.D. WRIGHT, P. NIELSEN, A.D. SHORT, F.C. COFFEY and M.O. GREEN		8. CONTRACT OR GRANT NUMBER(s) Grant N-00014-80-G-0001
9. PERFORMING ORGANIZATION NAME AND ADDRESS University of Sydney Coastal Studies Unit Sydney, N.S.W., 2006, Australia		10. PROGRAM ELEMENT, PROJECT, TASK AREA & WORK UNIT NUMBERS NR 388-157
11. CONTROLLING OFFICE NAME AND ADDRESS Office of Naval Research Coastal Sciences Program, Code 422CS Arlington Virginia, 22217		12. REPORT DATE JUNE 1982
		13. NUMBER OF PAGES 154
14. MONITORING AGENCY NAME & ADDRESS(if different from Controlling Office)		15. SECURITY CLASS. (of this report) Unclassified
		15a. DECLASSIFICATION/DOWNGRADING SCHEDULE

16. DISTRIBUTION STATEMENT (of this Report)

Distribution of this document is unlimited

17. DISTRIBUTION STATEMENT (of the abstract entered in Block 20, if different from Report)

18. SUPPLEMENTARY NOTES

19. KEY WORDS (Continue on reverse side if necessary and identify by block number)

Beaches, Surfzones, Nearshore, Morphodynamics, Oceanography, Bass Strait

20. ABSTRACT (Continue on reverse side if necessary and identify by block number)

    A field investigation of inner shelf, surf-zone, and beach processes and associated morphodynamic changes was carried out on and seaward of Eastern Beach, on the Gippsland Coast, in Eastern Bass Strait, Australia. The beach is part of a long straight beach system fronted by a wide continental shelf. Frequent passage of gales through Bass Strait results in relatively high energy but variable and rapidly changing deepwater wave conditions. Time series of benthic currents (u and v) were recorded at

DD FORM 1473 1 JAN 73 EDITION OF 1 NOV 65 IS OBSOLETE
S/N 0102-LF-014-6601

depths of 20m and 10m over the nearshore profile and from different regions of the surf zone.

Over the nearshore profile, wave-induced oscillatory flows dominate to depths of 20m and are responsible for agitating and suspending sediments. Despite the microtidal range, reversing shore-parallel currents and super-imposed wind driven currents are second in importance and determine the fate of sediments suspended by waves. Frictional dissipation of the obliquely incident waves over the rough, rippled and low-gradient nearshore profile is particularly pronounced and, as a result, bottom orbital velocities measured at 10m depth were slightly weaker than those measured at 20m. Of fundamental importance to surf zone processes, nearshore energy dissipation by bed friction causes not only a reduction in average breaker height but also significantly reduces the temporal range of breaker conditions.

The morphodynamic state of the surf zone and beach remains intermediate between the reflective and dissipative extremes and is characterized for most of the time by pronounced longshore bar-trough or rhythmic bar and beach topography. A relatively deep ($h \simeq 2m$) trough separates a dissipative bar from a steep reflective beach face. In addition to the oscillations at in-cident wave frequency which are dominant throughout the surf zone, important roles are played by surf zone standing waves at subharmonic and infragravity frequencies and by longshore currents and rips. Vertical profiles of long-shore current velocity within the trough revealed velocities as high as $0.25m \ sec^{-1}$ to within 0.075m above the bed and were not at all logarithmic. The profiles are explained in terms of the large near-bottom eddy viscosity caused by wave induced vortices over a rippled bed. Direct measurement of vertical profiles of suspended sediment concentrations showed that, des-pite the presence of longshore currents, sediment suspension can be well modelled in terms of entrainment by waves alone.

Although temporal variability of deepwater wave conditions is very large, the substantial reductions in breaker variability caused by increased near-shore dissipation of larger waves also reduced the range of morphodynamic variability of the beach and surf zone. The longshore-bar-trough and rhythmic-bar-and-beach states represent the modal states and other states rarely develop. However, profile mobility is considerable. Most of this mobility is expressed by onshore-offshore migrations of the bar and, to a lesser extent, by longshore migrations of rhythmic features. The mobility of the subaerial beach face is comparatively low and this is attributable to the relative constancy of the shore-break amplitude. The Eastern Beach model is compared to an analog at Duck, North Carolina, U.S.A.